Understanding the effect of daylight on circadian rhythms through High Dynamic Range (HDR) measurements and simulations

Amber Wu

A thesis submitted in partial fulfillment

of the requirements for the degree of

Master of Science in Architecture

University of Washington

2023

Committee:

Mehlika Inanici

Christopher Meek

Program Authorized to Offer Degree:

Architecture

University of Washington

Abstract

Understanding the effect of daylight on circadian rhythms through High Dynamic Range (HDR) measurements and simulations

Amber Wu

Chair of the Supervisory Committee:

Professor Mehlika Inanici

Department of Architecture

A growing body of research suggests that the built environment affects the circadian rhythms of building occupants inhabiting indoor spaces. This stems from the fact that the average modern human being spends about 90% of their lives indoors, which presents a need for architectural design to take into consideration how indoor spaces are able to support human health and well-being. Having a means to predict melanopic light levels through digital simulation will greatly facilitate the conversation of how design choices affect indoor circadian entrainment.

LARK is a multi-spectral lighting simulation tool that can simulate indoor circadian lighting. It was developed in 2015, which makes it a relatively new tool and it is still under development. Validation is required to assess its accuracy in simulating the spectral qualities of the sky and indoor material spectral properties to give a quantitative value of circadian entrainment. This thesis compares real-world measurements with simulation results to assess LARK's circadian lighting simulation capabilities of indoor environments and identify shortcomings that require further development.

Field measurements of the spectral characteristics, Correlated Color Temperature (CCT), and photopic lux of the sky and indoor data collection site are taken. The Equivalent Melanopic Lux (EML) values are derived from spectral measurements. Year-long measurements recorded one day a month between 9:00 am to 5:00 pm are analyzed to understand the dynamic patterns of photopic and melanopic daylight availability. The field measurements also serve as inputs for LARK simulation. Comparative analysis of the simulation results against measurement values shows that LARK performs well in predicting melanopic light levels under clear sky conditions with high CCTs, but discrepancies start to arise for skies with cloud cover and low CCTs. False color analysis of the sky luminance distribution shows a difference between the LARK simulation sky model and real-world skies. This highlights a need for sky models that are better able to represent the full spectral characteristics of real-world skies as it affects the resulting simulated EML values. With further validation and development, LARK has the potential to be extensively utilized by researchers and designers to identify architectural design strategies that can satisfy both visual and circadian needs of occupants in indoor spaces.

Acknowledgements

I would first like to express my deepest gratitude to my thesis supervisor Dr. Mehlika Inanici for her continued and unwavering support, guidance, and invaluable insights throughout my master's degree journey and especially this thesis. I feel extremely fortunate to have her as my thesis committee chair and mentor; she is a wealth of knowledge in the field of lighting research and could answer any questions that I had with ease and enthusiasm and helped me shape the direction of this thesis. She is also a great teacher who taught some of my favorite classes that I took in my graduate studies.

I am also extremely grateful to my thesis committee member, Prof. Christopher Meek, for his kind words and encouragement, as well as providing me with the opportunity to work at the Integrated Design Lab. My interest in daylight first stemmed from his introduction to daylighting class that I took as an undergraduate at the UW, and I am glad that I got to continue working with him through my master's degree.

I would also like to thank my good friend and classmate Nico Lomas, who has been an incredible source of inspiration, support, and camaraderie as we both went through this academic journey together.

Words would not be able to describe my heartfelt gratitude to my parents for their love, support, and understanding. Their continued support allowed me to pursue this master's degree, and stay focused and motivated to further my knowledge in a topic that I am passionate about. I am also indebted to my in-laws, for their support and encouragement.

Lastly, I would like to thank my husband, Dino de Raad, for his exceptional expertise and creativity in statistics and his advice on how to represent the data in this thesis. Most importantly, his continued love and support have been a constant source of strength and inspiration to which I attribute the success of my academic endeavor.

Table of Contents

List of Figures

Chapter 1 – Introduction

The human eye functions in a dual manner – visual and non-visual. The visual side comprises rods and cones and allows humans to see and perceive the world around them by processing light signals received by the eye. The non-visual side, on the other hand, is the main driver of the circadian rhythm. The circadian rhythm, derived from the Latin word *circa* and *diem*, or around a day, describes the body's internal regulation of the sleep-wake cycle, and it controls various daily biological processes in cycles of approximately 24 hours. The circadian rhythm is regulated by the non-visual system's exposure to light and darkness, which sends signals to the suprachiasmatic nucleus (SCN) in the brain to synchronize the body's internal clock to the external environment (Rea et al. 2010). The circadian rhythm affects various aspects of human health and well-being, such as the sleep-wake cycle, hormonal regulation, metabolic processes, and cognitive function and alertness (Figueiro 2008, Brown 2020, Figueiro et al. 2019, Rea et al. 2020).

The light exposure pattern of the average person in modern society greatly deviates from the natural light-dark diurnal cycle that shaped the circadian rhythms of humans through evolution. This is due to extensive reliance on electric lighting and indoor spaces in the built environments, which effectively reduces opportunities for exposure to natural daylight. The disruption of circadian rhythm can result in a myriad of health problems in the long term, such as sleep disturbances, mood disorders, reduced cognitive function and alertness, and increased susceptibility to cancer, diabetes, depression, and Alzheimer's disease (Richard et al. 2013). It is thus imperative that the design of our indoor spaces are able to support the circadian needs of its

occupants, providing a passive way to receive the necessary daily level of circadian entrainment to avoid disruption of the circadian rhythm.

1.1 – Goals and Objectives

The overarching goal of this thesis is to improve design decisions through holistic evaluation of lighting in the built environments. There are two main objectives: 1) to understand the changes of EML throughout the year and 2) to evaluate the tool LARK Multispectral Lighting, which is a lighting simulation tool capable of simulating indoor circadian lighting. Validation is done via comparative analysis of measurements versus simulation results. Field measurements of the luminance, Correlated Color Temperatures (CCTs), and spectral characteristics of the sky as well as the indoor data collection site are collected at multiple points in time. The Equivalent Melanopic Lux (EML), which is the quantification of circadian entrainment, is derived from the measurements. The measurement values are used as inputs for the LARK simulation, which generates an EML value at each point-in-time simulation. The measurements also allow us to identify trends and patterns in the characteristics of Seattle skies throughout the year, as well as highlight factors that may cause discrepancies in simulated results.

1.2 – Overview of Thesis

Chapter 2 is a literature review of current research in circadian rhythm, daylight, and the state of lighting simulation tools and software. Chapter 3 describes the methodology in which field measurement was undertaken, as well as how these measurements relate to the LARK simulation workflow. The simulation parameters are discussed. Chapter 4 discusses the results of

the year-long data collection and comparative analysis between measurements and simulation results. Finally, chapter 5 covers a summary of results, the conclusion, contributions, and future work.

Chapter 2 – Background

With the advent of electric lighting, its rapid adoption in the built environment effectively prolonged the hours of the day that people can utilize the indoor environment. In the modern era, the majority of the modern population spends about 90% of their lives indoors (Klepeis et. al. 2001). No longer were peoples' vision impaired by the lack of daylight or the low illuminance of candlelight. For decades, the solution to insufficient light within an indoor environment has been to simply turn on the electric lighting until the necessary light levels are reached. In commercial buildings, in order to minimize heat loss or gain through building envelope, small, punched windows are used which limits building occupants' views to the outside. The advancement of mechanical heating and cooling technology also meant that the floorplate depths were increased due to financial incentives for greater floor area use. These factors brought about the disruption of circadian entrainment to the modern population, as people no longer had a patterned exposure to daylight (Rea et al. 2002). The circadian rhythm is defined as a cycle that follows an almost-24 hours cycle, and is a natural process responding to light and dark that affects living things. The circadian rhythm can affect physical, mental, and behavioral responses in human beings. In addition, the beneficial qualities of daylight such as illumination and passive heating, are becoming increasingly recognized, and a great percentage of architecture projects in the 21st century puts a strong emphasis on the quality of daylight design. The introduction of better building envelope insulation techniques and advanced fenestration systems allow for more freedom in façade designs. The discovery of the circadian rhythm and its importance to the human body's functioning brought about a greater degree of value to daylight for the health and well-being of building occupants, which is weighed heavily in some extensively used building

standards such as the WELL v2[1] and Living Building Challenge[2]. Daylight has a unique spectral quality that cannot be substituted by current electric lighting technology to have the same effect on the circadian rhythm and human well-being.

2.1 - Chronobiology

Chronobiology is defined as the study of time and its effects on biological systems, and examines the interaction of external events and cues with the internal biological clock. In other words, it is the study of the circadian rhythm. It is a transdisciplinary field of research due to a multidisciplinary interest in how the circadian rhythm can affect general medicine as well as psychiatry (Çalıyurt 2017), and non-medical fields such as in the built environment. To understand the extents of how and why the circadian rhythm has such a significant impact on the human body, it is important to understand the various processes occurring in the body that affects these changes based on external stimuli. The systems for discussion in this chapter are the visual and non-visual system in the eye (, as seen in Fig 2.1), the brain, and the endocrine system.

[1] https://www.wellcertified.com/certification/v2/
[2] https://living-future.org/lbc/

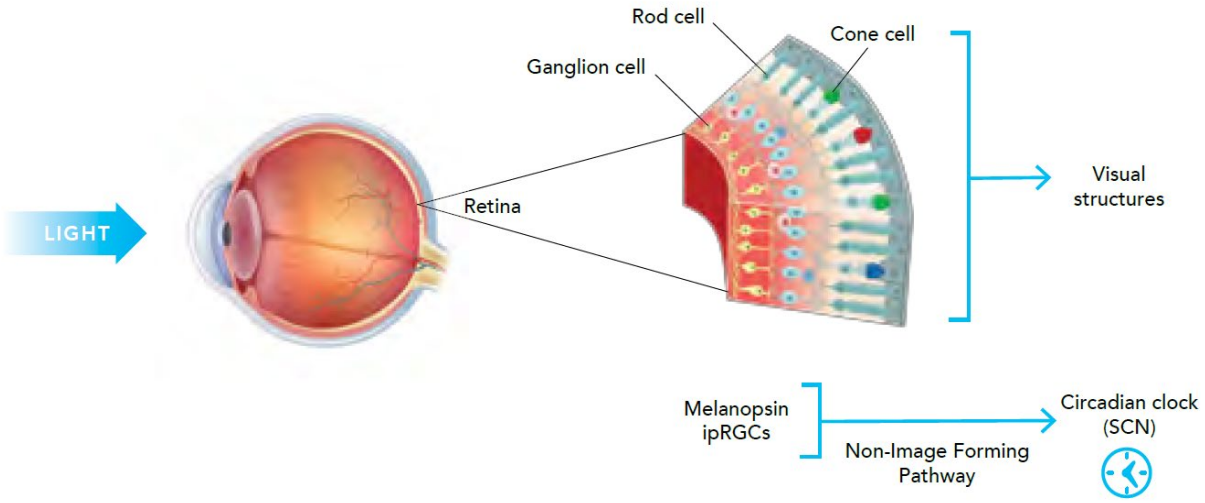

Fig. 2.1: Light entering the eye affects both the visual and non-visual systems (Jackson and Bollinger 2022).

2.1.1 - Visual System

A significant body of research has been done on the complex visual system of the human eye, where a complicated network of nerves connect the eye to the brain. Light stimuli is first focused through the cornea and lens of the eye. When light touches the lens, the zonular fibers and ciliary muscles change the shape of the lens so that light can focus and reach the retina, at the back of the eyeball where the photoreceptors are located. The retina contains rods and cones, which are image-capturing photoreceptor cells that convert light into electrical impulses, and they transfer such signals to the brain via the optic nerve, where the signals are interpreted as an image. This process, known as the visual pathway, allows humans to see and perceive elements in their surroundings, such as color, complex geometries, and movement.

Color vision is achieved by the eye through the three types of cone photoreceptors sensitive to Long (L), Medium (M), and Short (S) wavelengths of light respectively (Fig 2.2). Each have their unique wavelength color of peak sensitivity – L = red, M = green, S = blue. This gives humans their trichromatic vision, or the ability to see in three primary colors and their derivatives. The eye detects the spectral distribution of the light it receives and stimulates the LMS cones. The overlap of the cones are interpreted as various colors which allows the brain to understand the perceived color of light entering the eye.

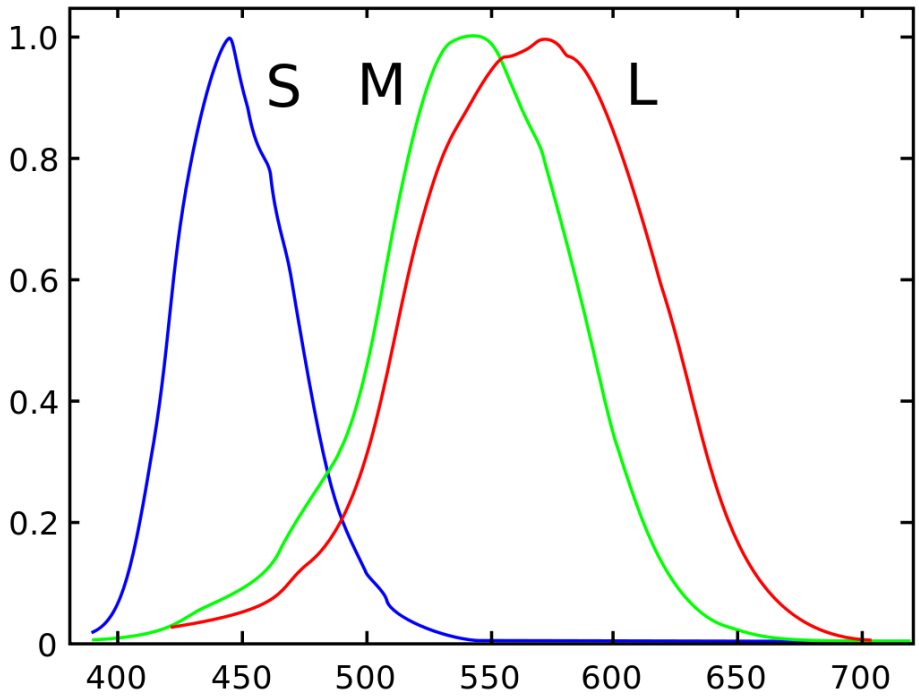

Fig. 2.2: Graph showing peak sensitivities of L, M, and S cones (Stockman et al. 1993).

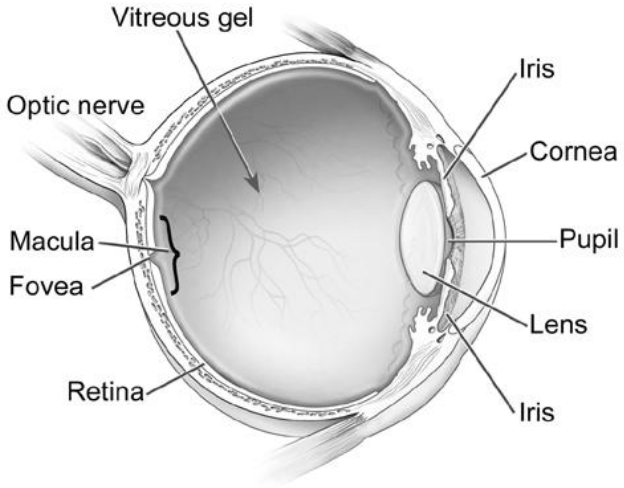

Fig. 2.3. Anatomy of the human eye[3]

The International Commission on Illumination, or the Commission Internationale de l'Eclairage (CIE), publishes standards that guide the science and art of light, color, and vision, among others. In 1924, they defined a standardized general photopic spectral sensitivity function based on the average human eye, called the CIE 1924 Luminosity Function, V(λ) (Wyszecki and Stiles 1982). The two classes of photoreceptors in the eye responsible for the visual system, rods, and cones, have different peak spectral sensitivities. The peak sensitivity of cones is concentrated around 555 nm wavelength, and is applied as the Y function in the CIE 1931 XYZ chromaticity diagram (Section 2.3.5.1). On the other hand, the peak spectral sensitivity for rods is at 498 nm. Above 3 cd/m², in everyday lighting conditions, the human vision is based on photopic vision, and the photopic luminosity function best represents the response of the human eye. In lower

[3] https://www.nei.nih.gov/

light levels, below 0.03 cd/m², the scotopic curve is used. Mesopic conditions refer to in-between photopic and scotopic when both rods and cones are active.

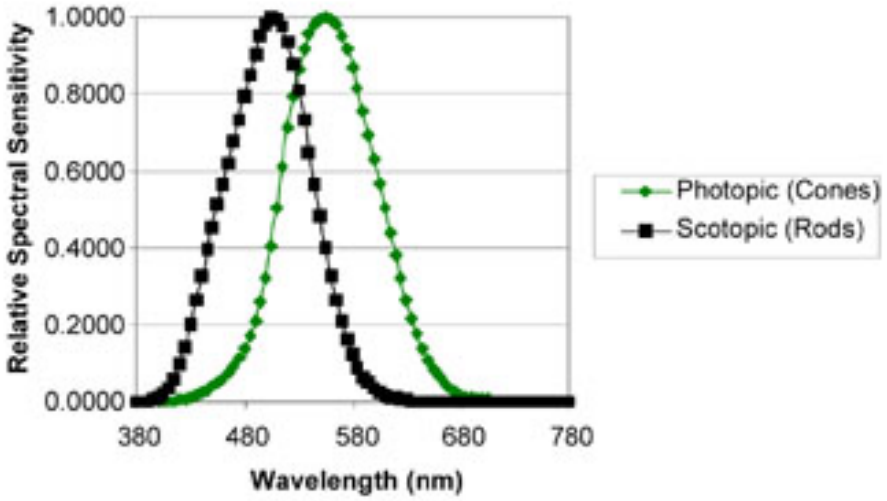

Fig. 2.4: Graph showing the spectral sensitivity curves of rods and cones (Schwiegerling 2004).

2.1.2 - Non-Visual System

The discovery of the intrinsically photosensitive Retinal Ganglion Cells (ipRGCs) in mice in the year 2001 by Brainard et al. and Thapan et al. opened doors to a new area of research of the eye. Unlike the rod and cones, the ipRGCs are non-image-forming (NIF) and can communicate irradiance information to an area of the brain called the suprachiasmatic nucleus (SCN). The ipRGCs only comprise about 1-5% of the Retinal Ganglion Cells (RGC) at the base of the retina. However, the ipRGCs express melanopsin, a photopigment that covers the retina and is most sensitive to blue light wavelengths of around 480 nm. In comparison, the rods are sensitive to wavelengths of 498 nm, while cones, comprising of S-cones, M-cones, and L-cones, are sensitive to 420 nm (blue), 534 nm (green), and 564 nm (red) respectively. The ipRGCs sends

signals to the brain in areas such as the suprachiasmatic nucleus (SCN), the olivary pretectal nucleus (OPN), as well as kick start signal transduction responses like the pineal melatonin production system, sleep regulation system, and the various processes regulated by the endocrine system.

The visual system responds to light stimulus rapidly (in milliseconds), whereas it can take several minutes of light exposure to affect the circadian system. Moreover, an individual's short-term history of light exposure affects the circadian system's sensitivity to light, as measured by nocturnal melatonin suppression (Acosta 2016). Light can cause non-visual effects such as melatonin suppression, circadian phase resetting, as well as cognitive alertness (Figueiro 2008, Brown 2020, Figueiro et. al. 2019, Rea et al. 2020).

The circadian rhythm is a natural biological "clock" controlled by the suprachiasmatic nuclei (SCN) in the hypothalamus in the brain, with an average intrinsic period of slightly greater than 24 hours in humans (about 24.5 hours) and modulated by the retina's exposure to temporal light and dark patterns (Rea et al. 2010). The circadian system is integral to several bodily functions in human physiology, ranging from metabolism, hormone-production, to daytime alertness via the suppression of melatonin production, and even affecting an individual's risk of certain cancers (Boyce 2014). This shows that both the presence and absence of daylight play important roles in human well-being in a daily cyclical pattern. However, studies and research conducted up to the year 2002 were limited by the gap in knowledge of the human eye as to the specific visual system that interacts with the non-visual aspect of light, primarily relying on the knowledge of melatonin suppression as a gauge for circadian entrainment (Rea et al. 2002). The discovery of the intrinsically photo-sensitive retinal ganglion cells (ipRGCs) was a significant milestone in research towards the role of light in circadian health as it identifies the retinal

photoreceptor in the eye responsible for the 'non-visual' processing of light, transmitting the neural signal to the SCN necessary to 'kick-start' a complicated network of neural and endocrine systems which send various hormones through the bloodstream that function to regulate both physical and psychological well-being (Brainard et al. 2001).

Phototransduction is defined as the process in which information obtained by photoreceptors in the eye is converted into electrical signals for interpretation by the SCN. These signals are sent to the pineal gland, which is connected to the SCN and responsible for melatonin secretion. Melatonin is a hormone that controls the sleep-wake cycle, and light exposure inhibits secretion while darkness allows for melatonin secretion. Hence, melatonin levels are lowest during the day, and highest at night (Rea et al. 2002, Rea et al. 2010, Arendt 1998). A higher concentration of melatonin in the bloodstream contributes to a more restful sleep with less interruptions through the night. On the contrary, a low level of melatonin is due to suppression in its production process, and light has a greater advancing effect early in the morning, which contributes to an individual's feeling of alertness (Alight 2021).

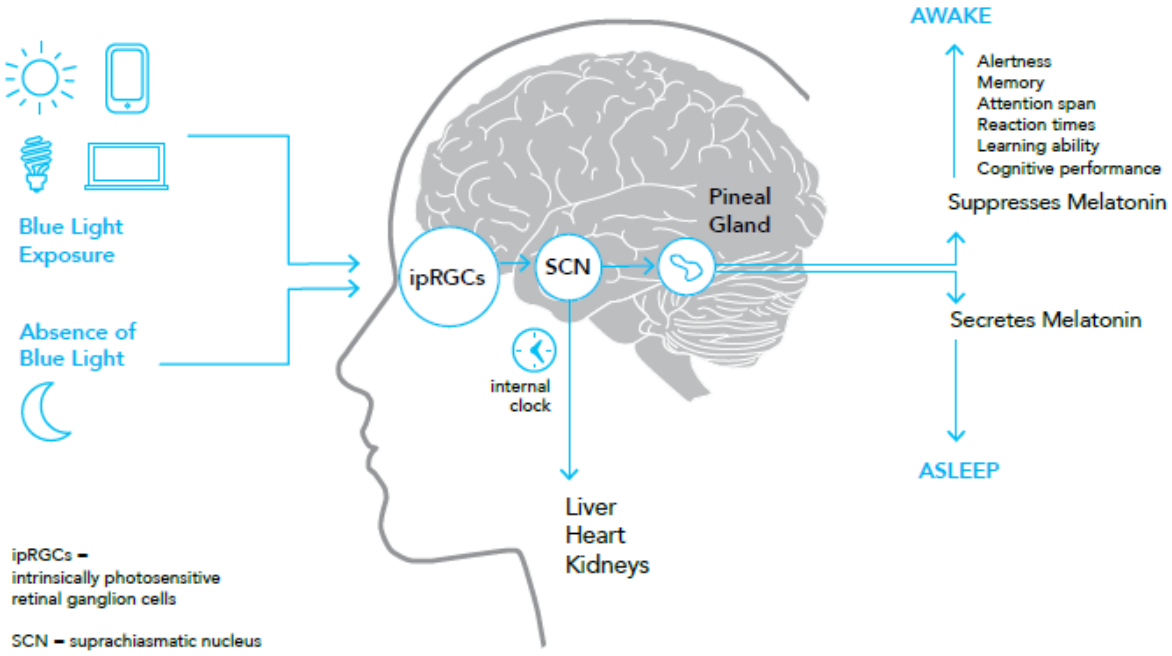

Fig. 2.5: How presence/absence of blue light affects melatonin production (Jackson and Bollinger 2022).

Our visual system peaks in sensitivity at about 555 nm, which is the green portion of the light spectrum. The non-visual system has a peak sensitivity to blue light at about 480 nm, but also is affected by wavelengths around it, as seen in Fig 2.6. This regular exposure to blue light regulates the SCN in hormone production, mainly melatonin secretion and suppression.

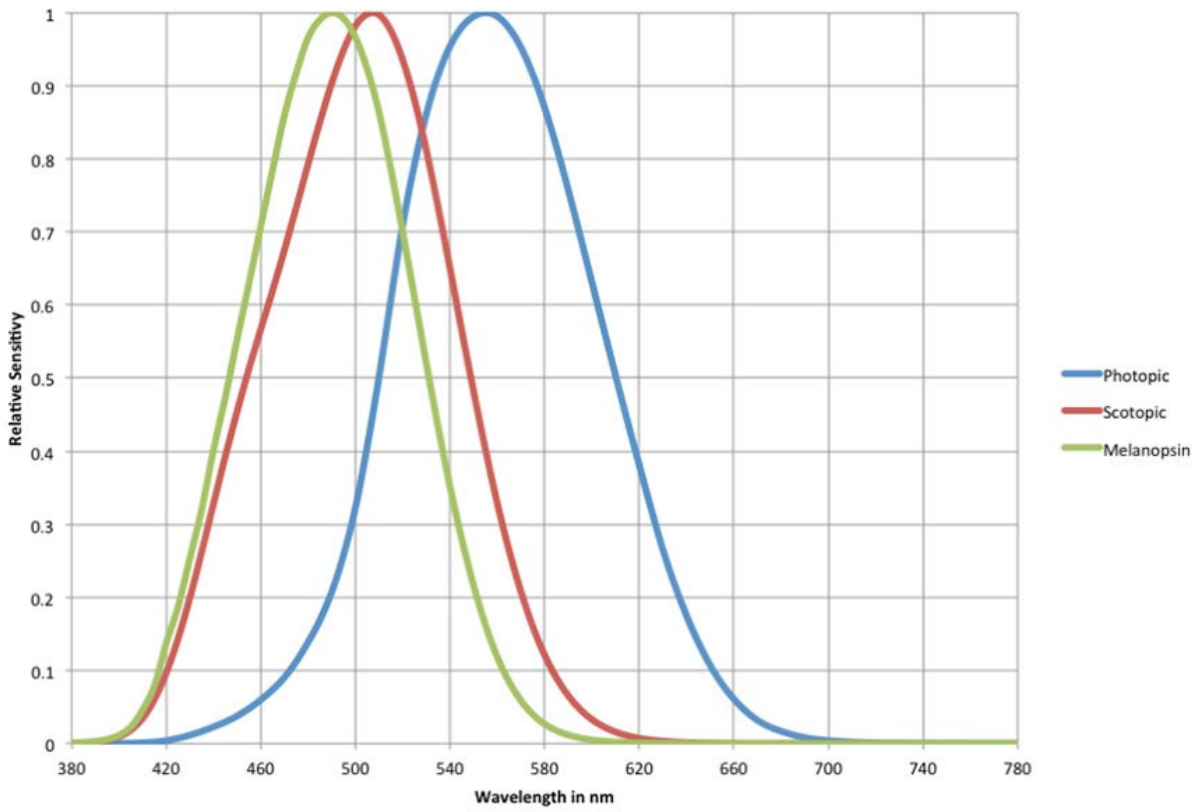

Fig. 2.6. Spectral sensitivity curve showing peak sensitivities of photopic (cones) and scotopic (rods) visions, and melanopsin based on Lucas et al. (2014)'s melanopsin function (Berman and Clear 2019).

Melatonin is a hormone that helps the human body prepare for restful sleep and its production is suppressed during the daytime when the blue light wavelength in natural daylight is at its peak. The result of this is providing alertness to the body and mind. As the day progresses towards the late afternoon, the signal to suppress melatonin production lessens, and around late evening to nighttime, when daylight is no longer present, melatonin production begins and is secreted by the endocrine system of the human body to signal that it is soon time to sleep. This cycle repeats the next morning where melatonin production is suppressed again. The lack of the blue wavelength in some electric light sources is attributed to low melatonin suppression which

sees lower productivity and mood in people working in spaces without adequate daylight access. Moreover, the endocrine system in the human body is delicate in that the various hormone levels in the body have to be in balance to avoid detrimental effects to the human physical and mental well-being. The circadian rhythm thus regulates alertness, core body temperature, blood pressure, and the production and suppression of melatonin. The short-term effect of a poor circadian rhythm is reduced alertness and poor sleep quality, whilst long term effects lead to more complex health problems such as increased risk of certain cancers (Richard et al. 2013). In examples of extreme circadian rhythm misalignment, it can cause Shift-Work Disorder and Jet-Lag Disorder, causing insomnia when workers try to sleep, and excessive sleepiness and fatigue at work (Gooley 2011).

2.2 – Light

2.2.1 – Daylight

Human beings evolved under the diurnal rhythm of external light and dark exposure. Daylight is a full-spectrum light source, and therefore it supports human vision and circadian entrainment with adequate spectral content. The color of light, be it natural daylight or electric light, is determined by their electromagnetic spectrum, determined by the intensity of each color between the wavelengths of 380nm to 780nm, which is the range of light that the human visual system is able to detect. A spectrophotometer is a device that can detect the spectrum of light that falls on its cosine corrected sensor.

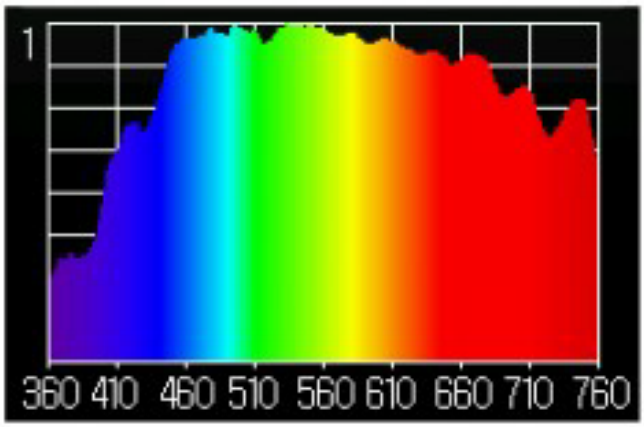

Fig. 2.7: Spectral power distribution graph of natural daylight (at one point in time) as read by a spectrophotometer.[4]

Correlated color temperature (CCT) is a description of the appearance of visible light emitted by a light source. This metric of color is derived from a hypothetical "black body" radiator (idealized to absorb and emit all wavelengths of light perfectly) heated to a certain temperature, and the color appearance of the light produced by the "black body" upon reaching this temperature. It is measured in Kelvin (K), and typically ranges from a scale of 2,000K to 10,000K. However, the CIE describes the CCT equivalent of the relative spectral irradiances of typical daylight on Earth to be from 4000K up to 25,000K (Wyszecki and Stiles 1982), and measured data in Granada, Spain suggests that the CCT of daylight can even reach up to 35,000K (Hernández-Andrés et al. 2001). Established by Hyde (1911), CCT is an extensively used quantification of color in lighting research and practice thanks to its simplicity in application. However, the simplicity is also a shortcoming as demonstrated by Durmus (2021)'s study, where two light sources with identical CCT can differ in perceived appearance due to

[4] https://www.sunlightinside.com/light-and-health/natural-light-vs-artificial-light/

differences in its spectral power distribution, and thus causes loss of information when used as a primary or only method of communicating the appearance of light. Instead, supplemental metrics, such as absolute spectral power distribution and accounting for chromatic adaptation, results in higher validity of research and improves repeatability of experiments.

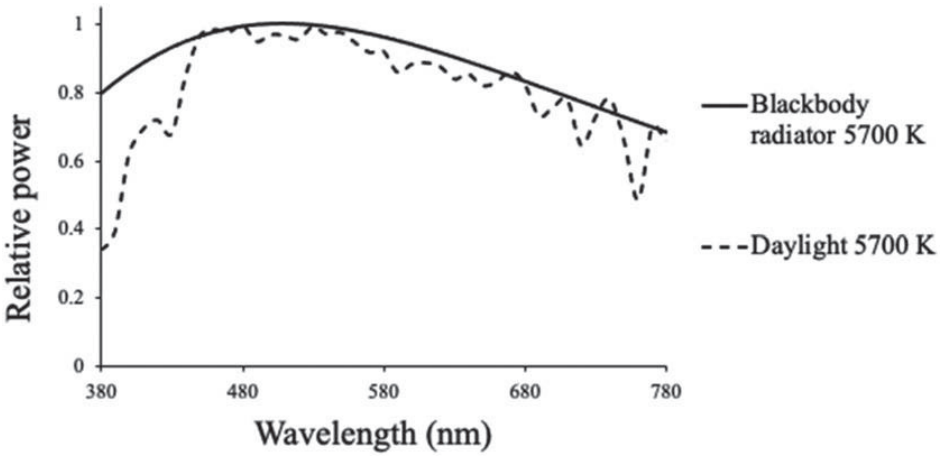

Fig. 2.8: Durmus (2021)'s graph showing two light sources with identical CCT but with different spectral power distribution.

Radiation emitted by a Planckian (blackbody) radiator and radiation emitted by the sun are similar (Fig 2.8). However, there is a difference in spectral power distribution between the two as light from the sun is absorbed and attenuated by atmospheric particles present within the Earth's atmosphere before it can be measured. The graph above shows that simply using CCT as a metric for evaluating the characteristics of light sources does not convey the full story.

2.2.2 – Variability of Daylight

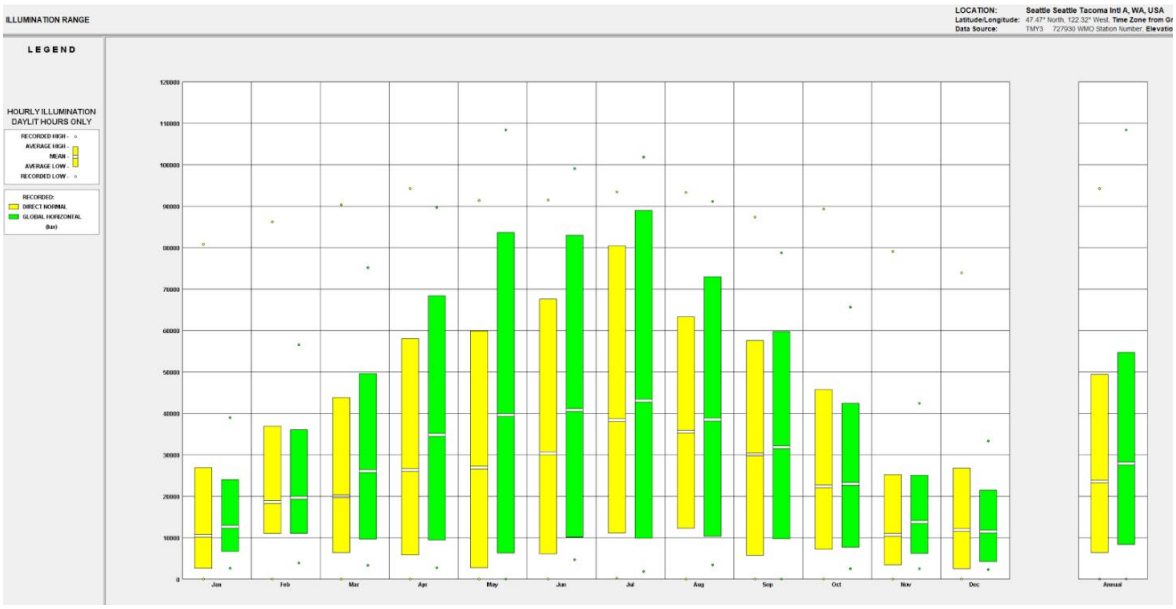

Fig. 2.9: Yearly recorded hourly variation of Seattle skies in illumination level from Climate Consultant software. The vertical axis is illuminance in lux.

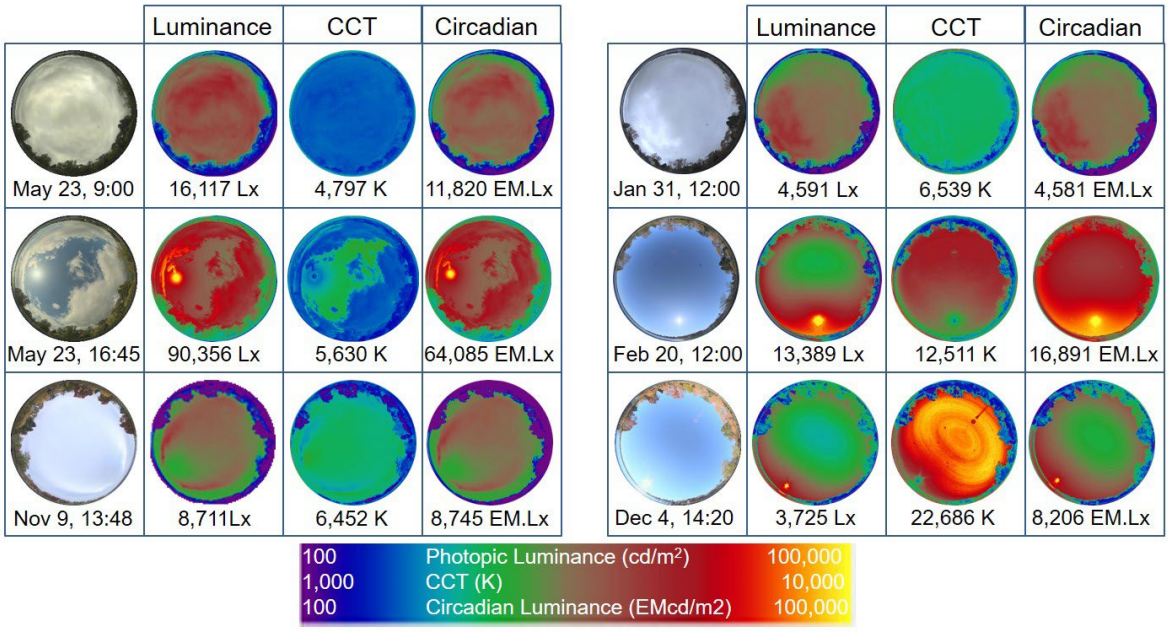

Fig. 2.10: HDR images captured under various sky conditions showing the variations in lux, CCT, and EM.Lx through per-pixel analysis (Inanici 2019).

Daylight is highly dynamic, and changes across days throughout the year due to various factors, such as sun position in the sky, weather conditions, color, and atmospheric particles. As it is a natural light source, daylight is more difficult to control, and different locations produce different outcomes owing to the daily, seasonal, and annual dynamics of daylight (Knoop et al. 2020). Evident from Fig 2.9, there is a wide variability in annual recorded illumination in Seattle skies, and Fig 2.10 shows how time of year and cloud conditions affect the CCTs and luminance of the sky, which affects the level of circadian stimulus in EML.

2.2.3 – Electric Light

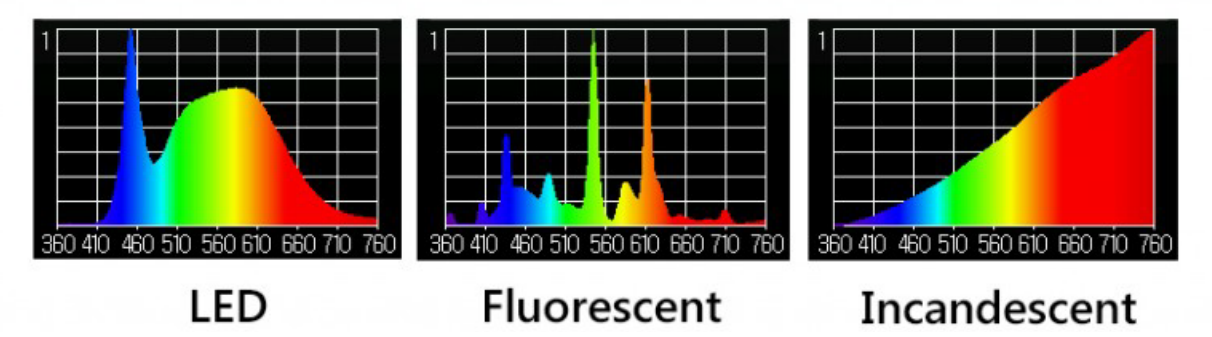

Fig. 2.11: Spectral power distribution graphs of 3 main types of electric light sources[5]

Electric light is defined as artificial illumination generated through converting electrical energy into radiant energy. The use of electric lighting is the main driver behind modern human beings spending most of their lives indoors, as it extends indoor productive hours beyond the presence of daylight by illuminating spaces enough to complete visual tasks. The most commonly used electric light sources are incandescent bulbs, fluorescent lamps, halogen lamps, and light-emitting diodes (LEDs).

[5] https://www.sunlightinside.com/light-and-health/natural-light-vs-artificial-light/

Fig 2.11 shows the spectral power distribution of typical LED, fluorescent, and incandescent light sources. Incandescent bulbs emit light by heating a wire filament using an electric current. The light emitted typically has a warm, yellowish color. Fluorescent and compact fluorescent lamps (CFLs) emit light by exciting a vapor inside of a glass tube that is coated with phosphor. The vapor emits UV light and the phosphor coating converts the UV light into visible light. They tend to provide a cooler, white light. Halogen lamps are similar to incandescent lamps, but are able to produce bright, white light by passing an electric current through a tungsten filament enclosed in a halogen gas-filled light bulb.

LEDs are the predominant type of electric light used today due to their ability to deliver high lumens using significantly lower wattages than their light counterparts. Invented in 1961 by Gary Pittman and James Biard, LEDs are solid-state devices that emit light when an electric current passes through a semiconductor material. The color of light produced is determined by the semiconductor material used. The bright blue emitting diode was invented in 1993 by Shuji Nakamura, which allowed LEDs to emit bright white light that fulfills most common lighting purposes. LEDs also offer a wide range of color options by utilizing different semiconductor materials, giving it a lot of versatility in spectral characteristics. Certain lighting manufacturers today are looking into creating lighting products that can mimic the spectra of natural daylight to drive circadian rhythms during the daytime, and offering timed color changing features to reduce melatonin suppression later in the day[6,7,8]. Nonetheless, electric light still greatly falls short of daylight in providing both illumination and circadian stimulus during the day due to a difference

[6] https://bioslighting.com/architectural-lighting/
[7] https://www.philips-hue.com/en-us
[8] https://www.lutron.com/en-US/Education-Training/Pages/LCE/ColorTuning.aspx

in spectral power distribution, and artificially providing the temporal characteristics of daylight through electric lighting requires significant energy use (Knoop et al. 2020).

2.3 – Design

2.3.1 – Designing with light

Designing with light can be a complex process involving balancing the light levels, color temperature, and position of the window. The lighting environment should provide building occupants with circadian entrainment, but at the same time there should also be adequate luminance contrast for visual tasks, without extreme light intensities that can cause discomfort due to excessive contrast and brightness in the field-of-view (Vos 2003). It will depend on the architect or lighting designer to consider the intentions of the project, and trade-offs are made to prioritize the building occupants depending on their specific needs or the architectural program of the space (Amundadottir 2017).

Design of indoor spaces are also complicated by integration of electric lighting and daylighting, as well as high contrast in spaces where uniform light is desired. Designing for circadian health and visual task performance can even be contradictory and challenging to control in the need to provide high light intensity but avoiding glare. Nonetheless, researchers are studying the design factors beyond electric lighting to potentially identify ways to achieve circadian lighting without compromising visual task performance and visual comfort.

Understanding how factors such as daylight and surface material reflectance affect the circadian entrainment of humans using the space is crucial to both simulation and design in the built environment.

2.3.2 – Surface material properties

Within indoor environments, the primary way by which light enters the eye is through inter-reflections on surfaces. The inter-reflect light spectra is a product of the spectra of the incoming light to a surface and spectral reflectance of the surface materials. Each reflection is weighted by the photopic and circadian efficacy curves to show the impact of material reflectance spectra on the visual and circadian response. Based on graph (e) below, the reflected light from the blue surface impacts the circadian response by almost four times as much as the red surface, both under 6500K daylight.

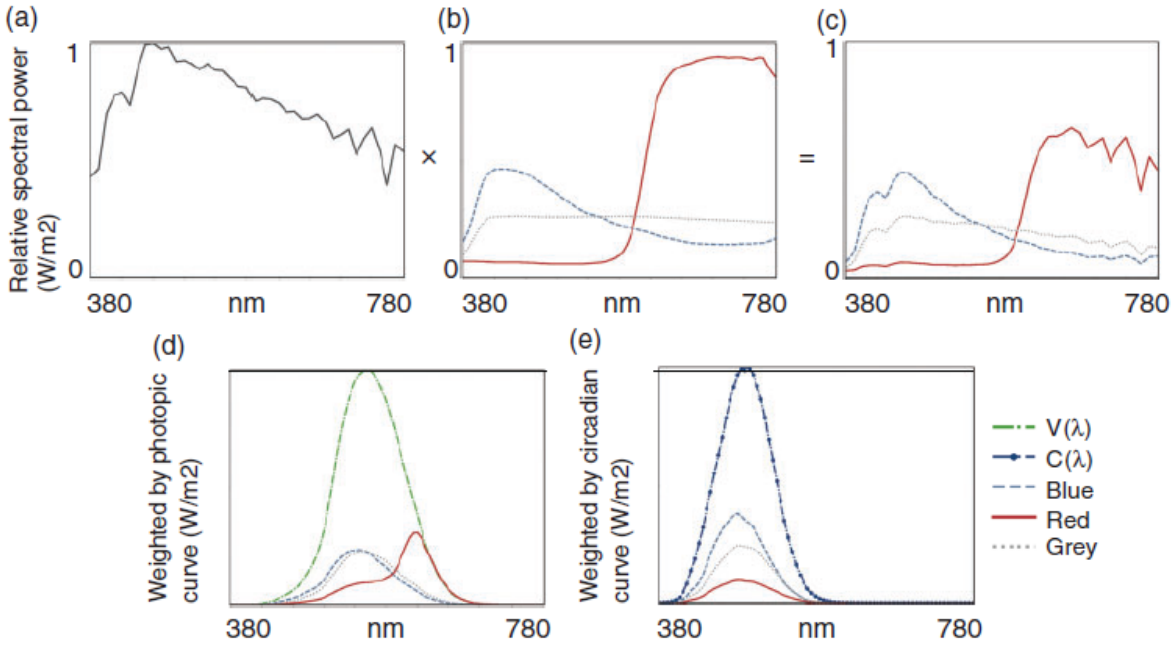

Fig. 2.12: graphs showing the relative spectral power of (a) incoming daylight of 6500K; (b) spectral reflectance of red, blue, and grey surface materials; (c) reflected light; (d) weighted photopic response; (e) weighted circadian response (Jung and Inanici 2019).

2.3.3 – Measuring circadian light

In order to measure and quantify circadian light, devices that are able to detect the non-visual characteristics of light and its spectral power distribution are needed. This can be achieved using a spectrophotometer.

2.3.3.1 – Dosimeter

The Daysimeter was developed by Rea et al. in 2004 at the Rensselaer Polytechnic Institute's Lighting Research Center (LRC). It is a research tool in the form of a wearable device at the eye level or as a pendant that measures personal circadian lighting exposures of its wearers, as well as track their daily rest and activity levels (Fig 2.13). It measures circadian light based on the model of human circadian phototransduction proposed by the LRC. The Daysimeter and its associated software allow researchers at LRC to interpret light as a stimulus to the human circadian rhythm, and thereby quantify circadian stimulus to further understand the impact of light on human health.

Fig. 2.13: The eye-level (left) and pendant (right) Daysimeter devices.[9]

[9] https://www.lrc.rpi.edu/programs/lighthealth/LightandDaysimeter.asp

The LYS Button is another wearable light sensing device that tracks light exposure, developed by LYS Technologies. The device can be clipped to clothing and even tracks movement with a built-in accelerometer. LYS aims to make light data collection more accessible. Based on their website, the LYS Button records RGB, Kelvin, Lux, movement values, and mEDI, while their phone application tracks chronotype, gender, age, social jetlag, and sleep-wake times.

Fig. 2.14: The LYS Button[10]

2.3.3.2 – HDR images

Although point-by-point measurement of photometric information is possible through traditional measuring devices, the process takes a long time and is highly prone to errors and uncertainties, especially with time-sensitive data that relies on the changing patterns of the sky. Inanici (2005) evaluated the use of photography-based data collection as an alternative that is able to capture data within a large field of view. This yielded the use of High Dynamic Range (HDR) images for the purpose of capturing luminance information. Multiple exposure

[10] https://lystechnologies.io/for-research/

photographs are taken for each scene by changing the shutter speed in increments, and these photographs are then computationally combined into a single HDR image. The multiple exposure photographs allow the camera to capture a wide luminance variation within a scene and the resulting HDR contains luminance information within each pixel of the image. A comparison of physical measurements showed that the luminance values derived from HDR images are within reasonable accuracy for the use of data collection.

Jung and Inanici (2018) recognized the lack of accessible technology for measuring circadian light and spectral data of daylight to researchers and practitioners. Equipment such as a luminance meter and spectrophotometer are specialized tools that can be expensive to obtain and fragile for field measurement and use. Many circadian lighting studies are done in laboratory-controlled settings, rather than real world settings within the built environment. In response, they developed a tristimulus color calibration procedure to tune HDR images taken by commercially available DSLR cameras such that circadian lighting information is available in the pixels of HDR images.

2.3.4 – Metrics for circadian rhythm in design

While further research is required in studying and quantifying the effects of light on the circadian rhythm of humans, the metrics most applied in current research are the Equivalent Melanopic Lux (EML) and the Circadian Stimulus (CS) (Gkaintatzi-Masouti et al., 2022b). Other metrics include the minimum reporting guidelines of stimulus conditions involving light by Spitschan et al. (2019) and the CIE Toolbox[11]. Both metrics have also been applied to

[11] https://cie.co.at/news/launch-cie-s-026-toolbox-and-user-guide

international standards and reports (Breslav et al. 2014), as well as circadian lighting simulation tools such as Lark Spectral Lighting and Adaptive Lighting for Alertness (ALFA).

The International WELL Building Institute (IWBI), an organization that focuses on the health and well-being of occupants in building design, introduced the WELL Building Standard (WELL). This is a guide towards a project achieving WELL certification, in recognition of the efforts made in design towards occupant health. The WELL guideline includes a section on health design standards for the circadian systems of building occupants. They propose the adoption of the Equivalent Melanopic Lux (EML), developed by Lucas et al. (2016), a metric that measures the biological effects of light on humans based on the ipRGCs, or more specifically the melanopsin which is the photopigment within the ipRGCs, and is recorded at the eye level of the occupant at a vertical plane. EML is calculated by multiplying the visual lux by a melanopic ratio that is dependent upon the spectrum of incident light, and the WELL requires a daily minimum threshold of 200 melanopic lux between the hours of 0900 to 1300 and considers all workstations where an individual regularly spends at least one continuous hour or cumulatively two hours per day (WELL 2021). Spectrophotometer measurements are taken in the field after project completion; thus, designers have to take into consideration the spectral power distribution (SPD) of glazing, surface finishes, daylight, electrical lighting, and the variability of daylight availability throughout the year (Brennan & Collins, 2018).

Rea et al. (2016) of the Lighting Research Center at Rensselaer Polytechnic Institute introduced the Circadian Stimulus (CS) metric which gives the functional effective relationship between circadian light (CLA), the spectral and absolute sensitivities of the circadian system to light (Rea et al., 2016) and acute melatonin suppression after a one-hour exposure, from a CS value of 0.1 at threshold to 0.7 at saturation. A laboratory and field study by the Light and Health

Research Center (LHRC) at Mount Sinai have revealed that exposure to a CS value of 0.3 or greater for at least two hours per day can positively affect sleep quality and alertness in humans (Figueiro et al. 2017; CIE 2018).

The non-visual direct response (nvR_D) model was first introduced as part of Amundadottir's thesis at Ecole Polytechnique Federale de Lausanne (EPFL) (2016), and further developed by Amundadottir et al. (2017). This is a dynamic metric that predicts the effects of light on humans based on non-visual effects, visual interest, and gaze behavior at the eye level of a building occupant, thus comparing light exposure patterns to potential health benefits in humans. It takes discrete time samples of light irradiance and weighs it to the peak sensitivity of ipRGCs, and coupled with light exposure duration to generate a response. Therefore, the nvRD model is a metric that considers how the non-visual system is affected by light exposure over a given duration of time.

2.3.5 – Predicting Light through Simulation

2.3.5.1 – Color Representation

The CIE 1931 color system, or the CIE chromaticity diagram, represents the limits of the human visual system for receiving light, by plotting the color space that is perceivable by humans. It is a standard for scientifically quantifying the characteristics of color as seen by humans in the LMS cones (Wyzsecki and Stiles 1982).

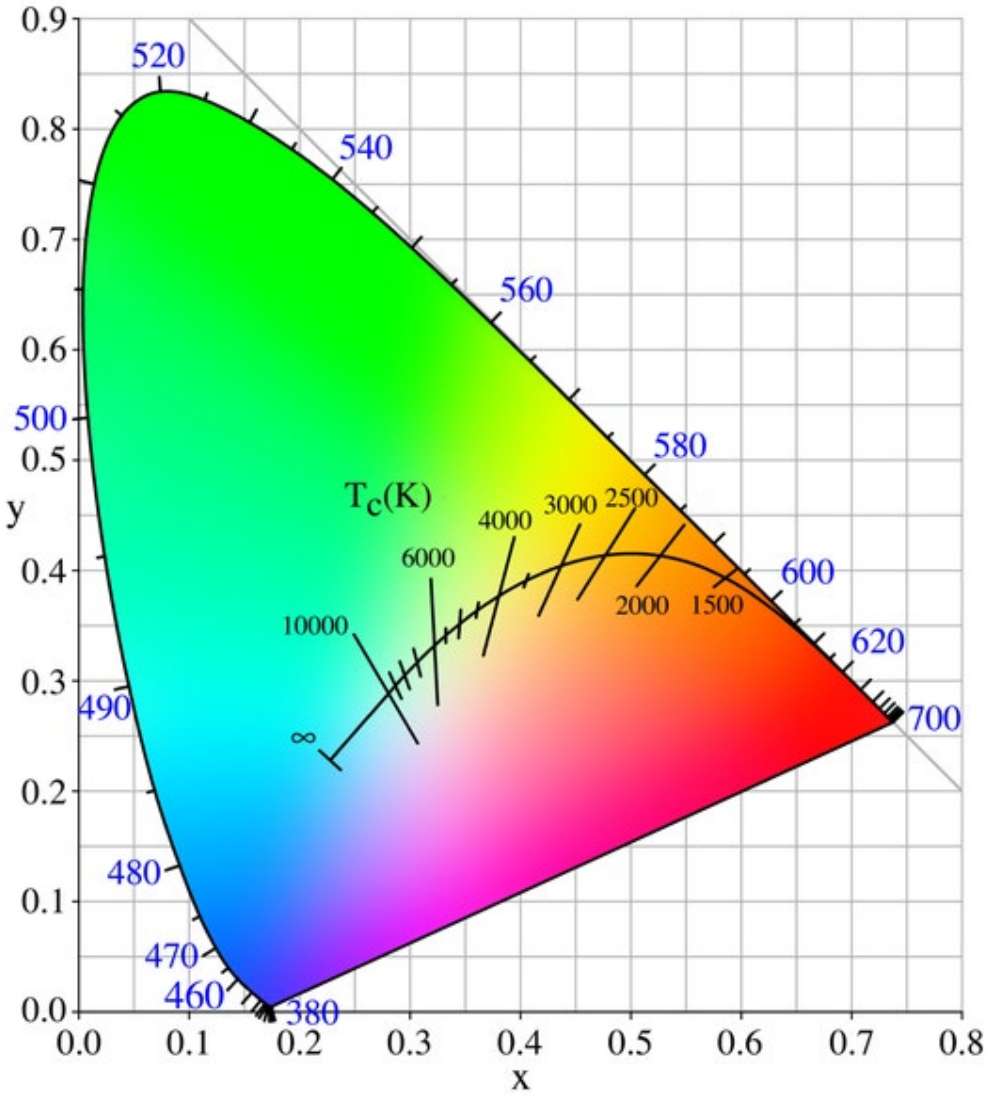

Fig. 2.15: CIE 1931 chromaticity diagram with the Planckian (black body) locus.

RGB is an arbitrary color space. Instead of using RGB, the CIE represents the 3 channels of XYZ in the human eye as humans are trichromatic (sensitive to the three primary colors RGB). The chromaticity diagram reduces the tristimulus values from 3 to 2 dimensions, by eliminating the intensity (or brightness) dimension, thus easily representing all colors perceivable by humans in a 2-dimensional diagram. The conversion from tristimulus values into chromaticity coordinates are based on the following equations:

$$x = X / (X + Y + Z)$$

$$y = Y / (X + Y + Z)$$

$$z = Z / (X + Y + Z)$$

These values are normalized ($x + y + z = 1.0$), so that the entire area within the chromaticity shape represents what the human color vision can perceive, and each color is a combination of x, y, and z. The perimeter of the chromaticity shape is a curve that represents the chromaticity coordinate of a spectral color, while every point within the shape represents the chromaticity coordinate of a non-spectral color, or colors that can only be created from mixtures of light.

The CIE 1931 chromaticity diagram also contains the Planckian (black body) locus, which gives a 1-dimensional representation of CCT and allows for the use of X and Y to calculate CCT.

2.3.5.2 – Lighting Simulations

In order to assess how design decisions made in the project interact with each other and have an idea of how the project may look like at its completion, mock-ups are used to create a model that is of a smaller scale to the actual building. Traditionally, physical models of a smaller scale than the final buildings were made to get a 3-dimensional (3D) representation of the project. However, with the advent of Computer Aided Design (CAD), this can be accomplished in digital space. 3D models can be created within CAD environments, such as Rhinoceros, and light sources can be simulated to understand the interaction of light with the building geometry and surface material, typically done via a render of a single point in time from a fixed point of

view. Lighting simulation tools are developed for the purpose of calculating the visual effects of light. Newer tools that utilize existing simulation engines are also being continually developed.

Although renderings are the preferred method to assess visual effects of daylight in architecture, a single rendering that represents one point in time with a single sky condition is inadequate in providing designers with information to evaluate the circadian entrainment of building occupants over time. Even with a time series of renderings for all daily and annual instances, it is difficult to compare the relative perceptions of architectural spaces under various sky conditions. Moreover, it is assumed that building occupants are stationary throughout the course of a day in simulation, but in reality they may circulate through the space and are exposed to changing sky conditions and light spectra throughout the day and year. In order to truly assess how circadian lighting design of an architectural space affects building occupants, a robust simulation model is needed that takes into account both spatial and temporal human behavior in space usage (Danell et al. 2020).

The primary engine for calculating light is Radiance, a suite of programs for the analysis and visualization of light. Greg Ward began developing Radiance in 1985, while he was at the Lawrence Berkeley National Laboratory (Ward and Shakespeare 1998). It is used by architects and lighting designers to predict illuminance, visual effects of light, and how light interacts with designed spaces before construction with both daylight and electric light. Radiance itself is a simulation software, and at the same time it is the background simulation engine for several other calculation or render tools. The inputs for Radiance simulation are geometry, light source data and properties, material properties. The scene's 3D geometry is compiled into an "octree", which is an efficient data structure for the purpose of raytracing. Raytracing is the algorithm that allows Radiance to emulate how light reflect and refracts, thus giving a more accurate description of

light's interaction with geometry. The Monte Carlo method is also used to sample light falling on a point. The outputs are spectral radiance, illuminance, luminance, and glare indices. The results of the Radiance simulation can be viewed as numerical values, contour plots, and color images.

Gkaintatzi-Masouti et al. (2022b) conducted a literature review on the current state of available simulation workflows and how they take into account metrics, predicting non-visual effects of light, and designing with light in architectural spaces. The review concluded that while there is increasing interest in simulating non-visual effects of light, there is a lack of consensus on a common method of performing these simulations. A preliminary simulation workflow was developed by Pechacek et al. (2008) that combines light quantity, light spectrum, and timing to obtain a "circadian potential" from daylight in a given space. This was later further developed using knowledge from photobiology by Andersen et al. (2012) and Mardaljevic et al. (2014) to incorporate a time-dependent effect of light exposure, as well as establishing a lower and upper bound for the effect of a given light dose on people. Amundadottir et al. (2017) refined the aforementioned workflow to develop a framework combining light quantity, spectrum, exposure duration, and photic light exposure history into a single mathematical model that translates light stimulus to their effect on humans.

Radiance is, in its most basic form, a 3-channel RGB renderer. Ruppertsberg and Bloj (2008) developed a methodology that will increase the number of channels that Radiance is able to render, thereby increasing the spectral resolution of simulations. An n-step algorithm is used to divide the visible spectrum into n wavebands, where n is the scale of spectral resolution of Radiance simulations.

2.3.5.1 – LARK

First developed and released by the University of Washington in collaboration with ZGF Architects in 2015, LARK[12] (Inanici et. al. 2015) is used in Grasshopper, a plugin tool for the 3D modeling software Rhinoceros. It utilizes the n-step methodology of 9-channel Radiance simulations to compute the effects of circadian light. It is used by design teams to evaluate the potential for circadian entrainment of their design decisions and material choices. LARK allows designers to set sky color, glazing type, and building material based on spectral data. Luminance renderings and data are also outputs of the plugin, which are used to analyze the effect of design decisions on the non-visual circadian system. Lark was subsequently improved upon by Gkaintatzi-Masouti et. al. and released as LARK 2.0 (2022a). This version of Lark officially includes electric lighting, daily simulations, and new metrics such as the melanopic equivalent daylight (D65) illuminance, as well as the relative ED65 non-visual direct response (based on Amundadottir et. al., 2016's research).

The LARK sky dome is colored using CCT derived from measured data, while the sun is modeled as a non-spectral equal energy white source without an atmosphere. This means that simulations are run without taking into account the spectral characteristics of the sun, and instead the result of non-visual stimulus heavily relies upon the CCT of the sky. Moreover, without an atmospheric-profile, LARK is unable to render the effect of low-angle sun in the morning or evening (Balakrishnan and Jakubiec 2019). LARK simulation skies also uniformly distribute the spectral properties throughout, but Inanici et al.'s (2022) study of vertical measurements at different orientations show differences in CCT values, SPD, and photopic and melanopic lux, suggesting that there are variations across the sky dome for that LARK currently does not take

[12] http://faculty.washington.edu/inanici/Lark/Lark_home_page.html

into account, and that simulation tools like LARK needs further development to accurately model the dynamic nature of daylight.

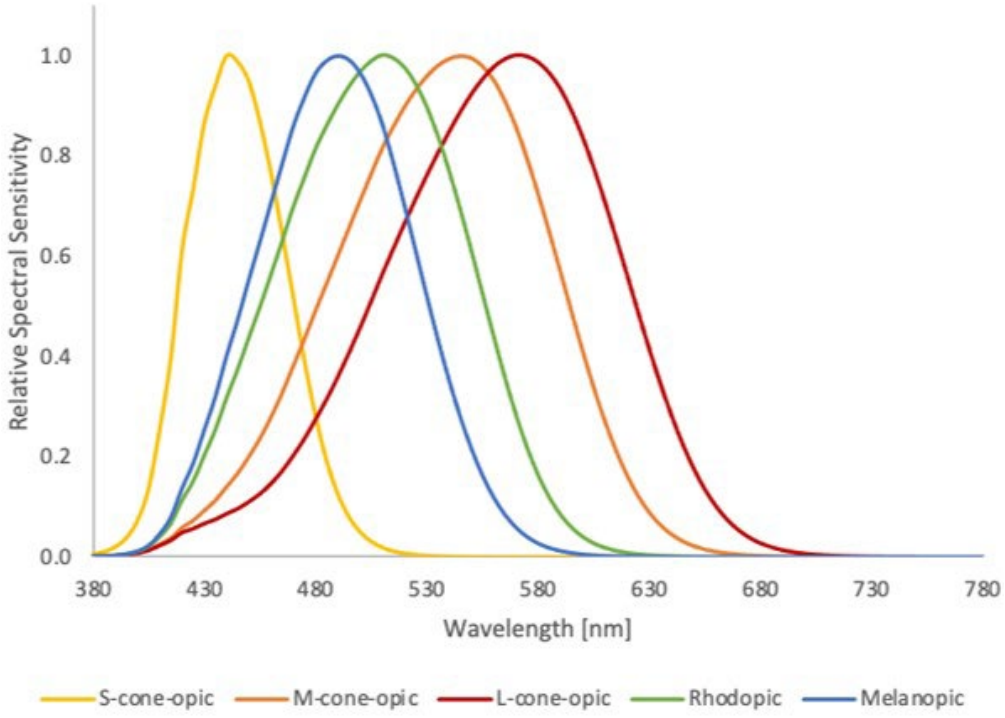

Fig. 2.16: normalized sensitivity curves of the 5 categories of photoreceptors in the human eye (CIE 2018).

Lark 3 is currently in development as a collaboration between the University of Washington and ZGF Architects as part of the College of Built Environments Applied Research Consortium alongside a recent study at the Cincinnati's Children's Hospital, where a specialized spectral lighting system is in place for the Newborn Intensive Care Unit (NICU) within the Cincinnati Children's Critical Care Building (Brennan & Cheng, 2022). Lark 3 reorganizes the 9 channel divisions for greater accuracy, and includes the metric for Opsin 5, a newly discovered receptor in the non-visual response system that affects the development of premature infants in

the neonatal intensive care unit (NICU) and peaks at the violet light wavelength of between 380 and 460 nm.

2.3.5.2 – ALFA

ALFA (Adaptive Lighting for Alertness) is a circadian lighting design software developed by Solemma[13]. It performs point-in-time calculations directly in Rhino 3D using Radiance with the three-color channels R, G, and B. ALFA then post-processes the Radiance ray tree and applies reflectance information at each ray intersection to generate 81 channels predictions for circadian lighting. The spectral sun and sky models used in ALFA are precomputed in libRadtran (Mayer and Kylling 2005), a radiative transfer library for locations available in ALFA's database generated using the U.S. Air Force Geophysics Laboratory's standard mid-latitude summer profile (Anderson et al. 1986). ALFA lets users choose between sky conditions – clear, overcast, hazy, and heavy rain clouds, as well as ground spectra.

[13] https://www.solemma.com/alfa

2.3.5.3 – LARK vs ALFA

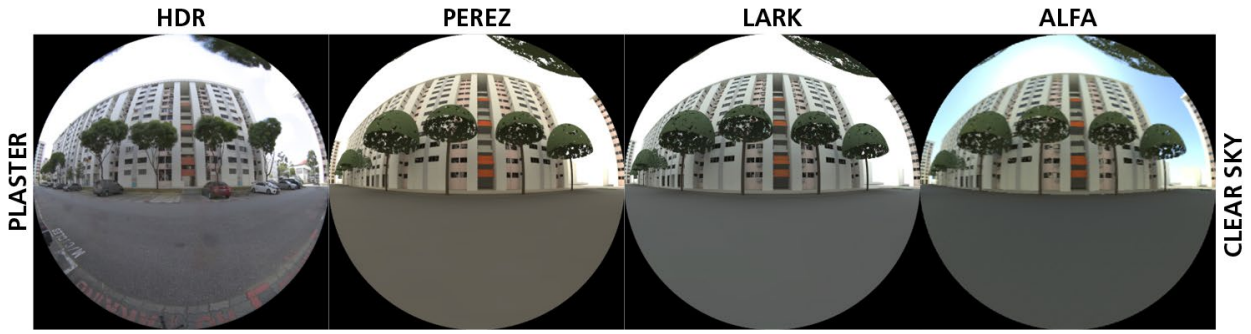

Fig. 2.17: Visual comparisons of urban environment renders of spectral and non-spectral simulations with HDR photographs (Balakrishnan and Jakubiec 2019)

LARK and ALFA are both tools capable of computing circadian lighting, as well as produce spectral renders with rich contextual color information and represent color perceptions which differs from non-spectral standard RGB simulations. Balakrishnan and Jakubiec (2019) compared the tools for their visual, spectral, and colorimetric accuracy of complex daylight scenes. Fig 2.17 displays the visual differences in render between spectral and non-spectral simulations with HDR images. ALFA's renders appear warmer in tone than that of LARK as ALFA renders direct light at a warmer color, while LARK models the sun as a non-spectral equal energy white source. However, this also caused a significant discrepancy in the appearance of the ALFA render to the HDR capture of the scene. In comparison, the LARK render has a closer appearance to the captured HDR image.

Using the Root Mean Square Error (RMSE) method computed for normalized spectral irradiance values to calculate errors in spectral distribution, the analysis showed that both LARK and ALFA performed better than non-spectral simulation tools in representing spectral information of scenes under various sky conditions, but LARK had a lower RMSE than ALFA

overall. Since LARK takes into account the CCT of the sky, it gives more accuracy in representing circadian stimulus than standard sky conditions provided by ALFA. Moreover, several types of measured sky conditions cannot be adequately represented by ALFA's pre-set cloud conditions, but LARK avoids this issue by taking the global horizontal irradiance and spectra for simulations. Ultimately, though, the study shows that both LARK and ALFA have significant errors for scenarios with cloud cover. LARK best performs under uniform sky conditions where the sun has minimal effect on simulation results, such as overcast days, and evening and morning skies. The reason for this is the global measured spectral irradiance is able to represent the entire sky dome, and hence the LARK generated sky model better aligns in colorimetric properties to real-world skies.

November 09, 14:02	(a) $Lark_{CIE}$ sky	(b) $Lark_{Perez}$ [2] sky	(c) Coloured Perez	(d) ALFA sky	(e) HDRI sky
					
Global horizontal illuminance	7167 lx[1] 7055 lx[2]	7044 lx[1]	7082 lx	12912 lx[3] 7528 lx[4]	7132 lx
Global horizontal CCT	5822 K[1] 5870 K[2]	5822 K[1]	5688 K	5868 K	6317 K
Global horizontal EML	7325 EML[1] 7651 EML[2]	7200 EML[1]	6862 EML	13797 EML[3] 8178 EML[4]	7595 EML

Fig. 2.18: Comparisons of cloudy sky conditions between LARK, Perez, ALFA, and captured HDR (Inanici et al. 2022).

November 7, 11:17	(a) $Lark_{CIE}$ sky	(b) $Lark_{Perez}$ sky	(c) ALFA clear sky	(d) ALFA hazy sky	(e) HDRI sky
	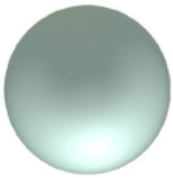	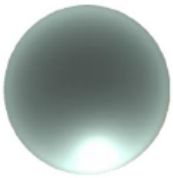			
Global horizontal illuminance	51 023 lx[1] 50 969 lx[2]	50 675 lx[1]	42 839 lx	24 263 lx	51 267 lx
Global horizontal CCT	5821 K[1] 5846 K[2]	5045 K[1]	5570 K	5143 K	5295 K
Global horizontal EML	52 146 EML[1] 50 751 EML[2]	48 683 EML[1]	43 702 EML	23 455 EML	44 599 EML

Fig. 2.19: Comparisons of partly cloudy sky conditions between LARK, Perez, ALFA, and captured HDR (Inanici et al. 2022).

November 17, 12:02	(a) $Lark_{CIE}$ sky	(b) $Lark_{Perez}$ sky	(c) Coloured Perez	(d) ALFA sky	(e) HDRI sky
					
Global horizontal illuminance	29 045 lx[1] 28 103 lx[2]	27 304 lx[1]	27 512 lx	38 518 lx	27 481 lx
Global horizontal CCT	5374 K[1] 5387 K[2]	5491 K[1]	5136 K	5555 K	5800 K
Global horizontal EML	28 181 EML[1] 27 309 EML[2]	27 213 EML[1]	27 513 EML	39 246 EML	25 628 EML

Fig. 2.20: Comparisons of clear sky conditions between LARK, Perez, ALFA, and captured HDR (Inanici et al. 2022)

Figures 2.18 to 2.20 show Inanici et al.'s (2022) study comparing LARK, Perez, and ALFA skies with captured HDR of various sky conditions, as well as their measured illuminance. There is consistently a significant discrepancy in global horizontal illuminance between ALFA sky and measured value of real skies, while LARK skies align better. Pierson et al.'s (2021) comparative analysis between ALFA and LARK also showed that although LARK had

significantly longer simulation times, it provided the most accurate results with no bias, with error distribution within the 20% range expected of standard Radiance RGB simulations.

Although both LARK and ALFA are accessible tools for circadian lighting to researchers, LARK is open-source, while ALFA is behind a paywall on Solemma's website, and its back-end is inaccessible. As more research findings pertaining to the non-visual system are being made, LARK can be improved upon more quickly.

Chapter 3 – Methodology

The project comprises two main processes – field data collection and LARK Spectral Lighting simulation. EML values are derived from both processes to assess circadian entrainment. The field data collection measurements are also examined to identify trends and patterns in the characteristics of Seattle skies across the year. Comparative analysis of measurements versus simulation results are done to validate LARK as a tool for predicting indoor circadian light levels and circadian entrainment.

3.1 – Setting

Data collection through measurement takes place primarily in three locations – Gould Hall 440 classroom (GLD 440), Gould Hall Roof, and Atmospheric Sciences-Geophysics Building Roof. GLD 440 is a south-facing classroom situated at the fourth and topmost floor of the College of Built Environments building at the University of Washington (UW) campus located in Seattle, Washington (Latitude 47.7, Longitude -122.3). This is where indoor illuminance, luminance, and spectra measurements are recorded on the vertical plane via HDR images, luminance, and spectrophotometer measurements. Data collection takes place once a month for over 12 months in duration, from 9am to 5pm local time to best mimic a desk worker's in-office hours. While daylight savings time is in effect, data collection proceeds from 9am to 5pm. Only daylight information is collected; all electric lighting is kept off. During winter months (Nov 2022 – Jan 2023), data collection concludes at 4pm local time as there is insufficient daylight to measure. Desks in the space are rearranged to mimic desk arrangement in an office space. The DSLR camera is positioned and aimed to closely mimic a person's eye-level

looking directly forward when seated at the desk. (Fig. 3.1) Two desk arrangements are used – one facing glazing directly and looking outside (Fig 3.2), and another perpendicular to the glazing facing a wood-slat wall such that the window and view to the outside is in the peripheral vision (Fig 3.3).

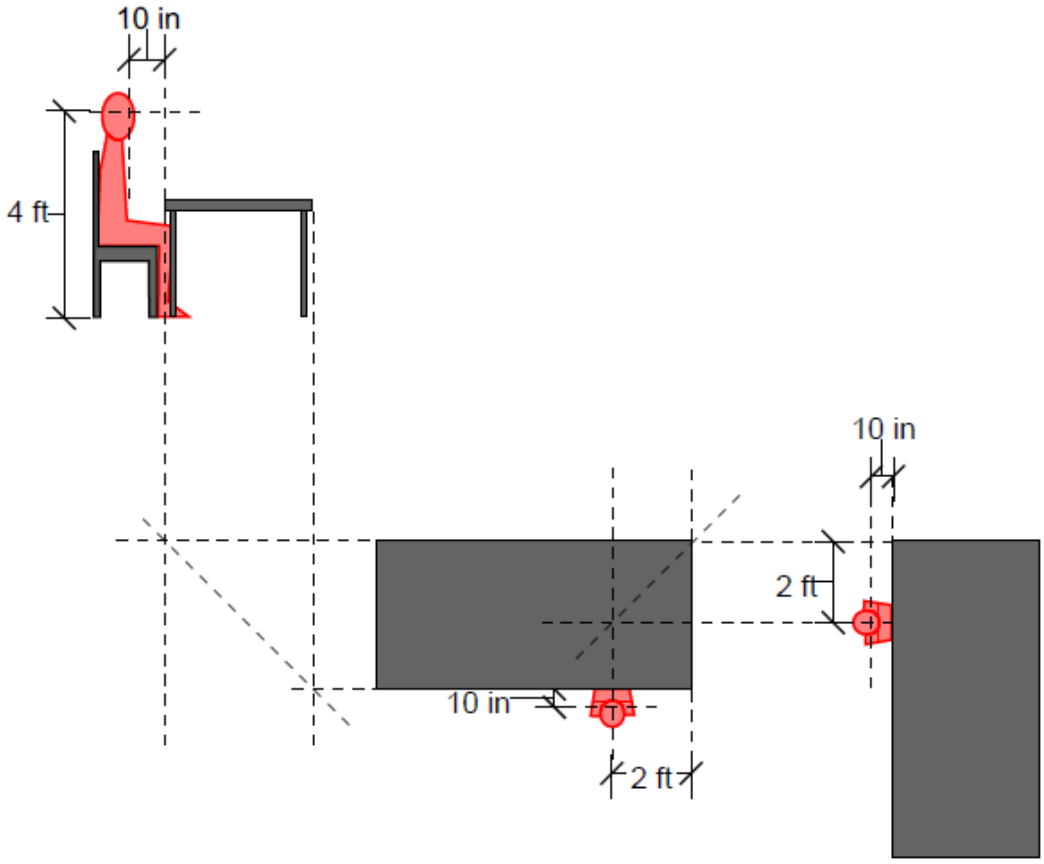

Fig. 3.1: Arrangement of desks and camera positions that will most closely mimic a typical person seated at the desks.

Fig. 3.2: Desk with camera pointed towards south-facing glazing

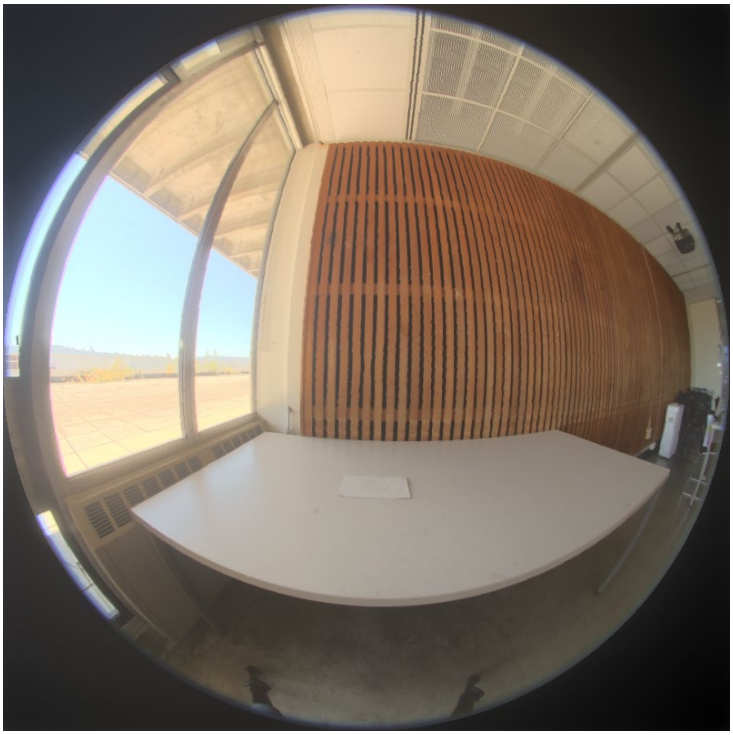

Fig. 3.3: Desk with camera pointed towards the wall and perpendicular to glazing

Directly above GLD 440 is a spectrophotometer on the Gould Hall roof taking horizontal sky spectra measurements. Not too far away from Gould Hall is the Atmospheric Sciences-Geophysics Building, where there is a pyranometer on the rooftop recording solar irradiation measurements (Fig 3.4). The outdoor measurements are collected simultaneously, the data matching the timestamp of indoor measurements are utilized for input and analyses.

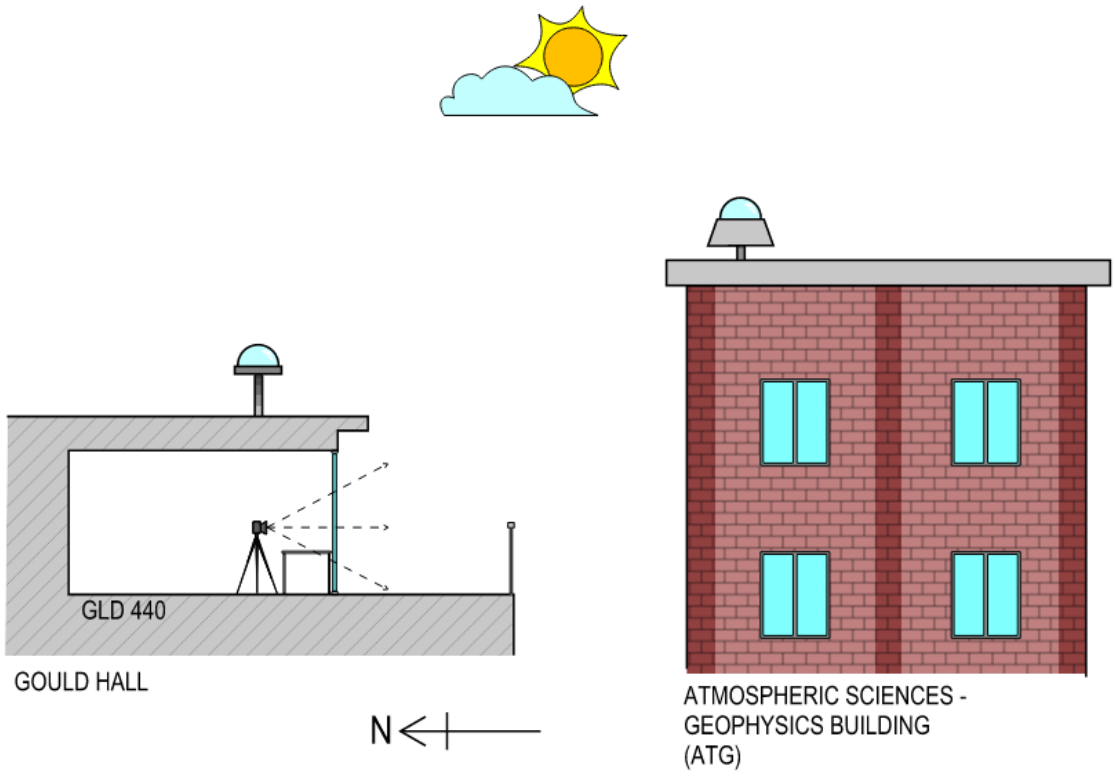

Fig. 3.4: Setting for field data collection

3.2 – Field Measurements

3.2.1 – HDR

The data collection process utilizes the photography-based data collection method (Inanici 2005, Jung and Inanici 2019). Using a DSLR camera and the software Photosphere, the Low Dynamic Range (LDR) images captured for each scene is combined into a single HDR image. The HDR images are post-processeed for vignetting correction and overflow correction in pre-written batch files and the software HDRscope to obtain the CIE trichromatic (XYZ) data as well as the photopic and melanopic luminance of these HDR images. These values are compared to field-measured values of the photopic lux and the calculated Equivalent Melanopic Lux (EML).

On or around the 21st of each month beginning May 2022 to April 2023, field data is collected in the form of HDR images; physical measurements via a luminance meter for fine calibrating the photopic luminance in a grey patch in the HDR image, and a spectrophotometer for photopic illuminance and spectra at the camera lens. A fisheye lens with a 180° angular field of view (Sigma 8mm F3.5 EX DG) is used to capture the human field of view in the resulting HDR photos (Fig. 3.2, 3.3). A set of photos is taken at each desk position at one-hour intervals from 9am to 5pm (4pm during the winter months) similar to a typical office's hours of operation and where sufficient daylight is present for visual tasks. Using the DSLR camera's (Canon 5D) manual exposure mode, multiple photographs are taken through increments of shutter speeds from 4s to 1/8000s with a fixed aperture size (f/11.0) to capture the point in time lighting condition across a range of exposure levels. A grey card is placed on the desk that will be used for field luminance calibration during the HDR image calibration phase. Field luminance is

measured via a Konica Minolta LS-110 luminance meter pointed towards the center of the grey card from the position of the DSLR camera. A Konica Minolta CL-70F spectrophotometer is placed level with the camera lens and facing the same direction, and measurements are taken directly after each HDR image set is taken so that as little time as possible has passed since the images were taken. This is to ensure that sun movement and changes in cloud conditions are minimized between camera and spectrophotometer measurements. The only light source was daylight, electric lighting was turned off.

Global horizontal daylight spectra is collected via a sensor atop Gould Hall's roof, almost directly above GLD 440. The global horizontal irradiance is collected at the rooftop of the University of Washington Atmospheric-Geophysics (ATG) building.

At each data collection point, multiple exposure photographs were taken within a minute. Irradiance data from the ATG was checked for significant variations during data capture as a result of cloud movements. Data with such variations are flagged as erroneous.

A set of low dynamic range (LDR) photographs consists of about 10 raw JPEG format photos taken in various exposures as quickly as possible at the first minute of each hour between the hours of 9am to 5pm. The photos are taken at different exposures to capture the full extent of luminance in the field. These LDR photos are then combined in the program Photosphere[14] to create an HDR image. Prior to this, Photosphere creates a camera response curve that is a computational calibration process that relates the pixel's RGB values to real world luminance values. The camera response curve is camera-specific and is used by Photosphere to create the HDR images, which can then be stored in the computer as a Radiance RGBE (.hdr file extension)

[14] http://anyhere.com/

image format. The luminance value captured by the luminance meter pointed at the center of the grey card is used to calibrate the HDR image, where the luminance value is set on the corresponding grey card in the HDR image. This adjusts the entire HDR image to a constant (k) to show the correct luminance (L) cd/m^2 value in each pixel extending over the luminance span of the human visual system (Inanici 2006, Jakubiec et al. 2016) and creates an HDR image that contains useable information for the post-processing step to obtain the CIE trichromatic (XYZ) data as well as the photopic illuminance (Equation 3.1) and equivalent melanopic lux (EML) (Equation 3.2) of the scene (Jung and Inanici 2019).

$$L = 179 * (0.2127 * R + 0.7151 * G + 0.0722 * B) \ \text{(cd/m}^2\text{)} \qquad \text{(Equation 3.1)}$$

In order to obtain photopic illuminance and EML value from the HDR image, there are a few steps that occur during post-processing to correct for geometric aberrations and color discrepancies.

First, the images undergo correction for geometric aberrations to account for the difference in the projection of the fish-eye lens on the DSLR camera and the spectrophotometer. A circular fish-eye image can be taken when attached to a full frame camera. The Sigma 8mm F3.5 EX DG fish-eye lens used in the data capture has a 180° angle of view both horizontally and vertically, with an equisolid projection as listed by the manufacturer. This means that periphery objects are compressed, with more compression as distance from the center increases. On the other hand, an equidistant projection maintains angular distances. The lens exhibit aberrations from an equisolid angle. Jakubiec et. al.'s (2016) work has yielded a correction curve to achieve the ideal equidistant projection. Jung's (2017) thesis uses the very same camera and fish-eye lens with correction done according to the graph below. This correction is also applied

to HDR images created as part of this thesis project. The images were cropped to 800 x 800 pixels and exposure set to 1.

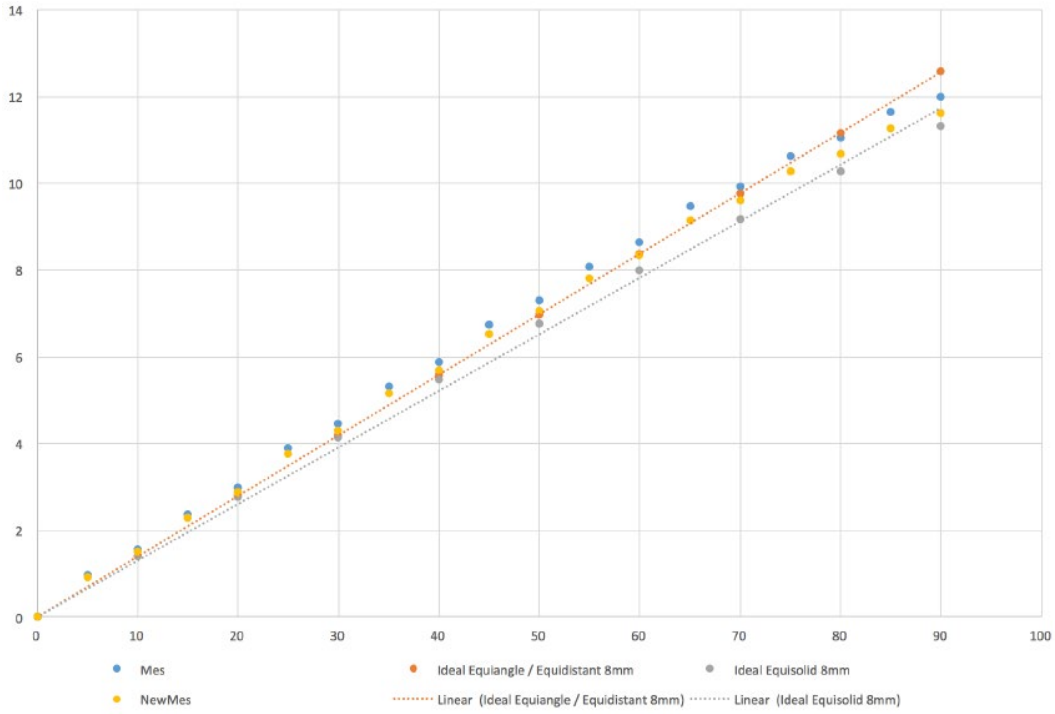

Fig. 3.5: the projection angle of the Sigma 8mm F3.5 EX DG lens (Inanici and Jakubiec 2016)

There is also a light fall off for pixels in the periphery of the fish-eye lens due to the physical structure of the lens. This light fall off was used to develop a digital filter to account for the loss in luminance of the pixels.

Fig. 3.6: Vignetting filter

Using regression analysis, Jung's (2019) study found that the typical camera overestimates the blue channel, and underestimates the red channel. This yielded a correction for the images captured based on the photopic measurements (CIE XYZ) to calibrate per-pixel RGB values such that they are similar to the CIE XYZ measurements from the spectrophotometer. The color corrected HDR image can then be used to obtain the per-pixel photopic and EML values.

Rather than yielding EML values of a small area, a HDR image allows for the capture of an entire scene to give EM.cd/m² values of each pixel and shows the circadian distribution of the scene. An EML value is given as a single number representing the entire fisheye image. The following equation was used to derive EML values in standard color space (sRGB):

$$EML_{sRGB} = 179 * (0.0013 * R + 0.3812 * G + 0.6175 * B) \quad \text{(Equation 3.2)}$$

3.2.2 – Gould Hall Roof Spectra

A spectrophotometer (Ocean Insight Flame VIS-NIR Spectrometer) atop the roof of Gould Hall (almost directly 1 floor above GLD 440) was installed to measure the spectral quality and variability of the sky in Seattle. This spectrophotometer takes hemispherical measurements of 180° both horizontally and vertically. It detects the intensity of each wavelength color present in the sky. The measurement results can be affected by a variety of factors, primarily location, date, time, CCT of skies, cloud cover. The instantaneous global horizontal spectral power distribution of daylight is used in the simulation step to create the sky model (more in section *3.3.3*).

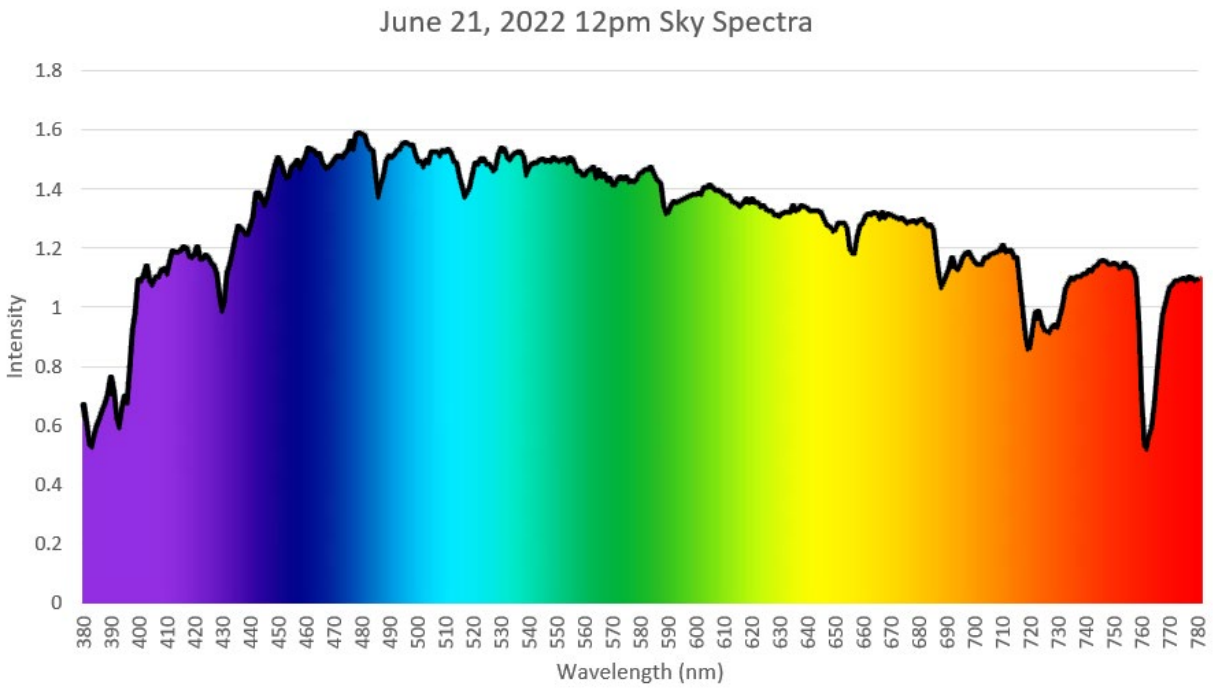

Fig. 3.7: Spectral Power Distribution (SPD) of daylight measured on June 21, 2022, at 12pm around the CBE area.

3.2.3 – Solar Radiation Measurements

Solar radiation is a measure of the power from the sun reaching a surface per unit area, and is measured in W/m². Global Horizontal Irradiance (GHI) is defined as the combination of direct and diffuse daylight hitting a horizontal surface. A pyranometer placed on a horizontal surface and pointed straight up measures the solar radiation in a 180° angle horizontally and vertically over a specific period of time. GHI is the sum of direct normal illuminance (DNI) cosined with the sun altitude and diffuse horizontal illuminance (DHI). DNI is defined as irradiance that is measured by a tracking surface that faces the sun, while DHI is irradiance that

reaches a horizontal surface but was not on direct path from the sun, but rather scattered by atmospheric particles along the way. The Perez Sky Diffuse Model (Perez et al. 1993) is used to split GHI into DNI and DHI. The DNI and DHI values are inputs to Perez all weather sky model (Perez et al. 1993) for simulating the luminance distribution patterns in the sky dome.

For this research, three sources of solar radiation measurements were considered – measurements taken by a weather station atop the Atmospheric Sciences-Geophysics (ATG) Building at UW, a weather station on the roof of Bertschi Middle School in Eastlake, and the National Oceanic and Atmospheric Administration (NOAA). The ATG data source was ultimately chosen as the necessary data points (dates and times that matched field data collection) were most consistently available, despite some missing data, and its geographic location is known and close to Gould Hall. When there was missing data for ATG, the Bertschi Middle School data is used as it came from the same source as ATG which most likely means similar calibration methods. In comparison, NOAA has several months of missing data for the year 2022, and no data for the year 2023 due to equipment faults.

3.3 – Simulations

LARK is a plug-in for the tool Grasshopper, which runs in the 3D modeling software Rhinoceros[15] (Rhino). A Rhino model of GLD 440 was created for the purpose of the LARK simulation, with the room furnishings modeled and placed at the position of their real-life counterparts during the field data collection. The visible spectral power distribution values of the surface materials are fed into LARK to create and assign the Radiance files to the corresponding

[15] https://www.rhino3d.com/

surfaces. Two sensor points in the model are set to the positions of the camera lens, and pointed towards the same direction as that of the camera during field measurement. LARK's 9-channel simulation workflow was used.

3.3.1 – Geometry

The geometry for use in simulation is a model of GLD 440 built in Rhinoceros 3D. Furnishings that will cause negligible changes in simulation results, such as chairs, were omitted. Only surrounding buildings visible in the captured HDR images are approximately modeled, and their RGB values are each set to 0.4. Trees are also omitted from the model. The model is only built slightly beyond the extents visible in the captured HDR images, with the exception of balcony floor and roof geometry as these can affect simulation results when light bounces off these surfaces.

3.3.2 – Material Definitions

As part of the LARK Spectral Lighting workflow, the spectral data of materials of room finishes and furnishings in the classroom GLD 440 have to be defined. As we did not have a spectro-reflectometer to measure in-situ, the GretagMacbeth ColorChecker chart (also known as a Macbeth chart) is used in combination with the Radiance macbethcal program to obtain the RGB values of materials that are used as input in the LARK simulation. The ColorChecker Chart was introduced in 1976 by McCamy, Marcus, and Davidson. The Macbeth chart contains 24 scientifically prepared colored squares that have a consistent color appearance under various lighting conditions. Note that while this technique allows us to measure in 3 channels, it is assumed that the 9 channel material definitions follow the 3-channel capture (R measurement is

applied to R1, R2, R3). Although this is a simplification, given that the measurement points are close to the window, the impact of interreflections are not significant on our measurement points.

The Macbeth chart is placed on the same plane as the surface of interest for measurement. An image is captured by the DSLR camera with the Macbeth chart and material surface present (Fig. 3.8), and another image is taken in the same camera position with the Macbeth chart removed (Fig. 3.9). The lighting condition is kept consistent between the two images.

The image with the Macbeth chart is cropped such that it only shows the Macbeth chart (Fig. 3.10). The image without the Macbeth chart is cropped to only contain a sample of the material surface of interest. In this case, it is the surface of the wood slat wall (Fig. 3.11). The Radiance macbethcal program is used to derive RGB values of the sample. A debug HDR file containing the cropped Macbeth chart image (Fig. 3.12) is created with the left side of the square representing the color under the lighting condition in the room when the image was taken, and the right side of the square represents what the color should look like under an equal energy white light source, as the Macbeth chart colors are standardized and known. The middle square is a corrected color that equals the difference between the equal energy white light source and the ambient lighting where the images were taken. Another calibration file then takes the corrected Macbeth chart to determine the dominant light conditions within the room where the image was taken and its difference from an equal energy white light source. The file generated is then used to color correct the material sample image to create a version of the sample image color corrected with its true RGB values (Fig 3.13). LARK is able to take these RGB values to generate Radiance files for use in the simulation (Fig 3.14 and Fig 3.15).

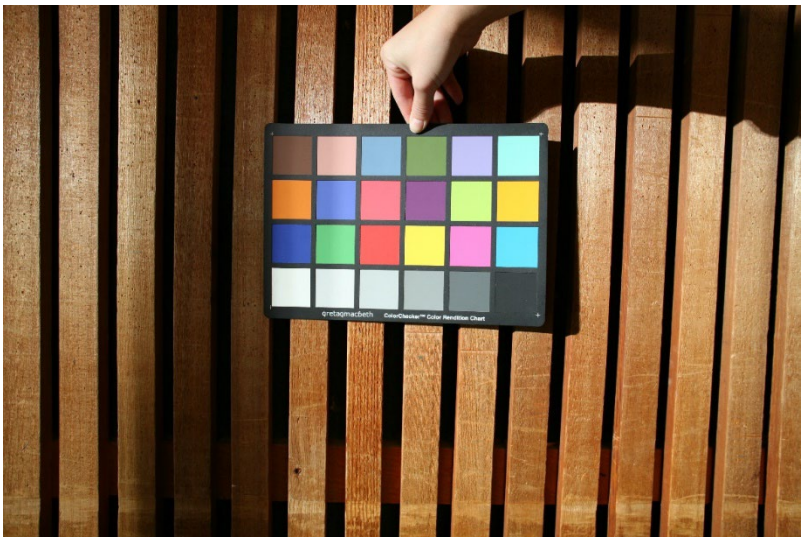

Fig. 3.8: Wood slat wall with Macbeth chart

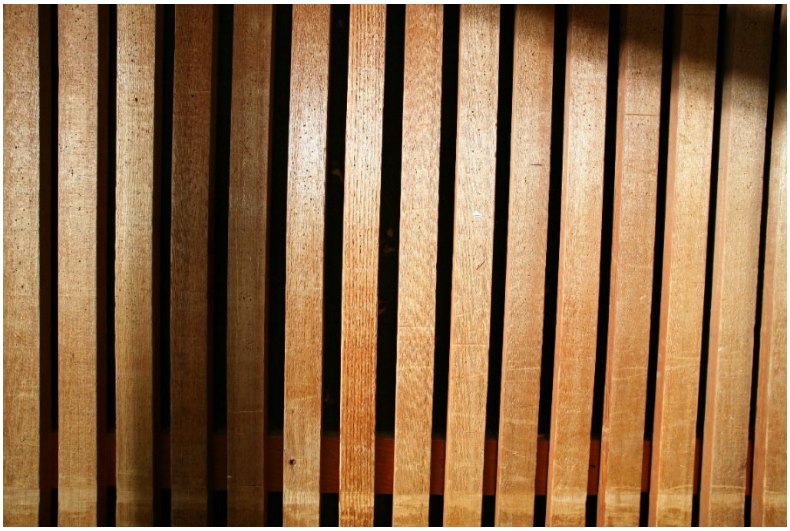

Fig. 3.9: Wood slat wall under same lighting condition as Fig 3a and without the Macbeth chart

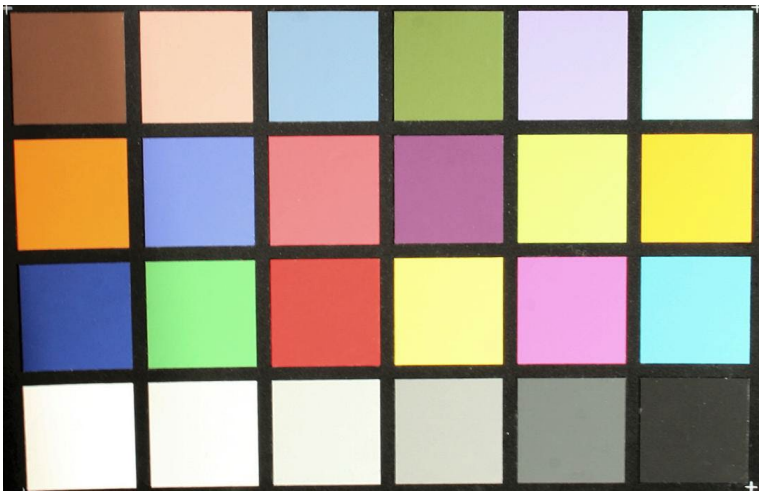

Fig. 3.10: Image of Macbeth chart under the lighting condition present at the time of image capture

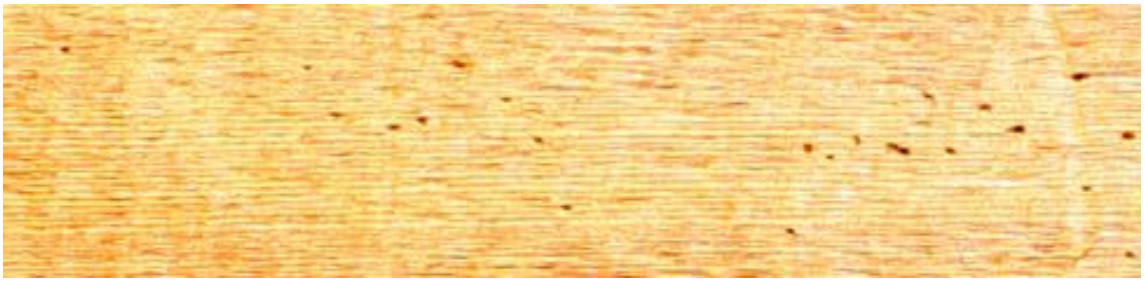

Fig. 3.11: Image sample of wood slat wall to be color corrected

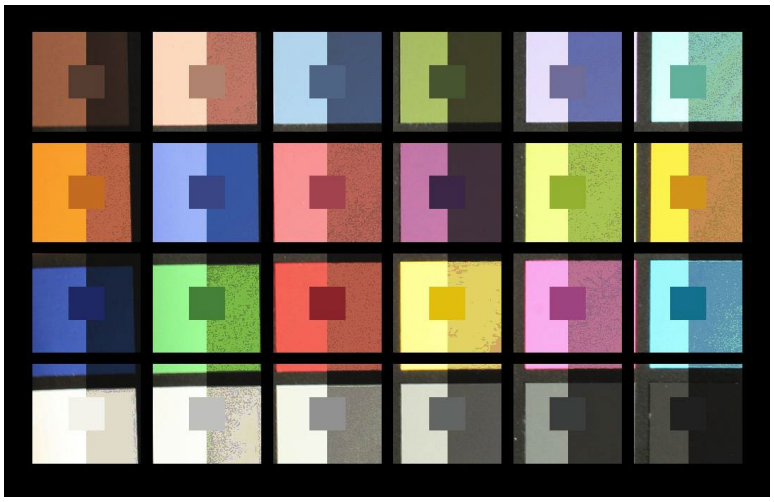

Fig. 3.12: Debug Macbeth chart HDR image

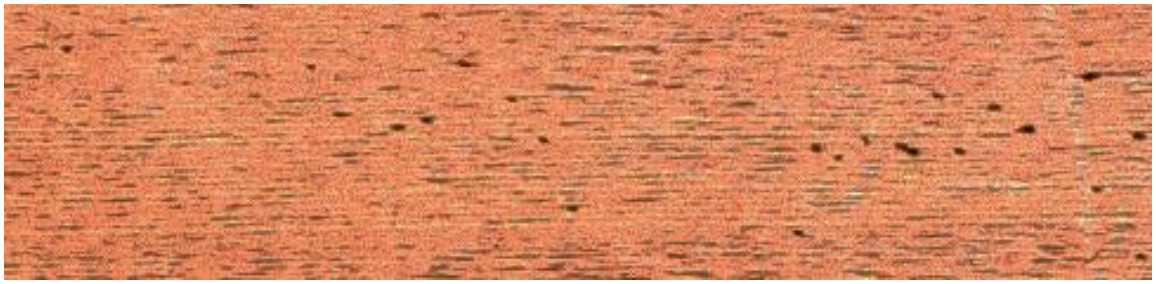

Fig. 3.13: Color calibrated wood slat wall material

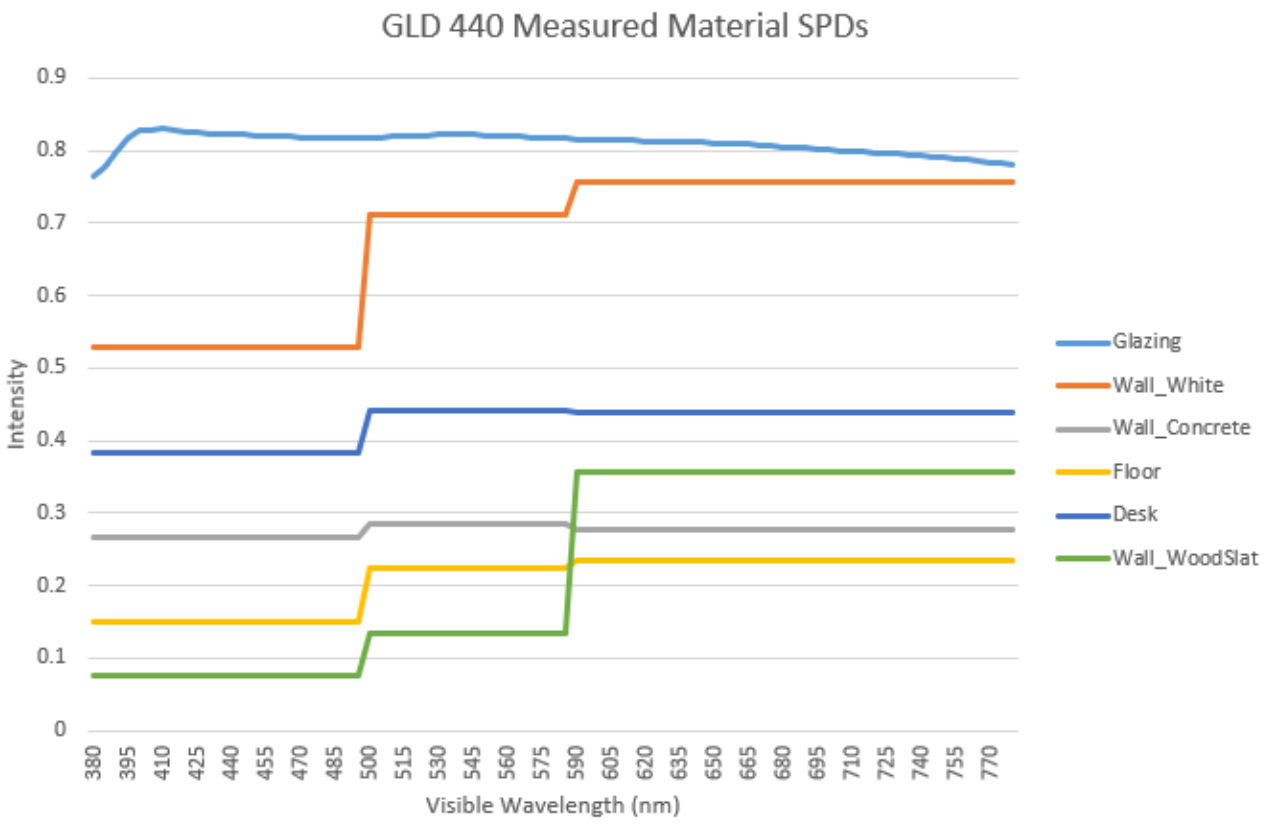

Fig. 3.14: SPDs of measured surface materials in GLD 440

	R	G	B
Blinds	0.732	0.764	0.623
Desk	0.438	0.442	0.384
Door	0.035	0.033	0.037
Floor	0.234	0.224	0.15
Wall_White	0.756	0.713	0.529
Wall_Concrete	0.278	0.284	0.267
Wall_WoodSlat	0.356	0.134	0.077
Wall_WoodSlat_Black	0.005	0.005	0.006
Other Buildings	0.4	0.4	0.4

Fig. 3.15: Table of RGB values fed into LARK for each material surface type used in simulation

3.3.3 – Sky Parameters

The parameters used to build the LARK simulation sky model are date, time, DNI, DHI, and spectra. These parameter values (except spectra) are shown in Table 3.1. The sky spectra used are represented in Figures 3.16 through 3.27. As field data collection takes into account daylight savings time, the time parameter is adjusted accordingly.

Table 3.1 – Measured Sky Irradiances

Date	Time	GHI	DNI	DHI
5/21	8:00	623.3	776	191
	9:00	243.9	14	234
	10:00	316.7	18	302
	11:00	849.8	730	220
	12:00	936	820	209
	13:00	896.6	822	181
	14:00	807.6	761	191
	15:00	679	690	188
	16:00	519.8	592	174
6/21	8:15	620	836	107
	9:00	614.1	532	236
	10:00	949.9	839	266
	11:00	942.8	820	218
	12:00	864.7	655	267
	13:00	827.1	605	283
	14:00	902.1	813	216
	15:00	702.8	658	208
	16:00	346.7	121	271
6/25	8:00	639	773	194
	9:00	717.6	823	134
	10:00	886.2	814	223
	11:00	939.6	819	216
	12:00	946.5	814	204
	13:00	906.1	779	205
	14:00	817.1	706	221
	15:00	695.5	636	216

	16:00	541.7	540	202
7/30	8:00	535.7	740	153
	9:00	681.9	767	178
	10:00	788.8	842	142
	11:00	854	800	180
	12:00	866	743	216
	13:00	832.8	692	235
	14:00	754.3	635	239
	15:00	636.5	568	228
	16:00	487.1	475	205
8/24	8:00	358.1	466	151
	9:00	583.3	793	118
	10:00	689.1	755	161
	11:00	753	717	198
	12:00	763.8	663	230
	13:00	723.4	600	249
	14:00	640.8	536	248
	15:00	519	455	230
	16:00	375	362	193
9/21	8:00	250.3	370	126
	9:00	399.3	495	163
	10:00	512	541	194
	11:00	613	643	191
	12:00	635.9	638	201
	13:00	599	593	208
	14:00	533.5	586	185
	15:00	448.3	640	136
	16:00	178.7	101	143
11/19	9:00	231.1	973	23
	10:00	294	681	82
	11:00	371.4	781	81
	12:00	371.9	690	103
	13:00	319.6	555	118
	14:00	240.1	452	106
	15:00	107.5	148	79
	16:00	25.4	0	25
12/21	9:00	64.4	85	53
	10:00	169.2	322	93
	11:00	184.3	185	128
	12:00	251.1	377	128
	13:00	360.6	763	124

	14:00	140.9	136	106
	15:00	68.1	46	61
	16:00	26.1	0	26
1/21	9:00	8.3	0	8
	10:00	296.3	739	98
	11:00	33.2	0	33
	12:00	44.6	0	45
	13:00	25.2	0	25
	14:00	191.5	163	139
	15:00	50	3	49
	16:00	24.4	4	24
2/26	9:00	84.5	7	82
	10:00	122.9	8	119
	11:00	515.5	806	108
	12:00	663.5	822	216
	13:00	255.9	48	230
	14:00	280.8	135	215
	15:00	347.1	552	129
	16:00	227.9	524	87
	17:00	98.7	566	34
4/1	8:00	50.5	0	50
	9:00	218.4	30	203
	10:00	317.3	78	270
	11:00	298.1	13	289
	12:00	349.6	43	319
	13:00	817.8	829	228
4/30	8:00	91.3	2	91
	9:00	143.9	3	142
	10:00	171.8	3	169
	11:00	203.6	4	200
	12:00	229.7	6	225
	13:00	313.5	16	300
	14:00	238.9	9	232
	15:00	203.2	9	197
	16:00	234.5	38	215

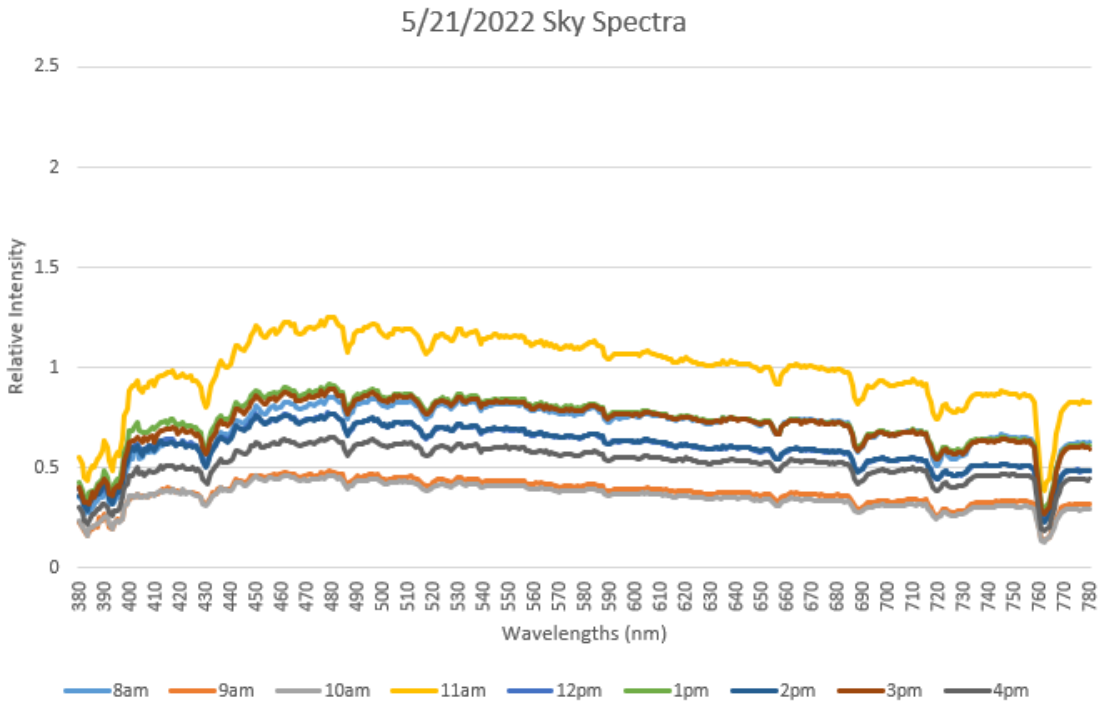

Fig. 3.16: Hourly sky spectra from 8am to 4pm PST on 5/21/2022

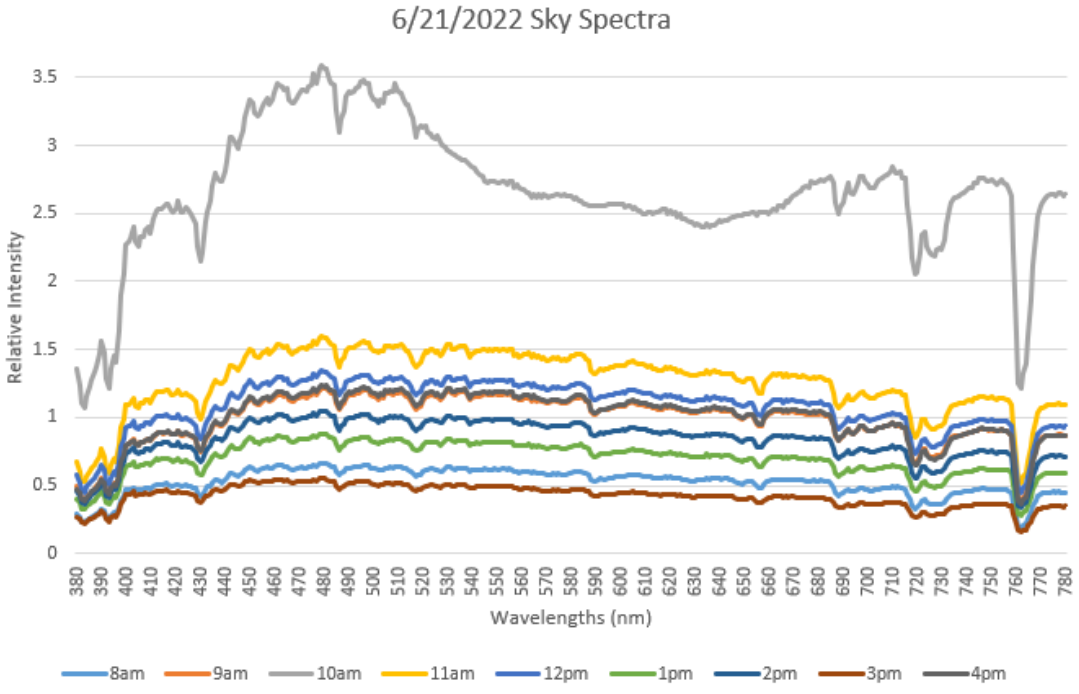

Fig. 3.17: Hourly sky spectra from 8am to 4pm PST on 6/21/2022

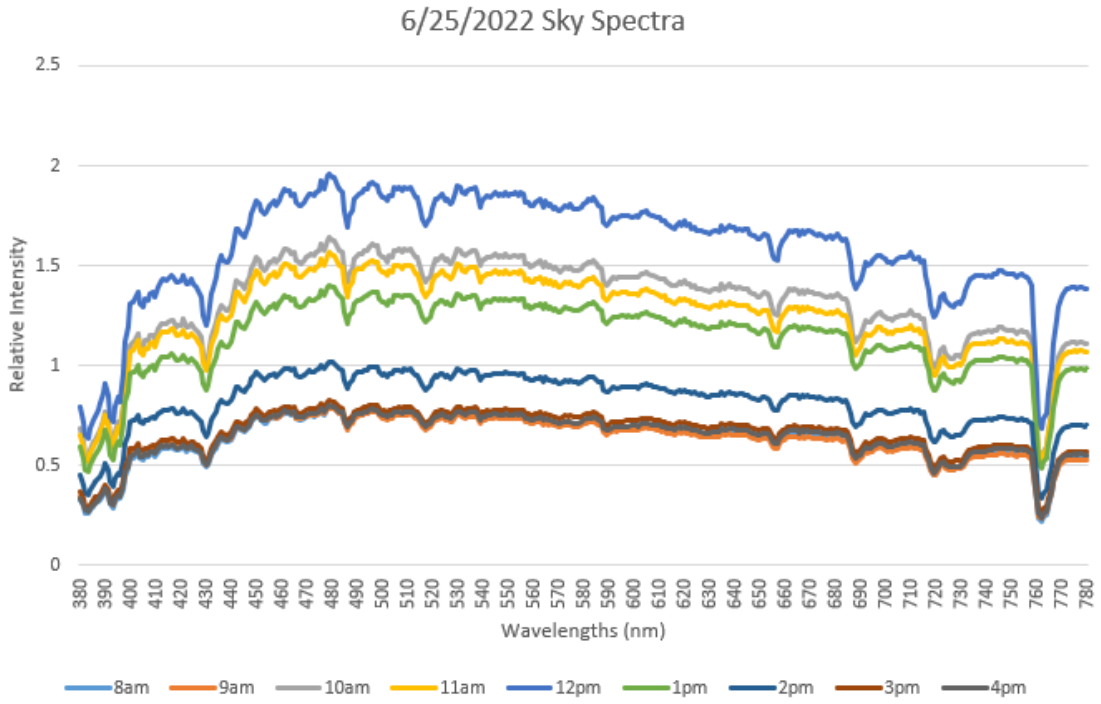

Fig. 3.18: Hourly sky spectra from 8am to 4pm PST on 6/25/2022

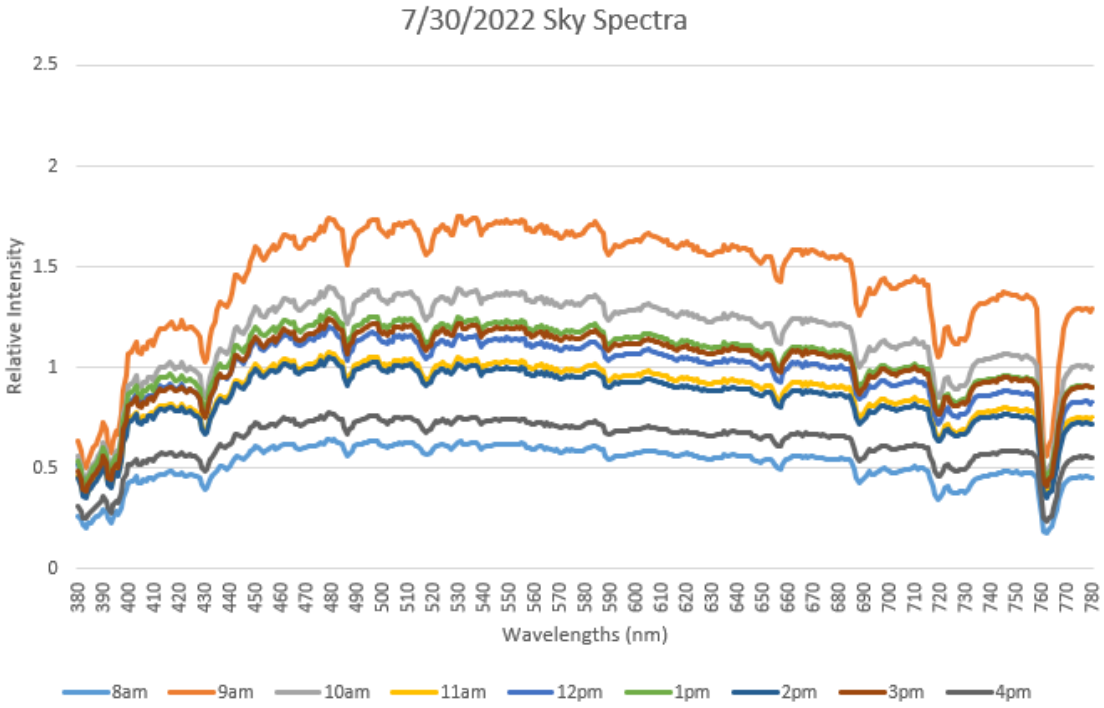

Fig. 3.19: Hourly sky spectra from 8am to 4pm PST on 7/30/2022

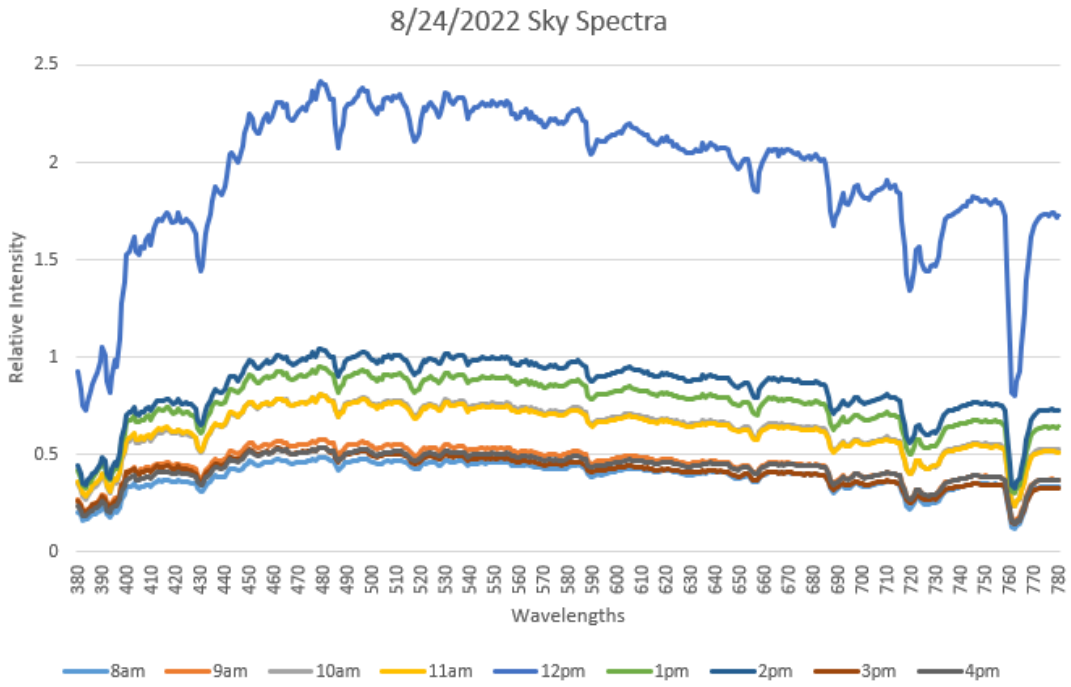

Fig. 3.20: Hourly sky spectra from 8am to 4pm PST on 8/24/2022

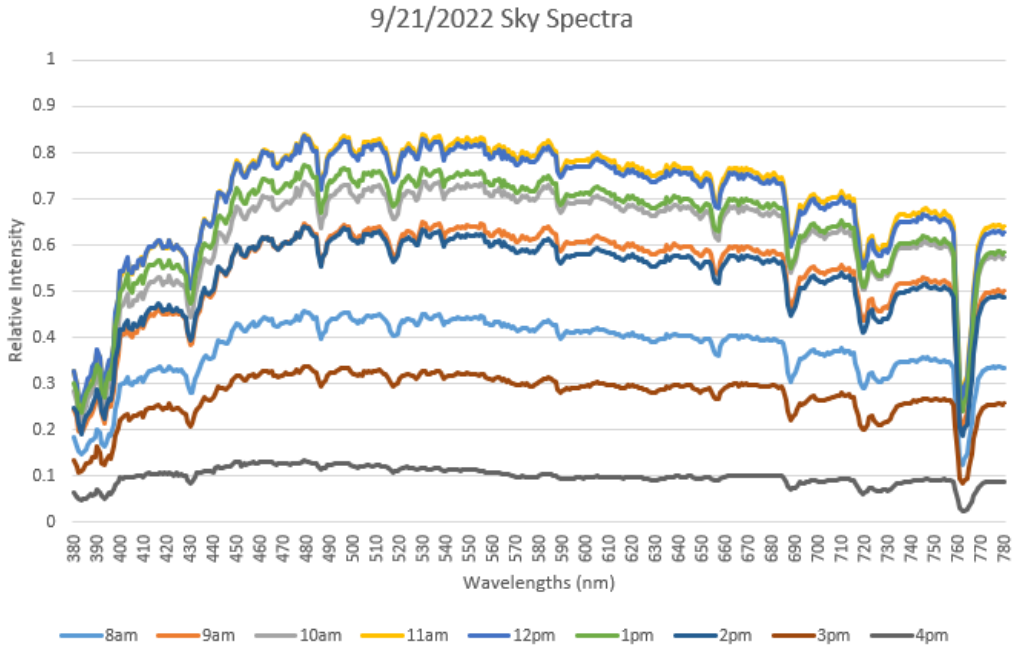

Fig. 3.21: Hourly sky spectra from 8am to 4pm PST on 9/21/2022

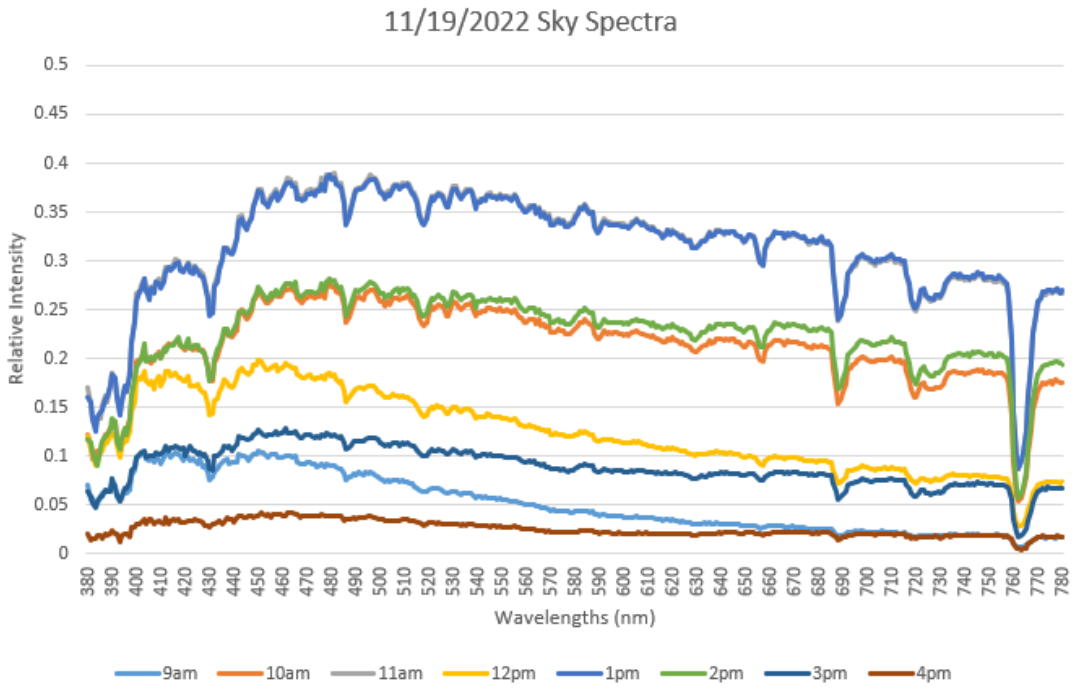

Fig. 3.22: Hourly sky spectra from 9am to 4pm PST on 11/19/2022

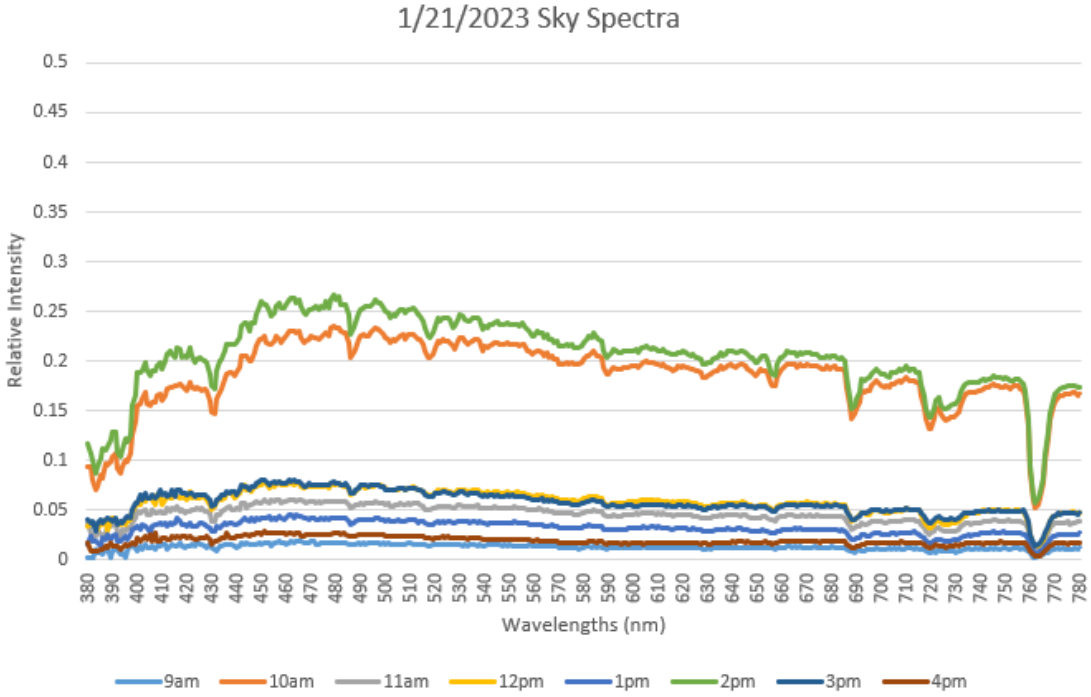

Fig. 3.23: Hourly sky spectra from 9am to 4pm PST on 1/21/2023

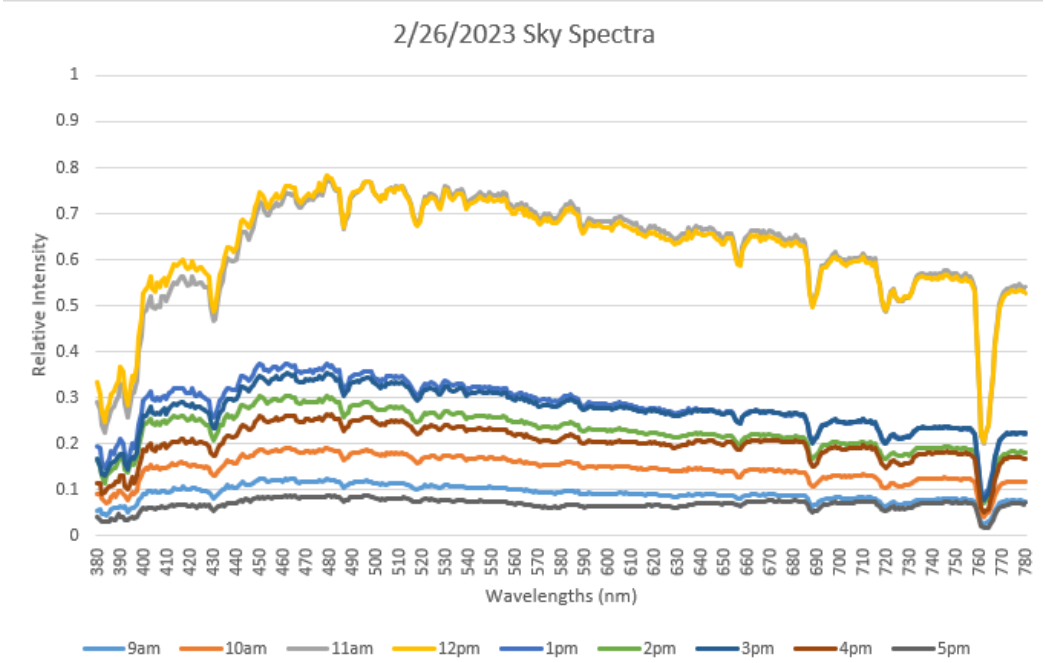

Fig. 3.24: Hourly sky spectra from 9am to 5pm PST on 2/26/2023

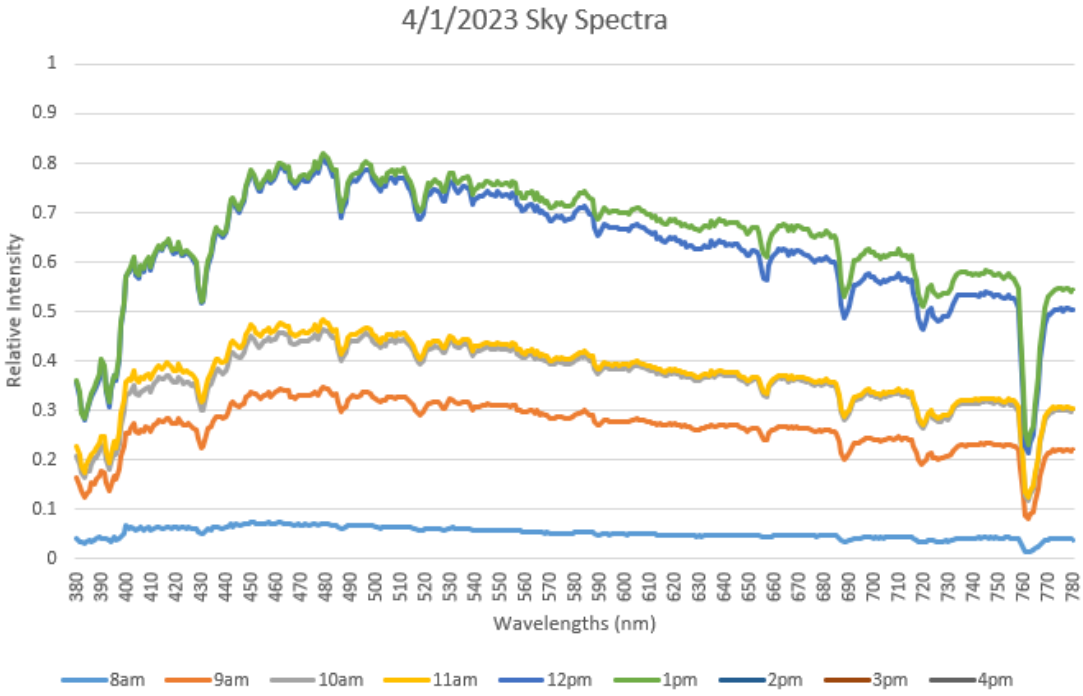

Fig. 3.25: Hourly sky spectra from 8am to 4pm PST on 4/1/2023

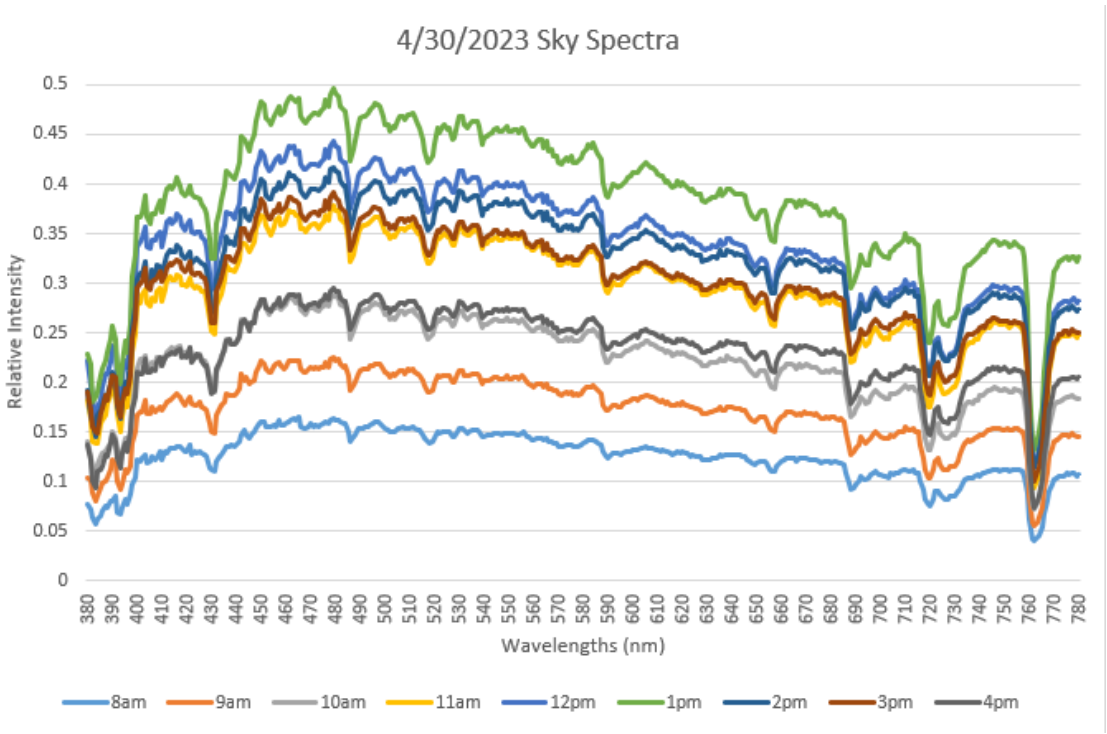

Fig. 3.26: Hourly sky spectra from 8am to 4pm PST on 4/1/2023

Chapter 4 – Results and Discussion

All field data collection measurements are studied to evaluate the variability of intensity, spectra, and CCT throughout the year. Simulation results are also studied and compared to measurement values.

4.1 – Measurements

4.1.1 – Overall Analysis

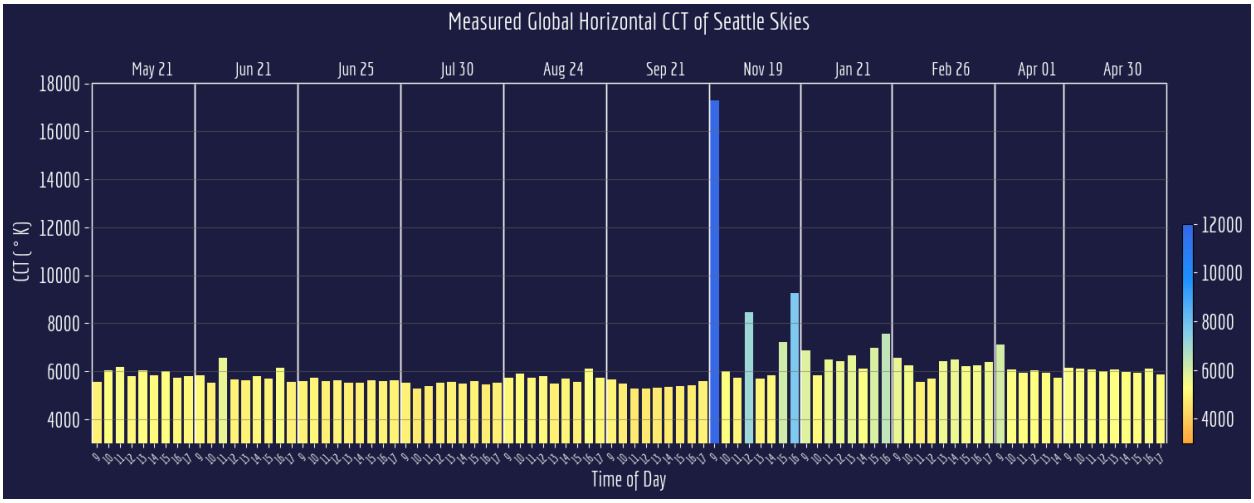

Fig. 4.1: Yearlong measurement of outdoor global horizontal CCTs

The global horizontal CCTs in Fig 4.1 were calculated from the global horizontal sky spectra measurements (Fig 3.16 to 3.26) using the Ohno method (Ohno 2013) through the web-based tool Luox[16]. The CCTs throughout the year tend to lie in the 5500K to 6500K range, although the peak CCTs in November 19 aligns with the extremely high LARK simulation

[16] https://luox.app/

results in Fig 4.27. These outdoor CCTs in Fig 4.1 also differ from the measured indoor CCTs in Fig 4.2 and 4.4.

In total, there are 223 usable measurement data points with measured CCTs, photopic lux and EML values, as well as the accompanying HDR image sets. Fig 4.1 illustrates yearlong measurements when the occupant is sitting at a desk facing the window. The solid green line represents all the photopic lux values measured, while the dotted blue line represents the EML values calculated from measured XYZ spectra-photometric data by the handheld spectrophotometer. The primary vertical axis demonstrates photopic and melanopic lux values. The vertical bars represent CCT; they are colored based on their corresponding CCT, and their heights are represented by the secondary vertical axis (on the right).

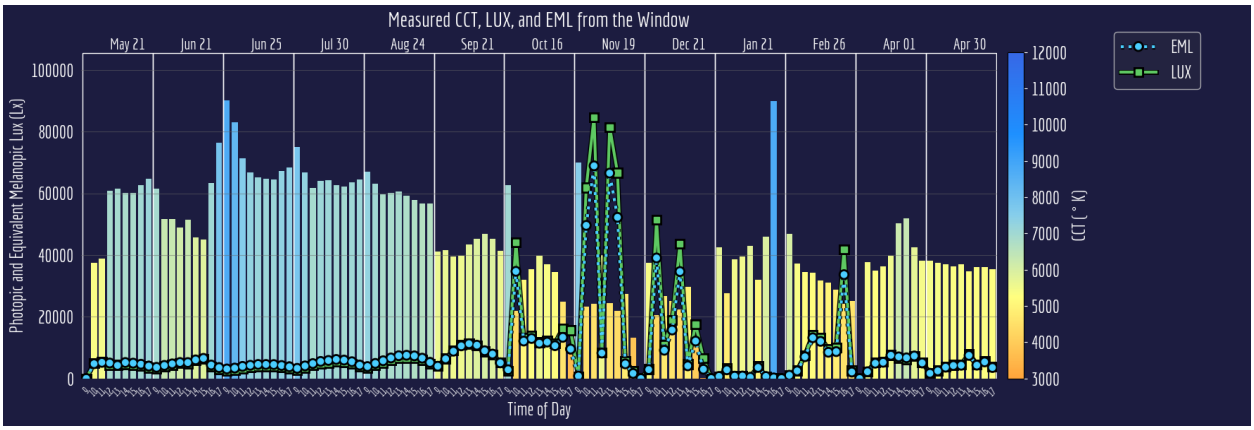

Fig. 4.2: Yearlong measurements of CCT, photopic lux, and EML facing the window

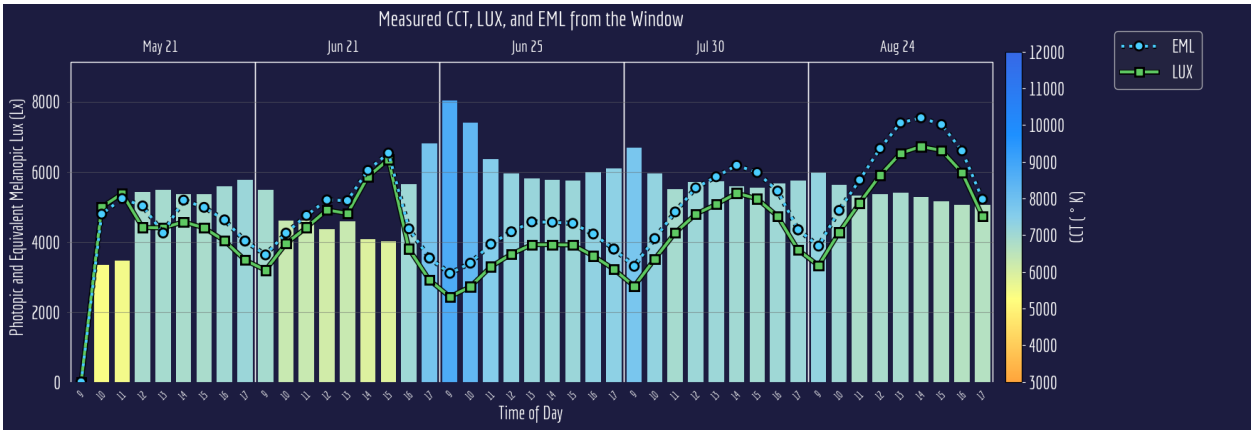

Fig. 4.3: Zoomed in view of May to August for measurements facing the window

Fig 4.2 shows that CCT of the sky is high in summer months at around 7000K to 9000K. The CCT and lux values measured are also more consistent, as the skies are mostly clear or have minimal clouds. The sun's altitude is higher, and most of the roof overhang outside the classroom prevents direct sunlight from entering. Fig 4.3 shows that the measured EML tends to be higher than the measured photopic lux values. This is mainly due to the higher CCT, which drives our circadian stimulus as there is a higher presence of blue-enriched daylight.

In the months of October to February, CCT is lower at around 5000K to 6000K, and we see a lot more fluctuations in lux. This is due to the presence of cloud cover resulting in the low measurement points. Moreover, the sun's position is lower, which means that when not covered by clouds, sunlight can enter the classroom and fall directly onto the spectrophotometer sensor, resulting in extremely high lux measurements. In the case of extremely high photopic lux, there is more than enough circadian stimulus received, but it also causes visual discomfort through glare. The measured EML tends to be lower than photopic lux during these months, due to the lower CCTs.

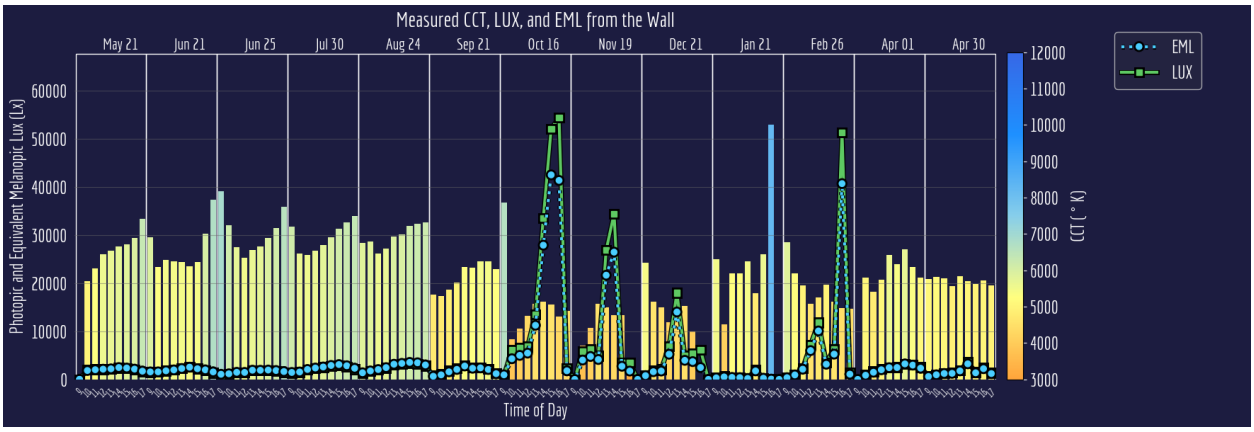

Fig. 4.4: Yearlong measurements of CCT, photopic lux, and EML facing the wall

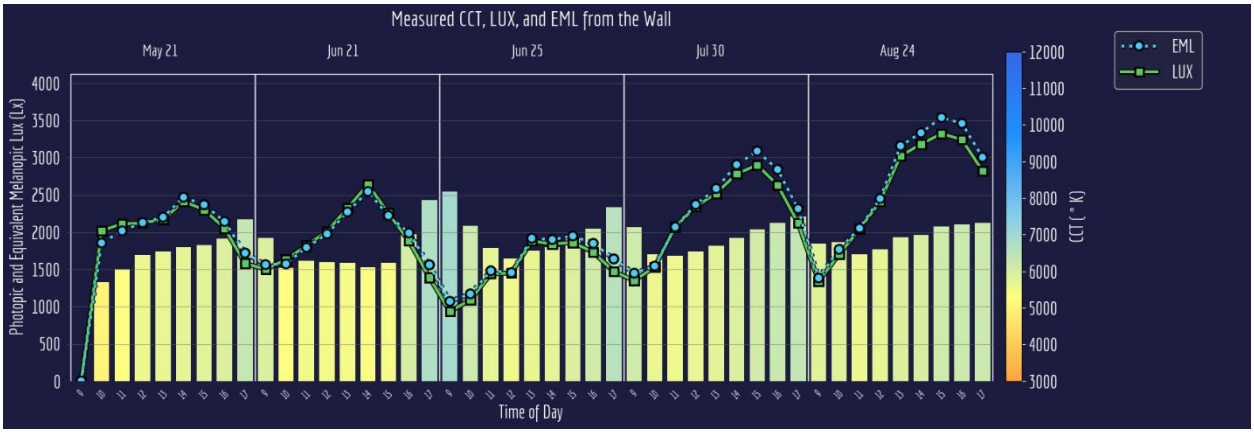

Fig. 4.5: Zoomed in view of May to August of measurements facing the wall

Fig 4.4 shows the measured CCT, lux, and EML facing the wood slat wall, perpendicular to the window. There are visible differences in measured values when compared to measurements facing the window (Fig 4.3).

The spectral qualities of the wood slat wall surface causes the measured CCT values to be lower than that facing the window during the summer months. However, during the other months, the CCTs measured facing the window and facing the wall are about the same, which shows that material surface spectral qualities affect the sky CCTs only to a certain extent. It may also be due to the wood slat wall having similar spectral properties to that of lower CCT skies.

Finally, as the sensor is not receiving direct exposure to daylight, the measurements are less varied through time each day, as they are not directly affected by the exterior sky conditions.

Fig 4.5 shows the measurements from May to August. As the spectrophotometer is not facing the window, photopic lux measured is lower throughout. Moreover the measured CCT are lower, at around 6000K to 8000K. As a result of both of these factors, the measured EML tends to be similar to photopic lux, and only slightly higher than photopic lux at a few measurement points. This contrasts with the EML measurement at the window, where it is consistently significantly higher than measured photopic lux during these months.

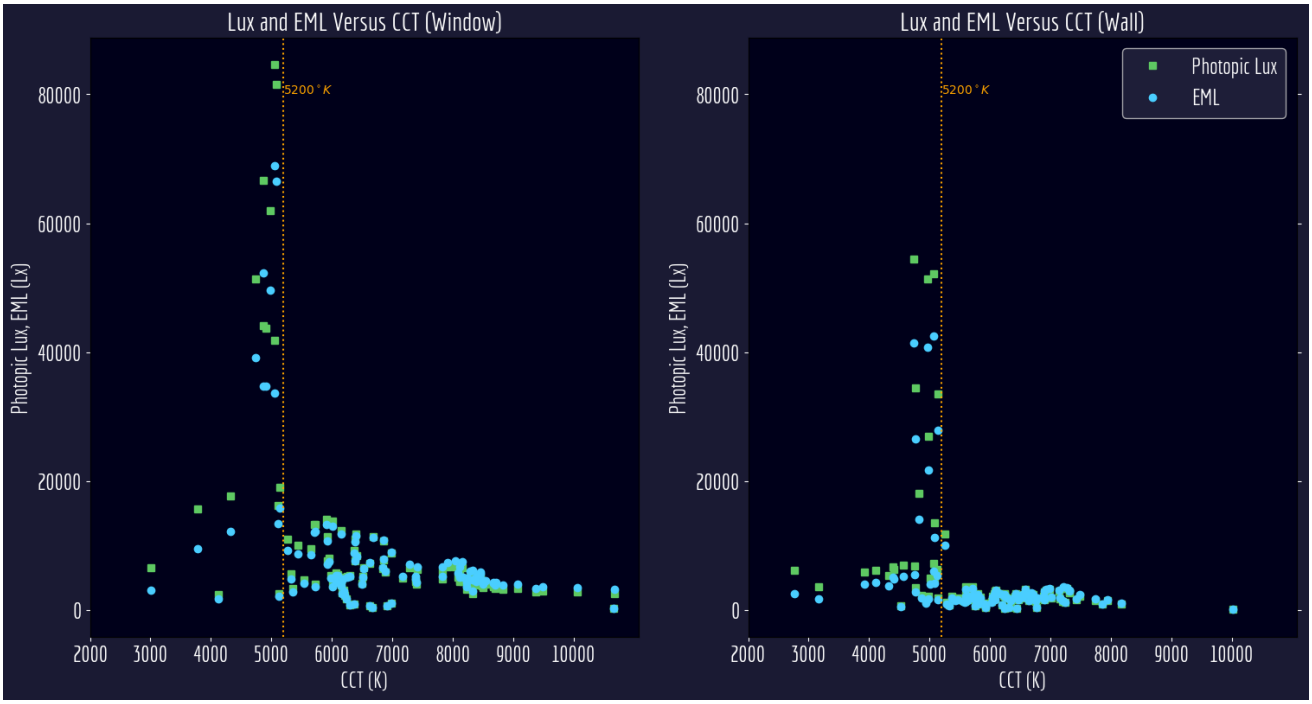

Fig. 4.6: Lux and EML measurements plotted against CCT for facing the window (left) and facing the wall (right)

The measured photopic lux and EML values are plotted against CCT in separate scatterplot graphs for measurements facing the window (Fig 4.6 left) and facing the wall (Fig 4.6 right). The points show that there are lux values measured across a wide range of CCTs, but the highest values tend to occur around 5200K. This is due to the sun having a color temperature of about 5200K – 5400K, and sunlight is hitting the sensor on the handheld spectrophotometer directly, completely overpowering the CCT of the sky. These extremely high values also tend to happen when the sun altitude is lower, which shows that shading strategies are important as these lux values cause extreme glare.

4.1.2 – Daily Variations

Figures 4.7 to 4.20 illustrate the daily measurements. While Fig. 4.2 shows all measured values throughout the year, viewing the measurements in a day-to-day view allows us to identify trends on an hourly basis and understand the changing sky conditions within a single day. Each clock represents the measured lux and EML values, and the slice of the hours are colored to correspond to the CCTs measured for that time of the day. In the summer months of May to August (Fig 4.7 to 4.9 left), the photopic lux and EML values measured were more consistent throughout the day, and EMLs are higher than photopic lux. In Figures 4.10 to 4.20, we begin to see more varied measurement values, as well as lower CCTs due to the presence of cloud cover.

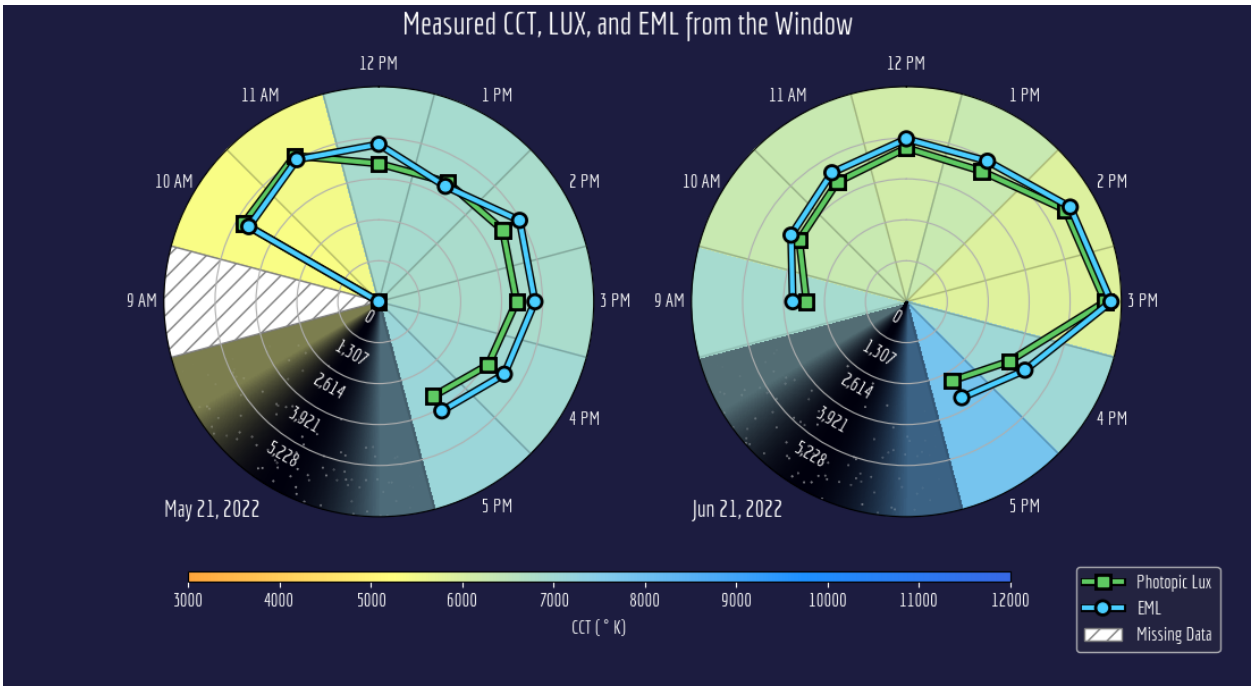

Fig. 4.7: Facing window – May 21, 2022, and June 21, 2022

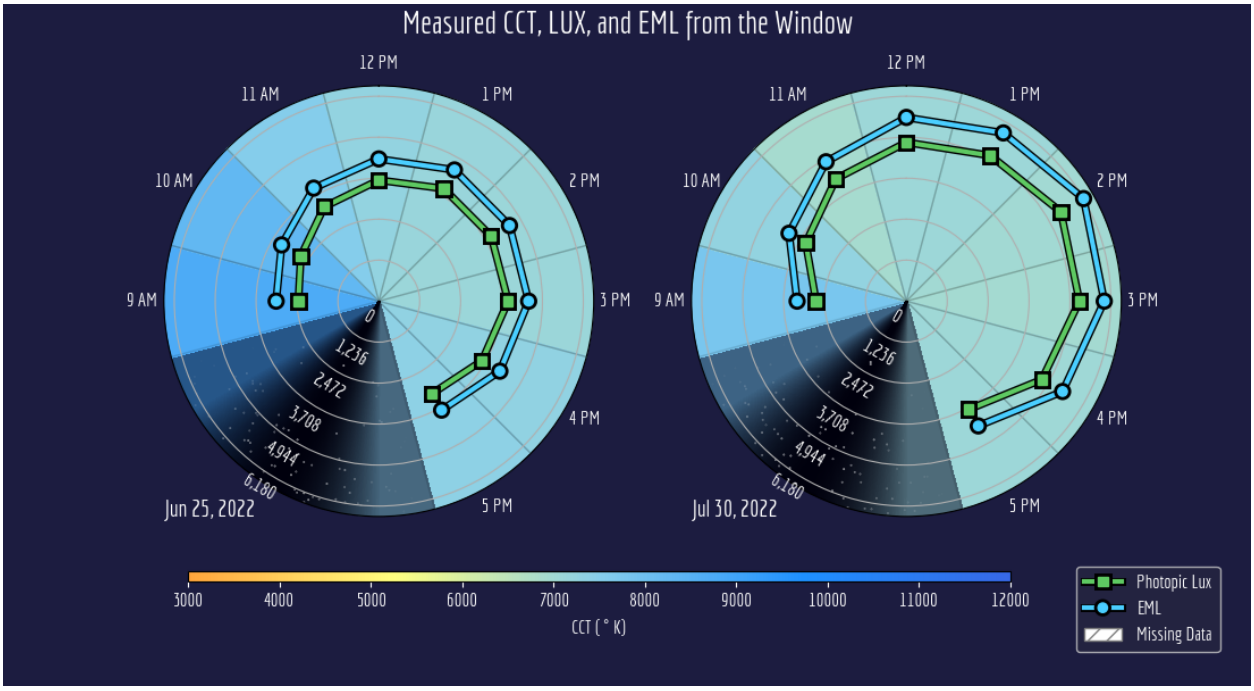

Fig. 4.8: Facing window – June 25, 2022, and July 30, 2022

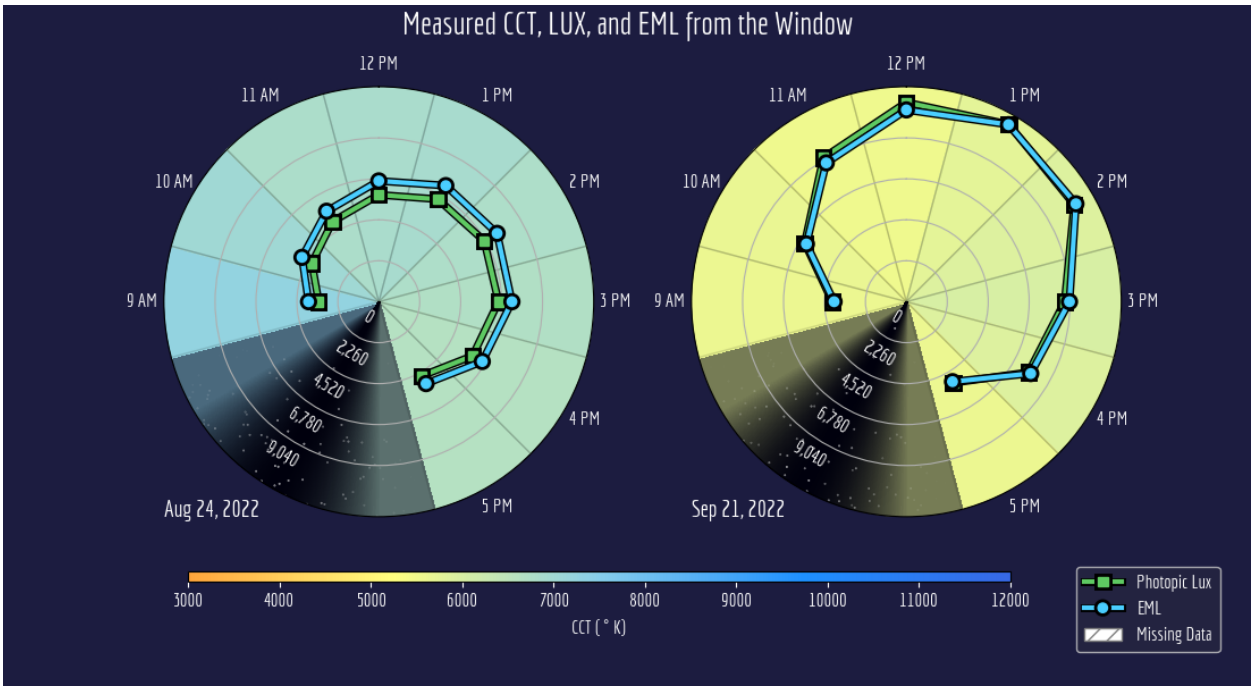

Fig. 4.9: Facing window – August 24, 2022, and September 21, 2022

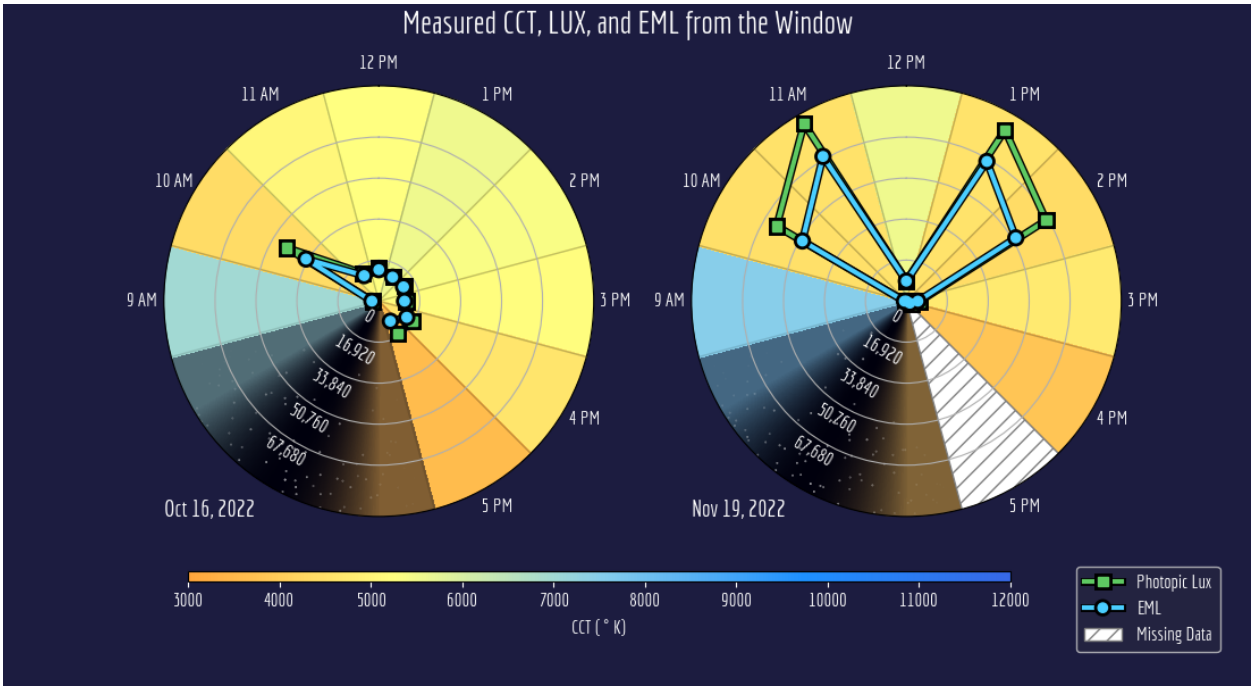

Fig. 4.10: Facing window – October 16, 2022, and November 19, 2022

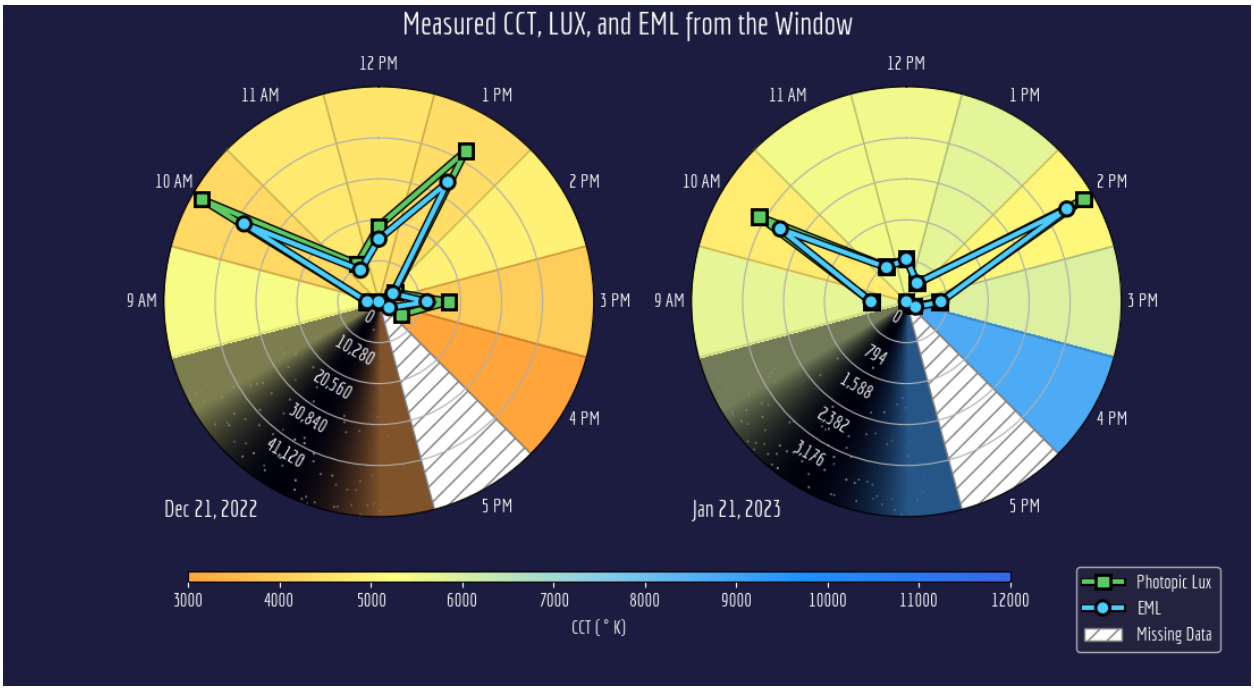

Fig. 4.11: Facing window – December 21, 2022, and January 21, 2023

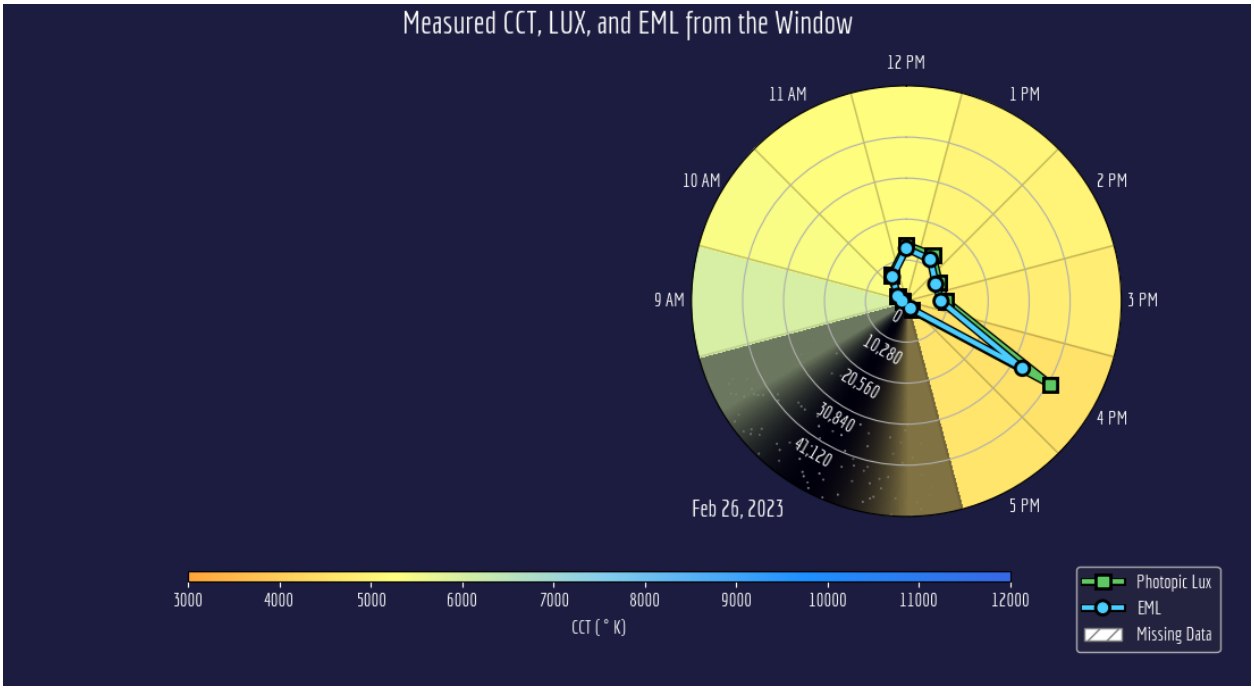

Fig. 4.12: Facing window – February 26, 2023

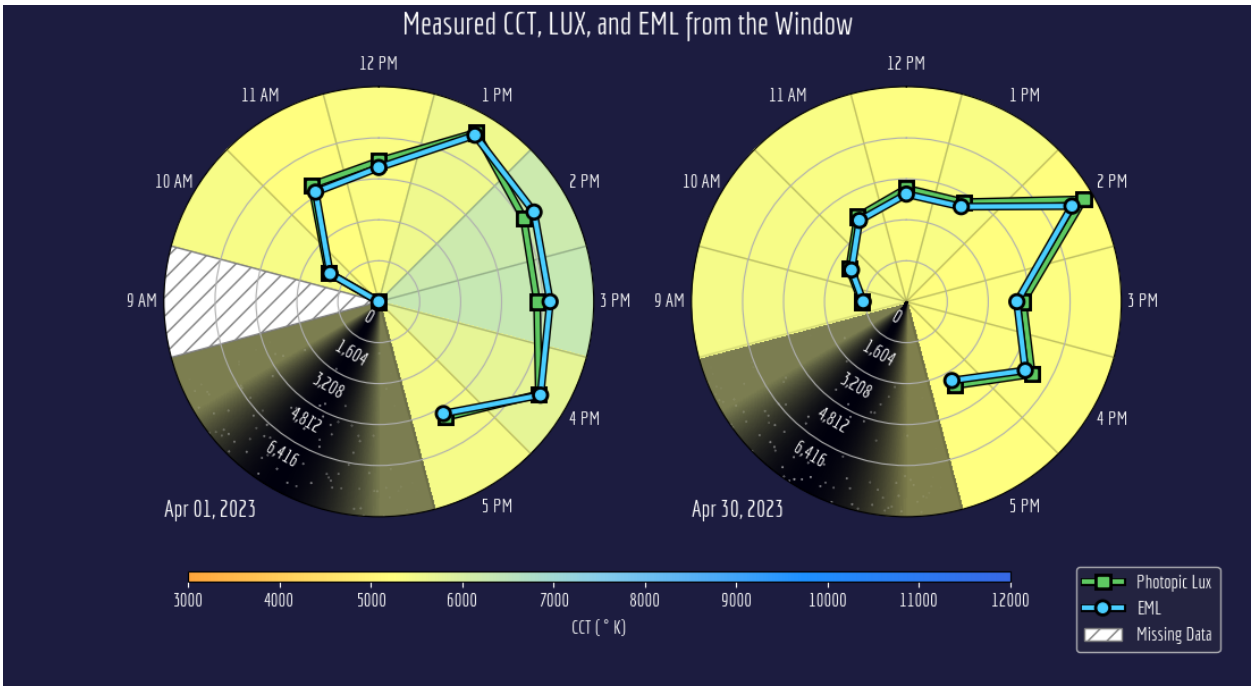

Fig. 4.13: Facing window – April 1, 2023, and April 30, 2023

Wall

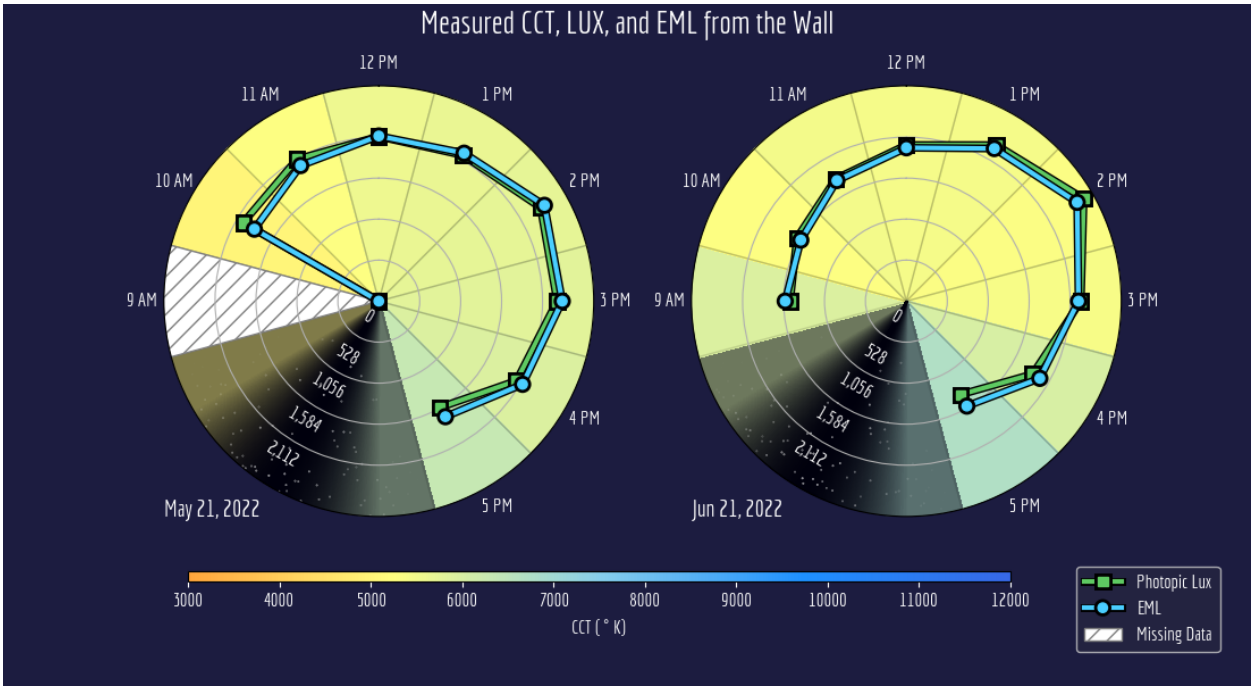

Fig. 4.14: Facing wall – May 21, 2022, and June 21, 2022

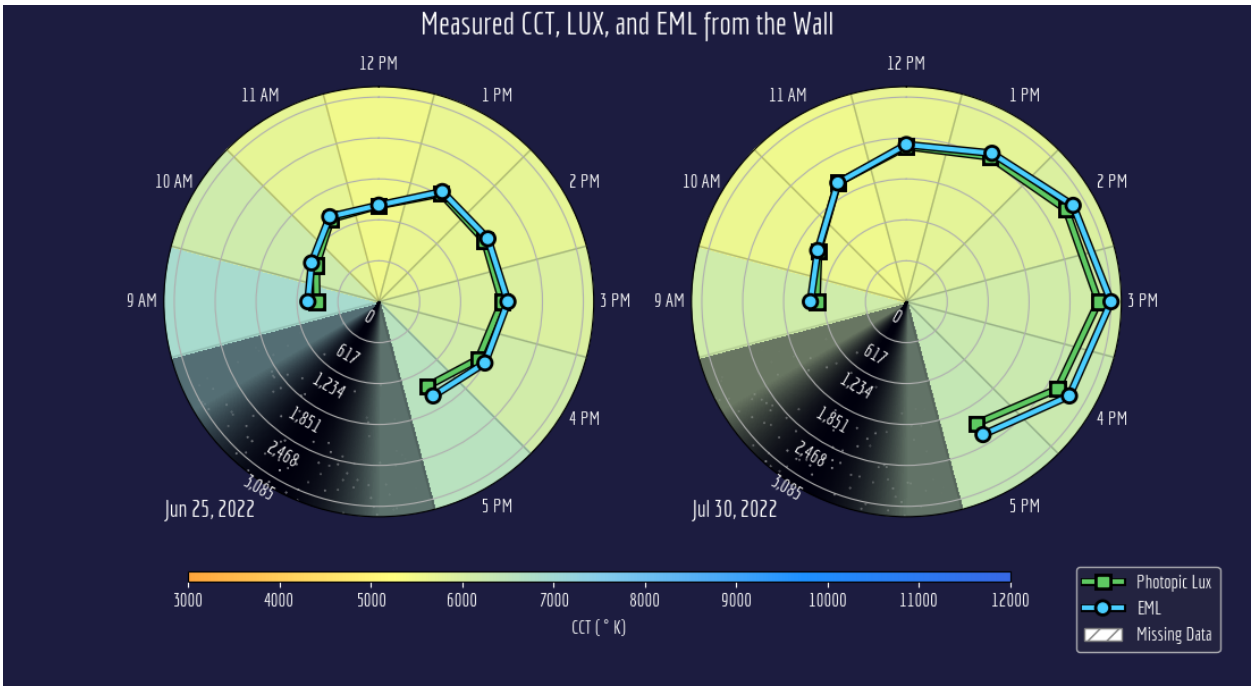

Fig. 4.15: Facing wall – June 25, 2022, and July 30, 2022

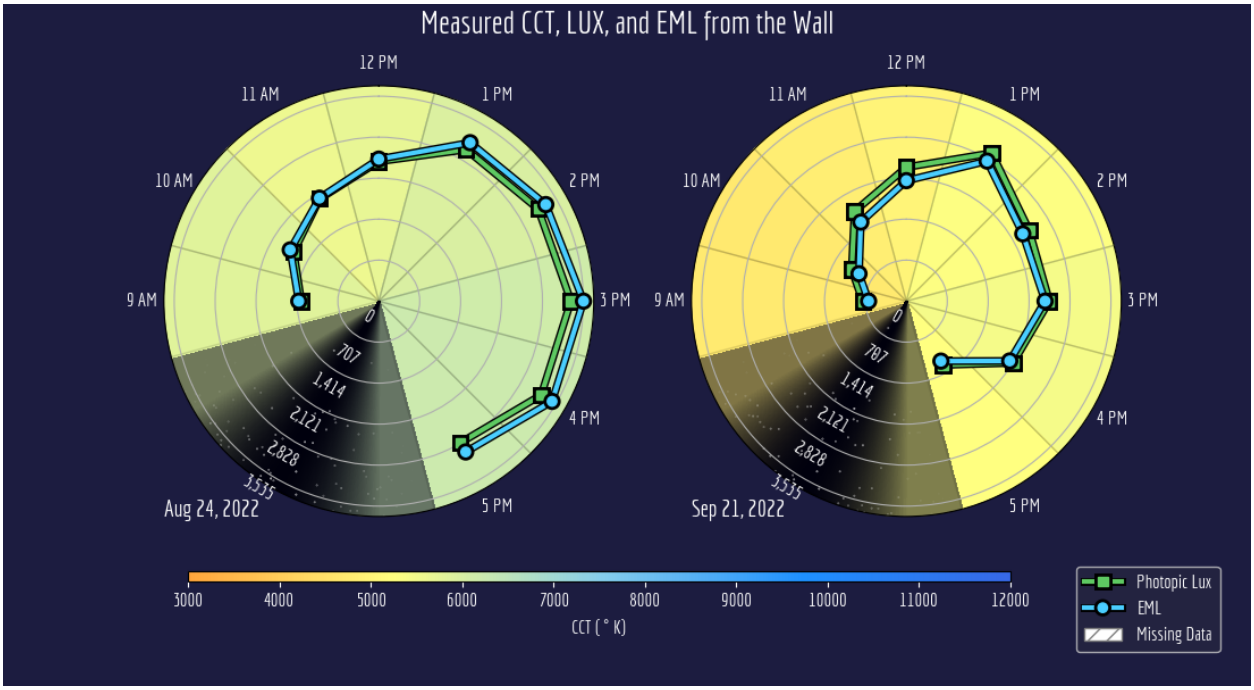

Fig. 4.16: Facing wall – August 24, 2022, and September 21, 2022

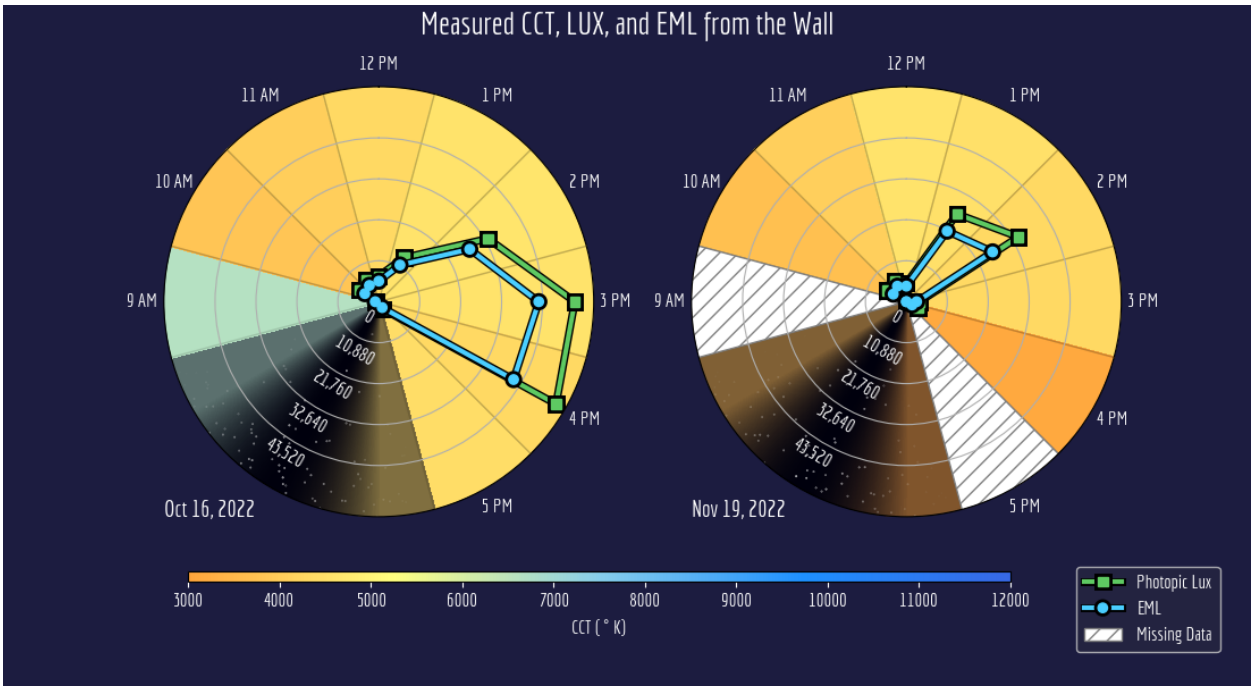

Fig. 4.17: Facing wall – October 16, 2022, and November 19, 2022

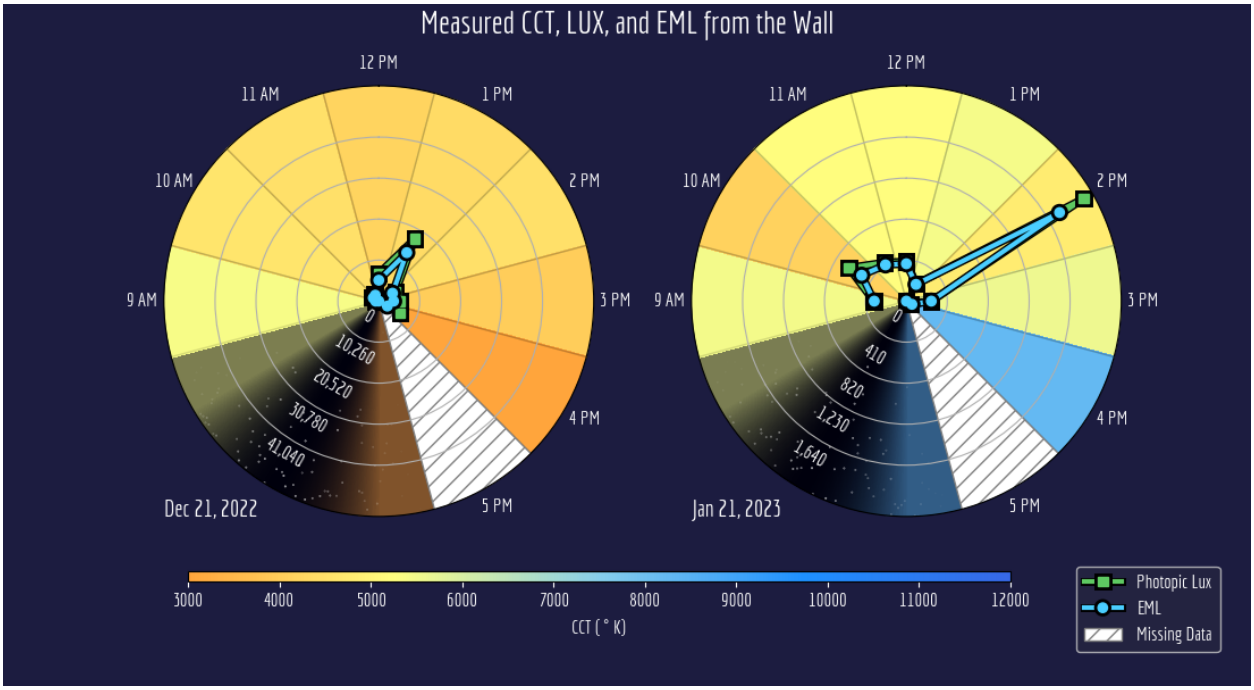

Fig. 4.18: Facing wall – December 21, 2022, and January 21, 2023

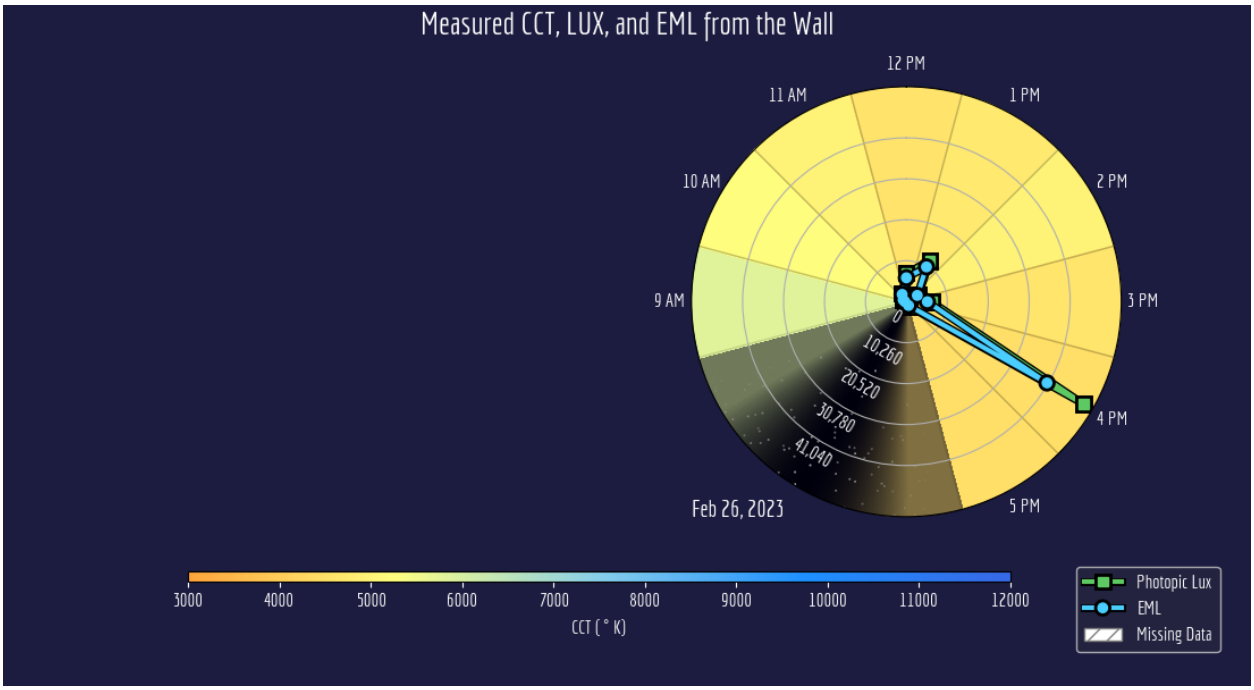

Fig. 4.19: Facing wall – February 26, 2023

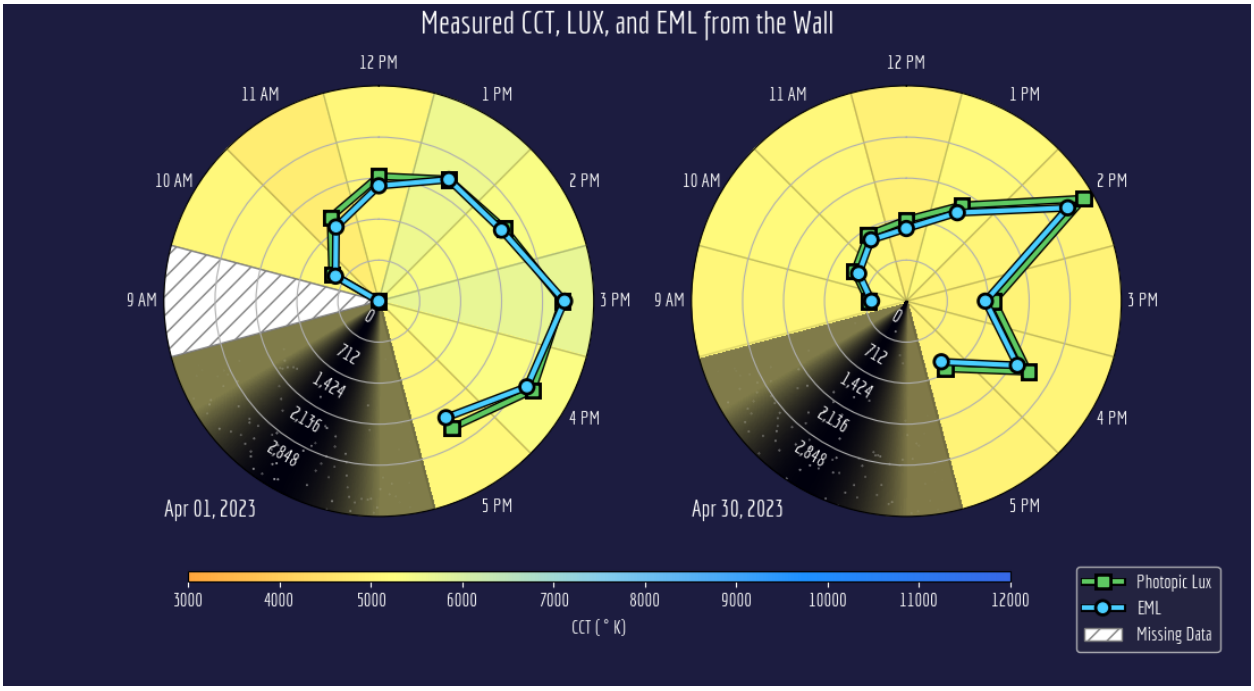

Fig. 4.20: Facing wall – April 1, 2023, and April 30, 2023

4.2 – LARK Simulation Results

4.2.1 – Measured values versus simulated results

In total, 97 simulations were performed. Fig 4.21 to 4.31 show the measured versus simulated photopic lux and EML values where available. Where there are discrepancies in values, the difference between measured and simulated results tend to be greater when facing the window. Moreover, as the results are almost directly affected by the sky inputs when facing the window, there are also greater fluctuations of results throughout the day, while results facing the wall are more consistent with less frequency or extremely high values. Overall, the results facing the wall aligns better than results facing the window.

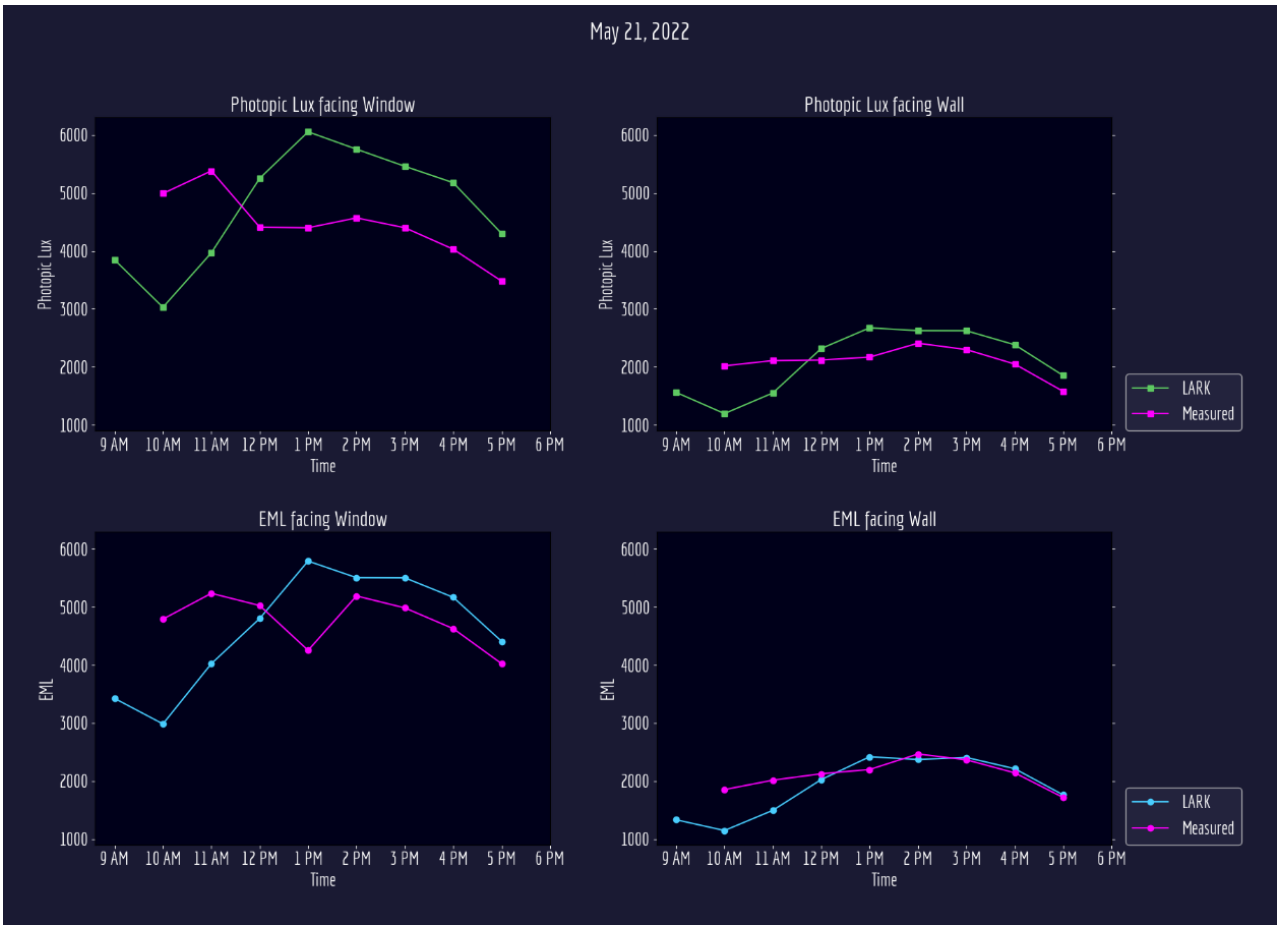

Fig. 4.21: Measured vs. simulated for May 21, 2022

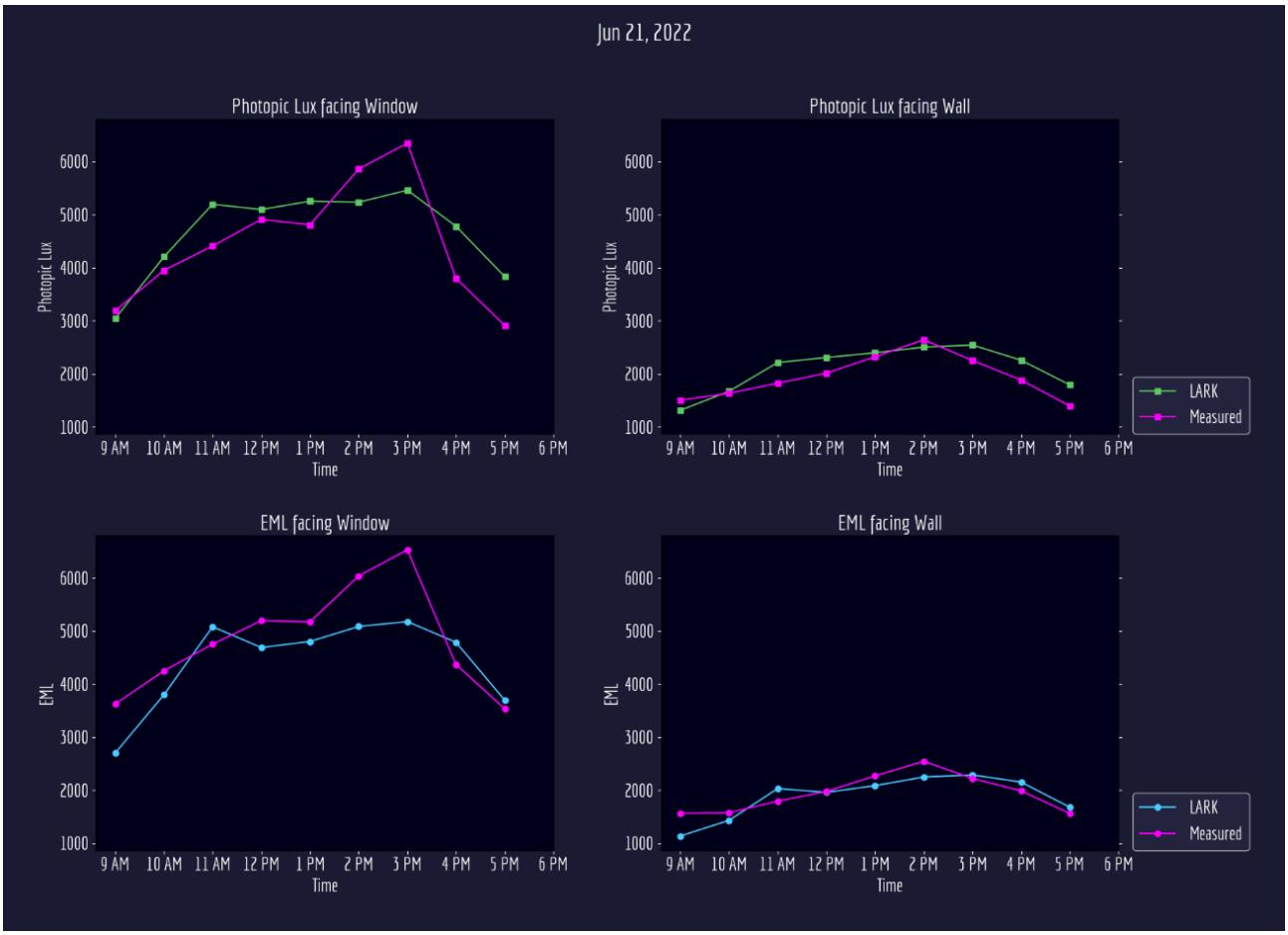

Fig. 4.22: Measured vs. simulated for June 21, 2022

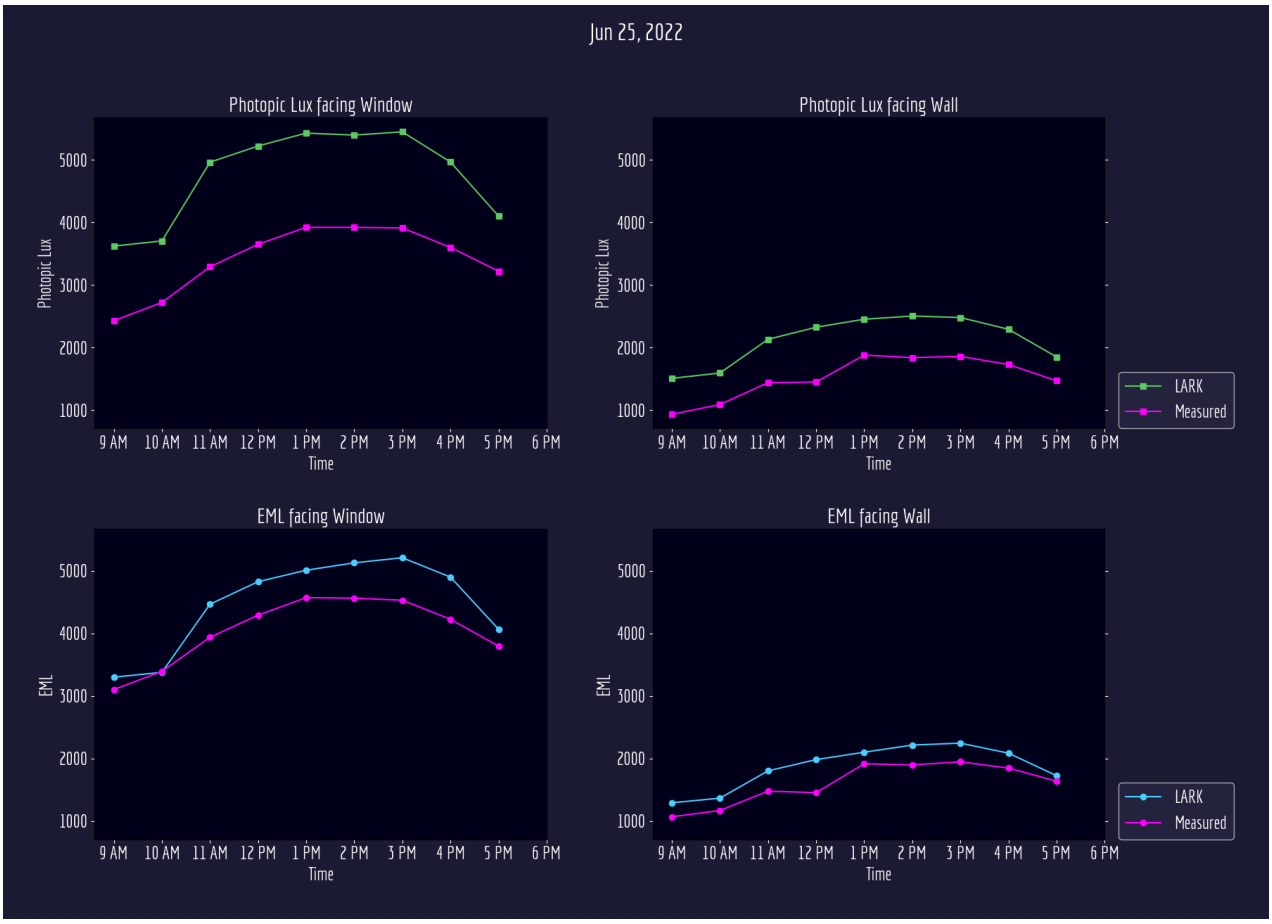

Fig. 4.23: Measured vs. simulated for June 25, 2022

Although the LARK photopic lux results are significantly higher than measured values, the overall trend of increase and decrease in lux values line up better. This is due to the presence of clear skies.

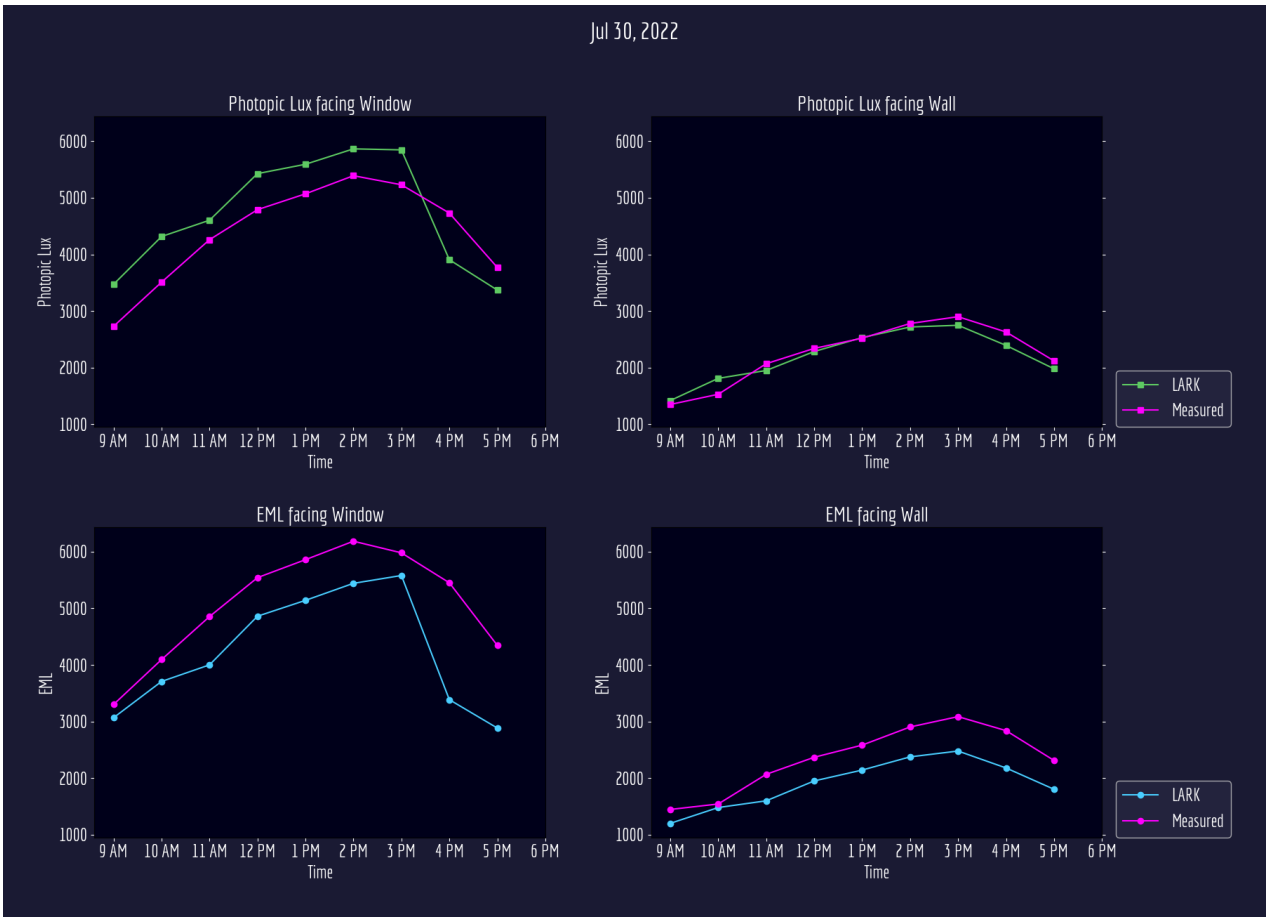

Fig. 4.24: Measured vs. simulated for July 30, 2022

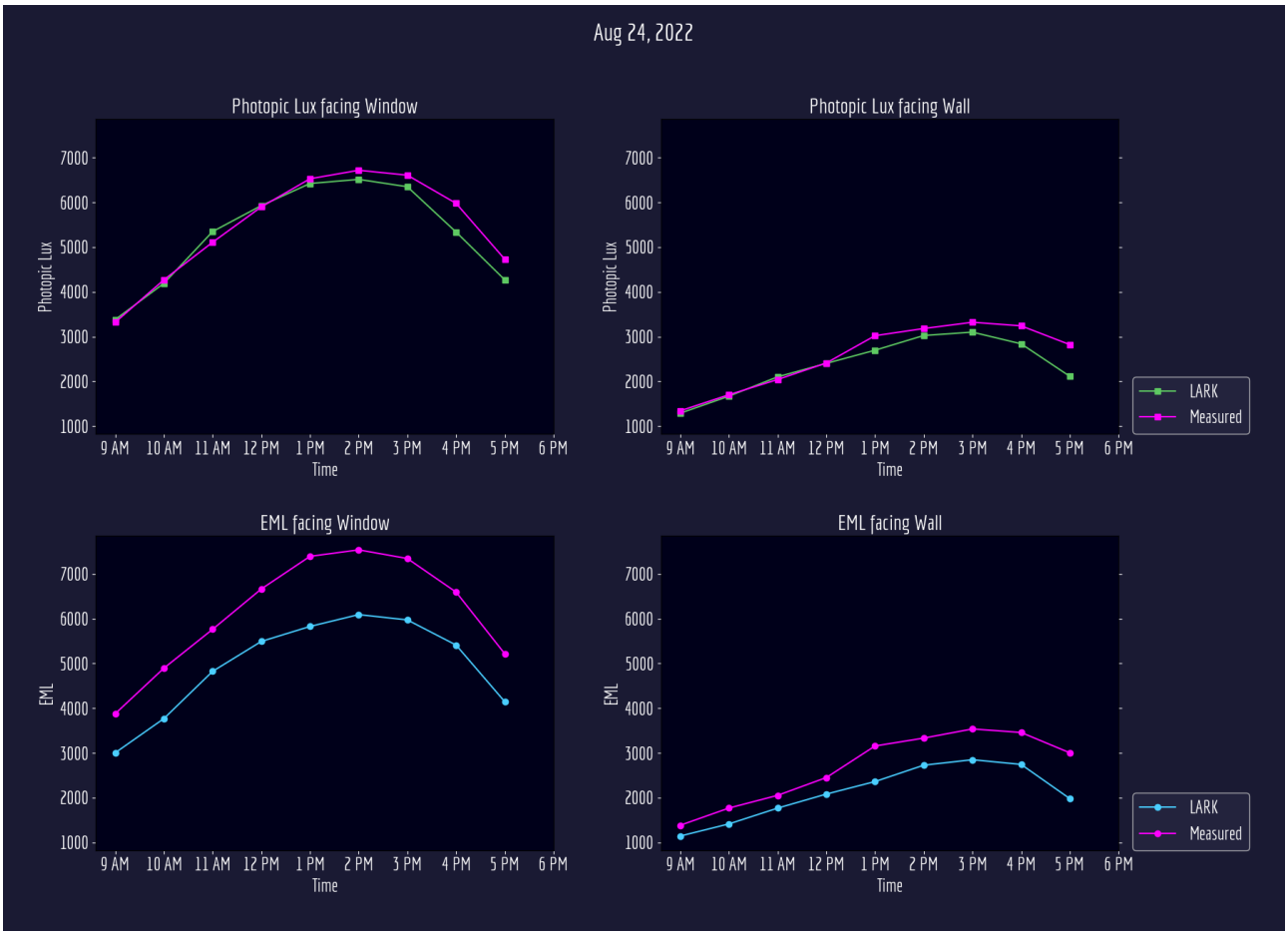

Fig. 4.25: Measured vs. simulated for August 24, 2022

It was noted that in Fig 4.25, the measured photopic lux facing the window is similar to the LARK simulated photopic lux. However, the measured EML is significantly higher than measured photopic lux for both facing the window and facing the wall. As the skies are clear, and sky CCTs are high, there is significant circadian stimulus from external skies. However, this is not reflected as such in the LARK results, where LARK EML is lower than the LARK photopic lux.

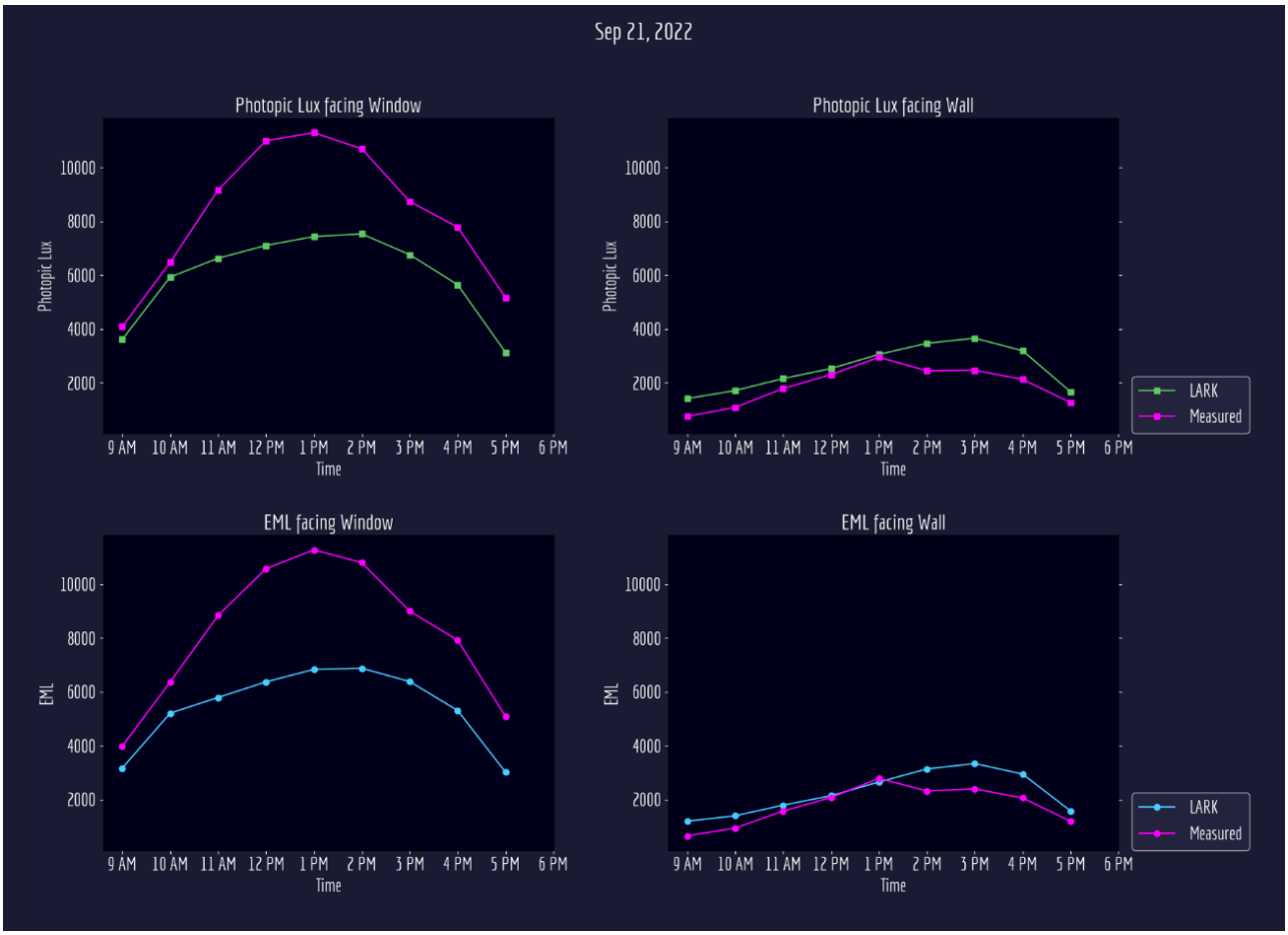

Fig. 4.26: Measured vs. simulated for September 21, 2022

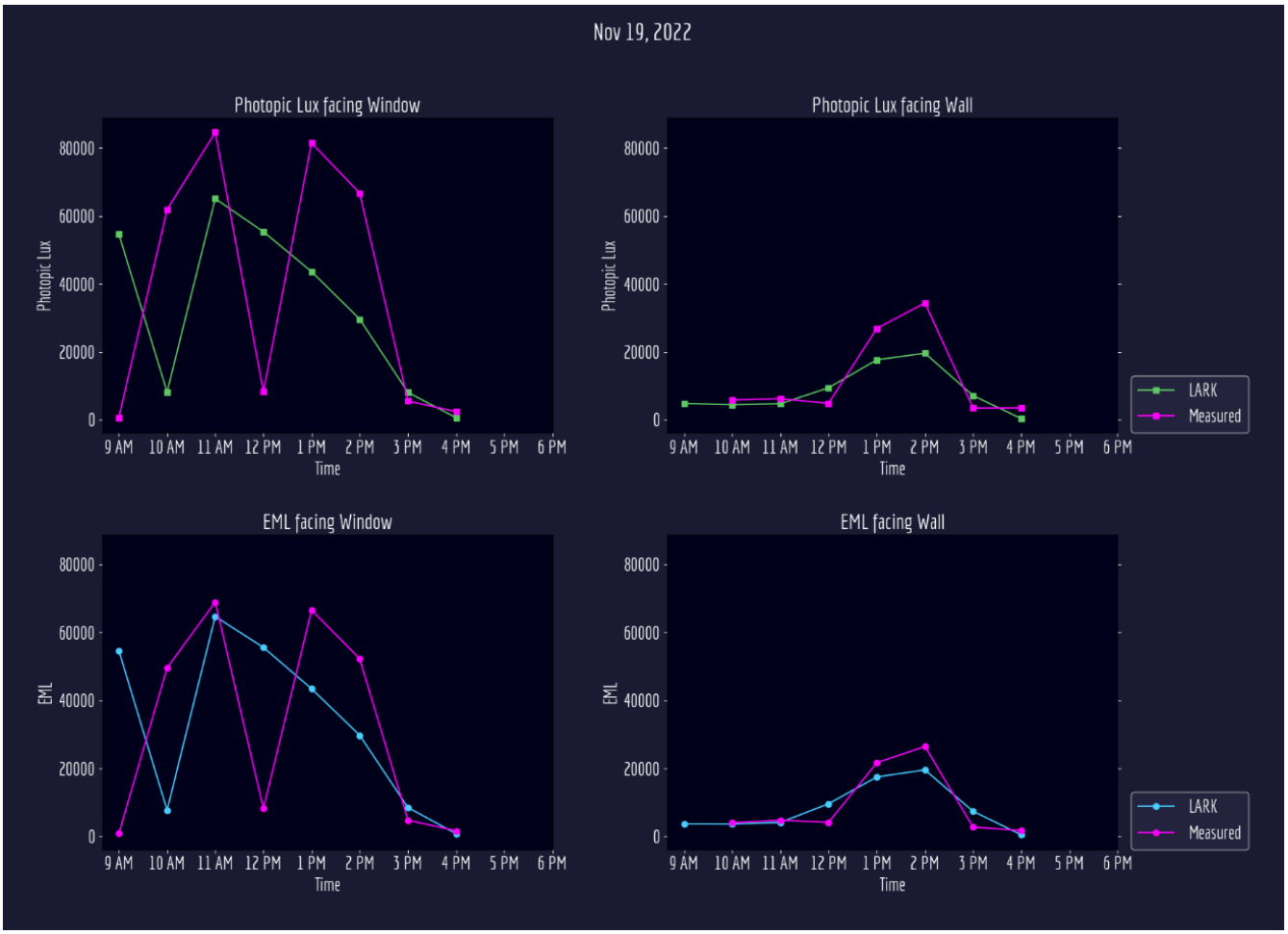

Fig. 4.27: Measured vs. simulated for November 19, 2022

Fig. 4.28: Measured vs. simulated for January 21, 2023

The consistently low measured lux values on January 21, 2023 (Fig 4.28) was due to overcast skies. However, the LARK simulation at 10am and 2pm does not reflect as such. A probable cause of this is shifts in cloud cover at time of measurement of global horizontal irradiance and spectra resulting in some daylight coming through the cloud cover.

Fig. 4.29: Measured vs. simulated for February 26, 2023

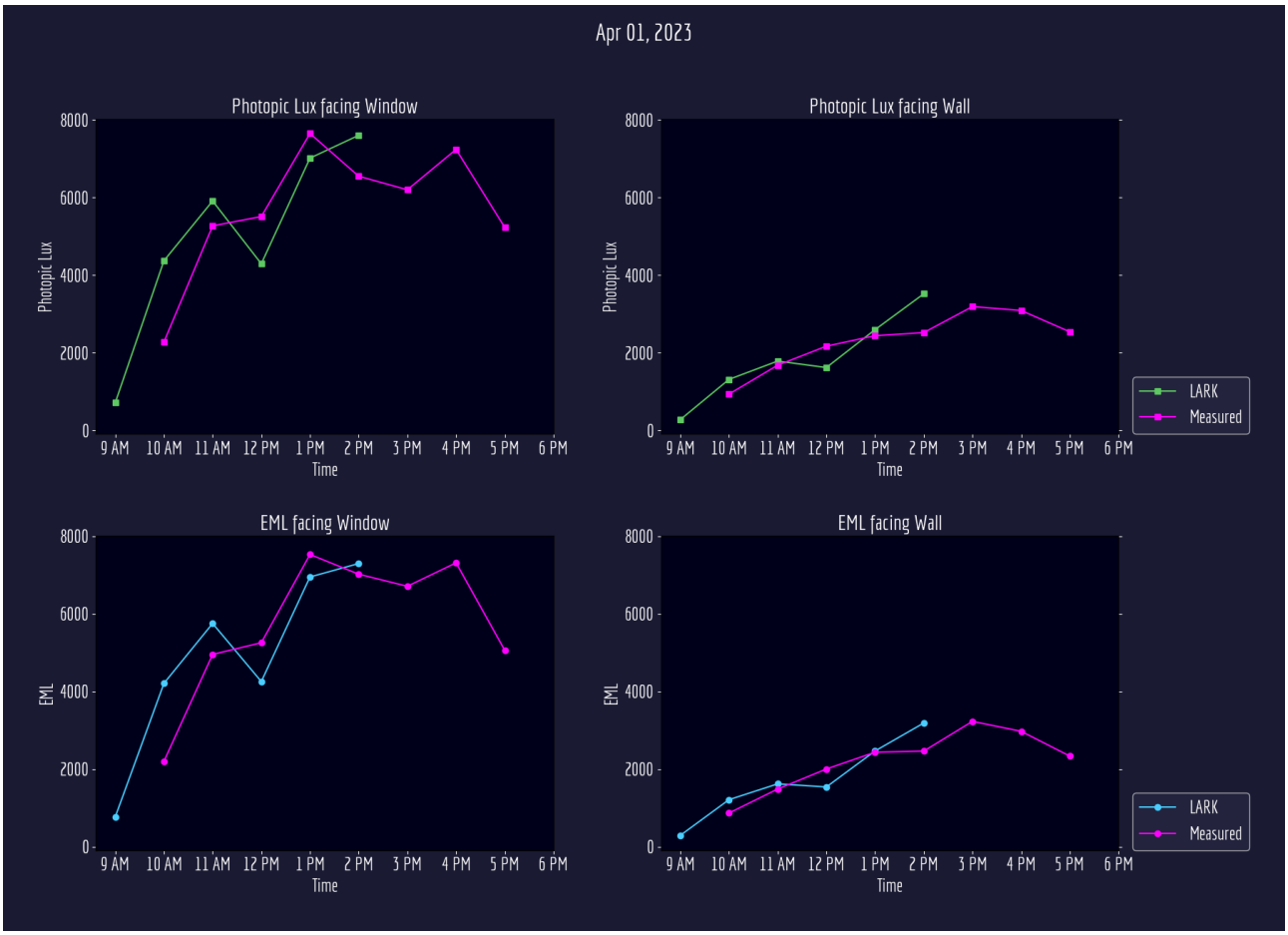

Fig. 4.30: Measured vs. simulated for April 1, 2023

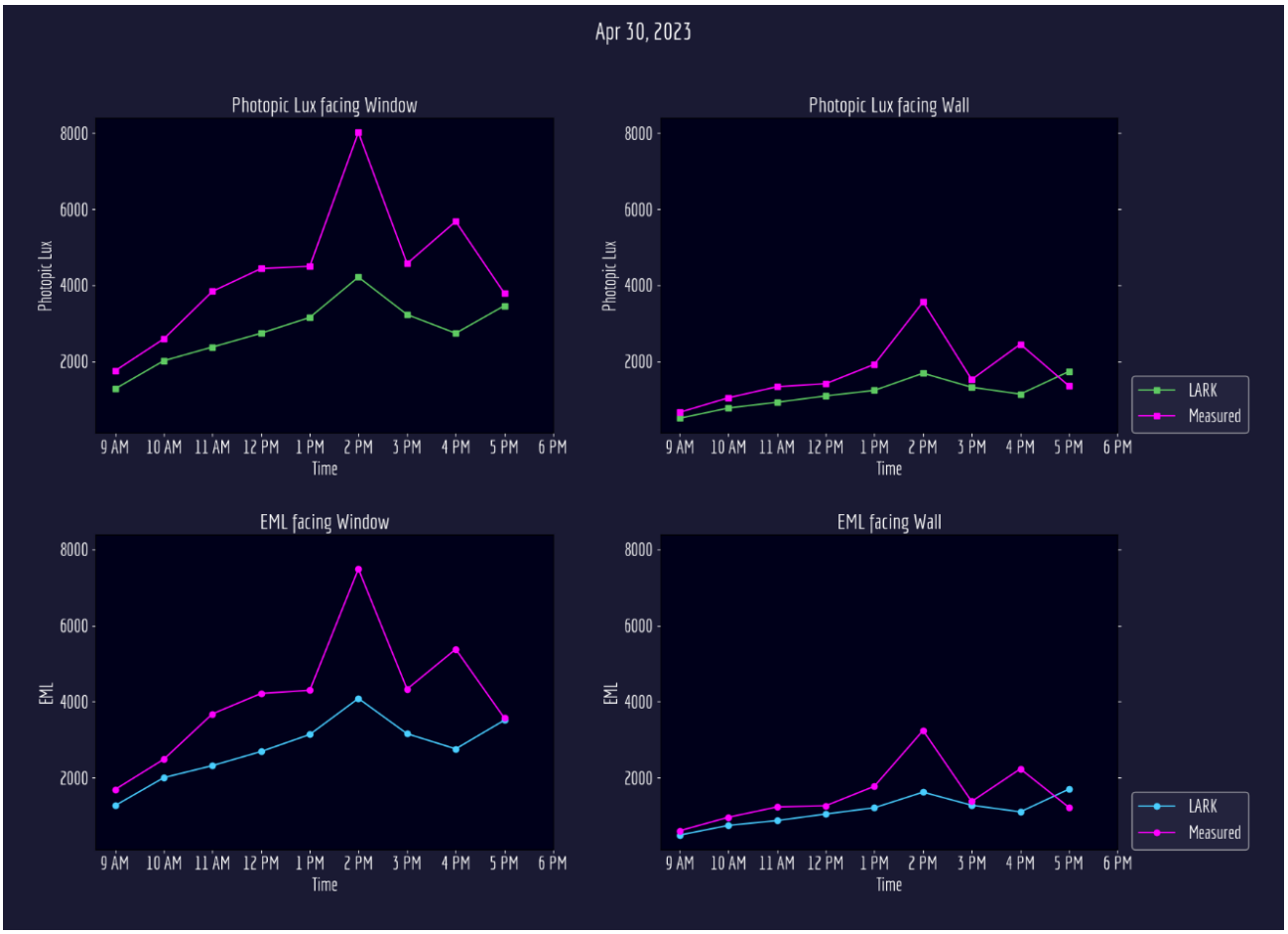

Fig. 4.31: Measured vs. simulated for April 30, 2023

4.2.2 – Image-based simulation comparison

LARK is able to produce spectral renders of its simulation (Fig 4.32 right). Using false color analysis, we can view if the overall luminance of the renders lines up with the captured HDR images at the matching times.

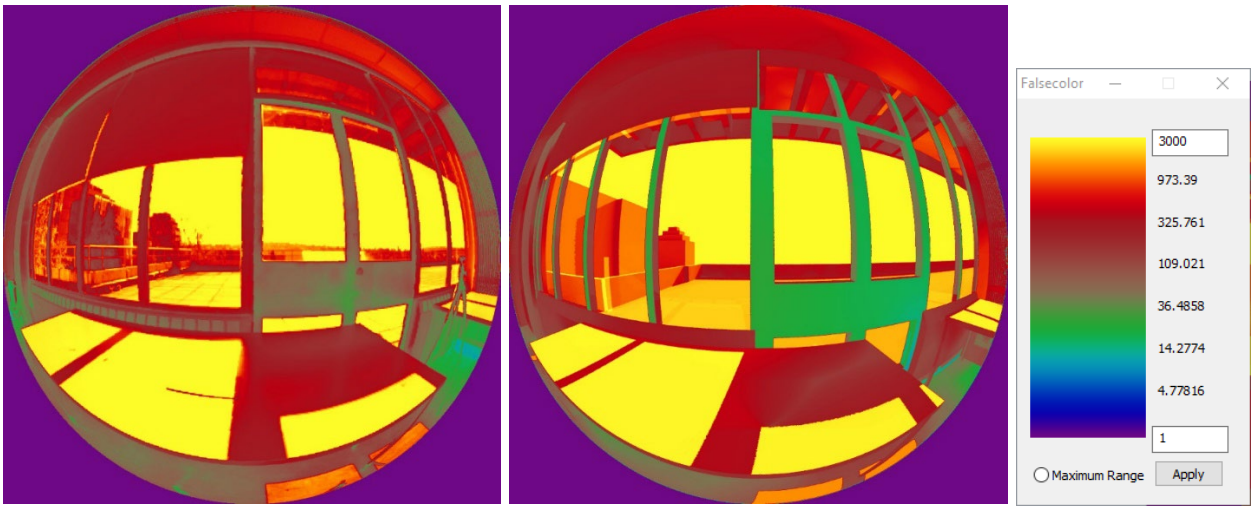

Fig. 4.32: Captured HDR (Left) and LARK image-based simulation output (right)

4.2.3 – Measurement vs simulation discrepancies

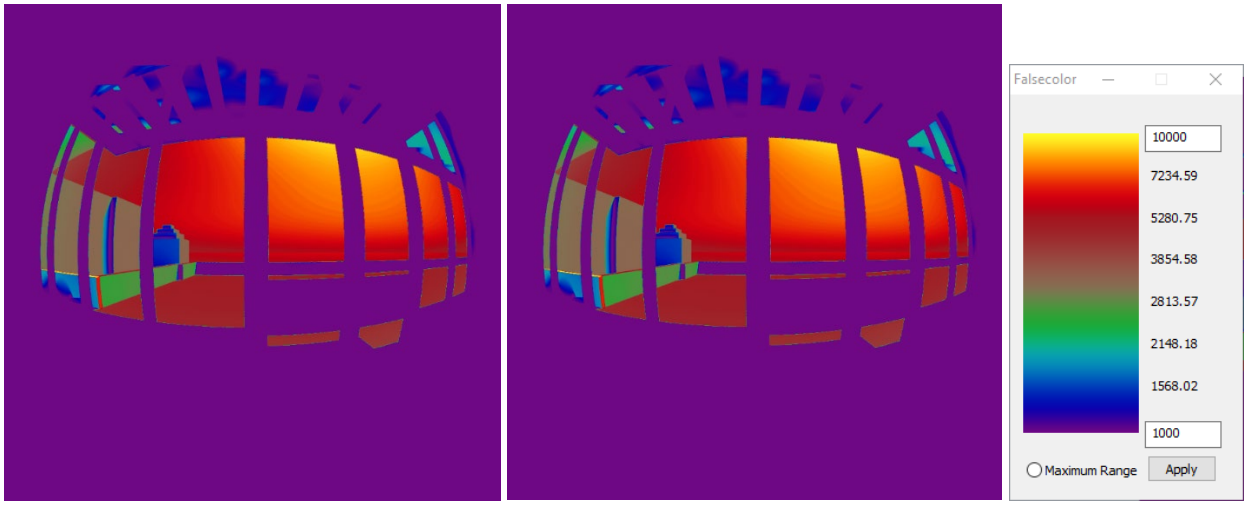

Fig. 4.33: Simulated HDR image: photopic luminance map (left), melanopic luminance map (center), and legend (right)

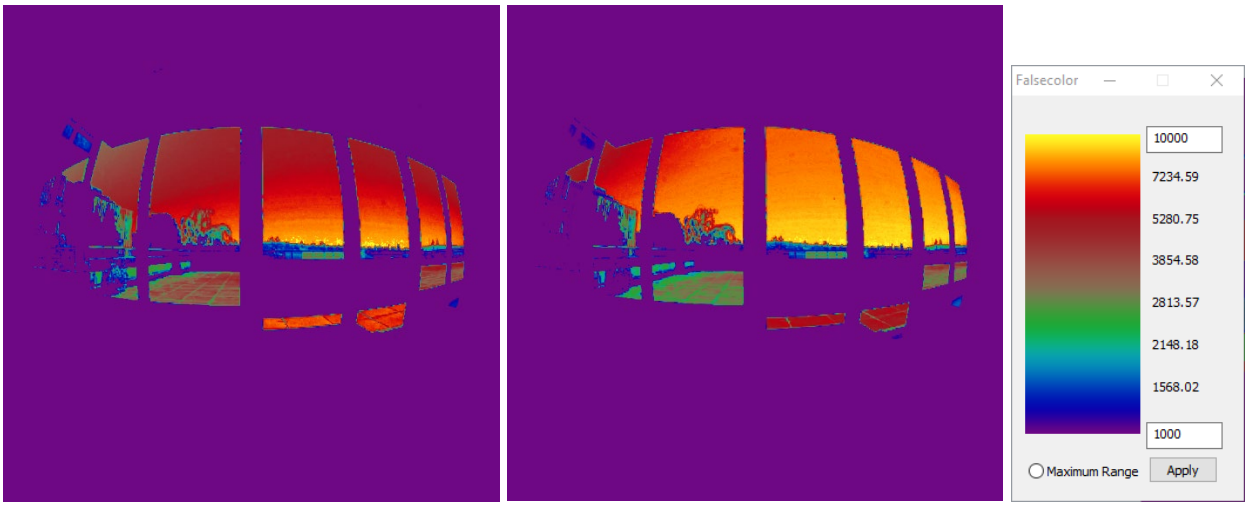

Fig. 4.34: Captured HDR image: photopic luminance map (left), melanopic luminance map (center), and legend (right)

To identify sources of discrepancy between simulation and measurements, an image-based simulation was run for July 30, 2022, at 1pm. All simulation parameters remain

unchanged. The aim was to assess if the discrepancies are a result of the LARK sky model, material spectral properties, or the model geometric differences. The resulting HDR image of the image-based simulation had its false color adjusted to 1000 – 10,000 cd/m² to display the luminance distribution of the simulation sky (Fig 4.33). The same false color scale is applied to the captured HDR image of July 30, 2022, at 1pm as well (Fig 4.34). The comparison between the two pairs of false color images show a significant difference in the sky luminance distribution. The error is more prominent in the melanopic image of the simulation HDR (Fig 4.33 right). This can greatly affect the EML values of our simulation results, and could be the main factor of discrepancies, thus highlighting a need for research into creating more accurate simulation sky models when it comes to simulating melanopic lighting.

4.2.4 – Grid-based simulation

LARK can perform grid-based simulations, showing the photopic lux levels and EMLs across the room. Vertical sensor points are set-up, facing north, south, east, and west for the purposes of these simulations. The legends are set up as between 150 – 1500 Lux for photopic (Fig 4.34), and 275 to 1100 EML for melanopic illuminances (Fig 4.35), respectively. Zones above red and below blue in false colors are not ideal. For photopic lux, values of above 1500 lux can cause visual glare, while values below 150 lux are too low to perform visual tasks. For EML, above 1100 EM.lx is enough as a single-dose of circadian entrainment. The WELL Building standard criteria requires 275 EM.lx over 4 hours, hence values less than 275 (in dark blue) are low and require a longer time to sufficiently entrain the circadian system.

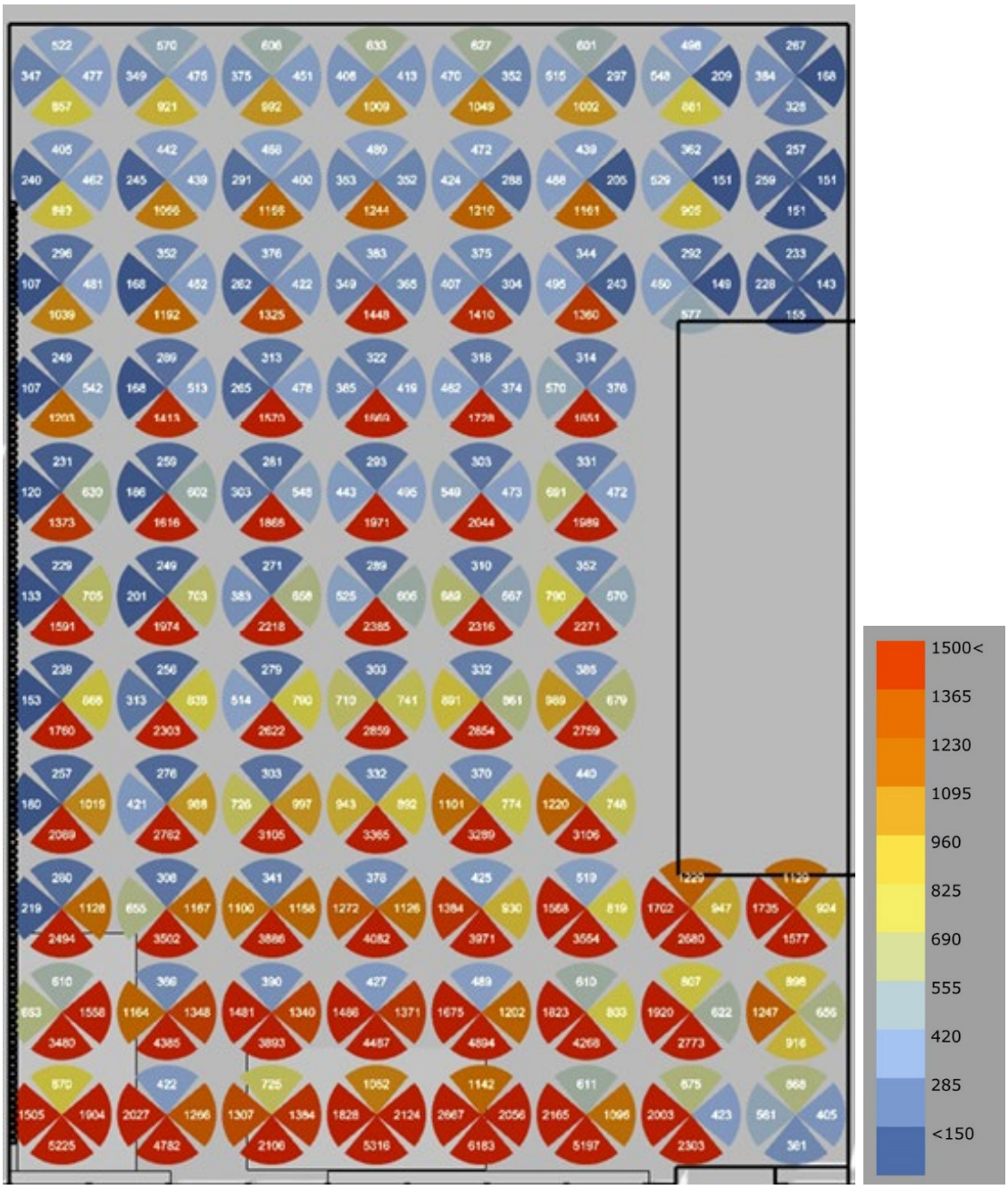

Fig. 4.35: Grid-based analysis of photopic lux on July 30, 2022, 1pm

When simulated for July 30 at 1:00 pm, most of the result values when facing south are above 1500 lux, as well as a few west-facing values (Fig 4.35). Glare is present at the front of the room for occupants facing south (window), west, and east.

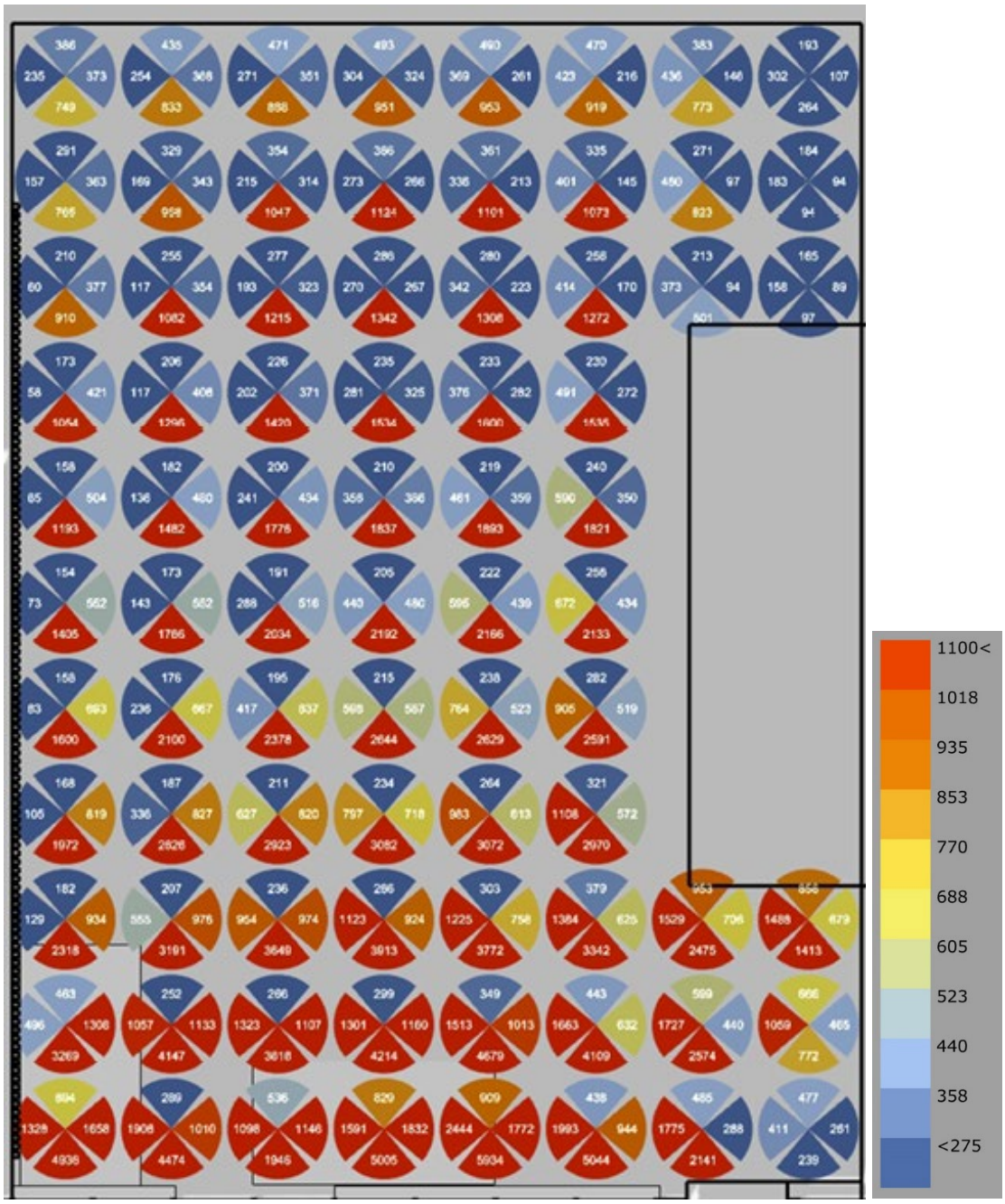

Fig. 4.36: Grid-based analysis of EML on July 30, 2022, 1pm

Most locations with unobstructed views towards the window (south) have EML results above 1100 EM.lx in Fig 4.36. This means that these locations and view directions are optimal for circadian entrainment when considering placing workstations in the room. Overall, all view

directions and locations have at least 275 EML, making the room appropriate for circadian entrainment on this day.

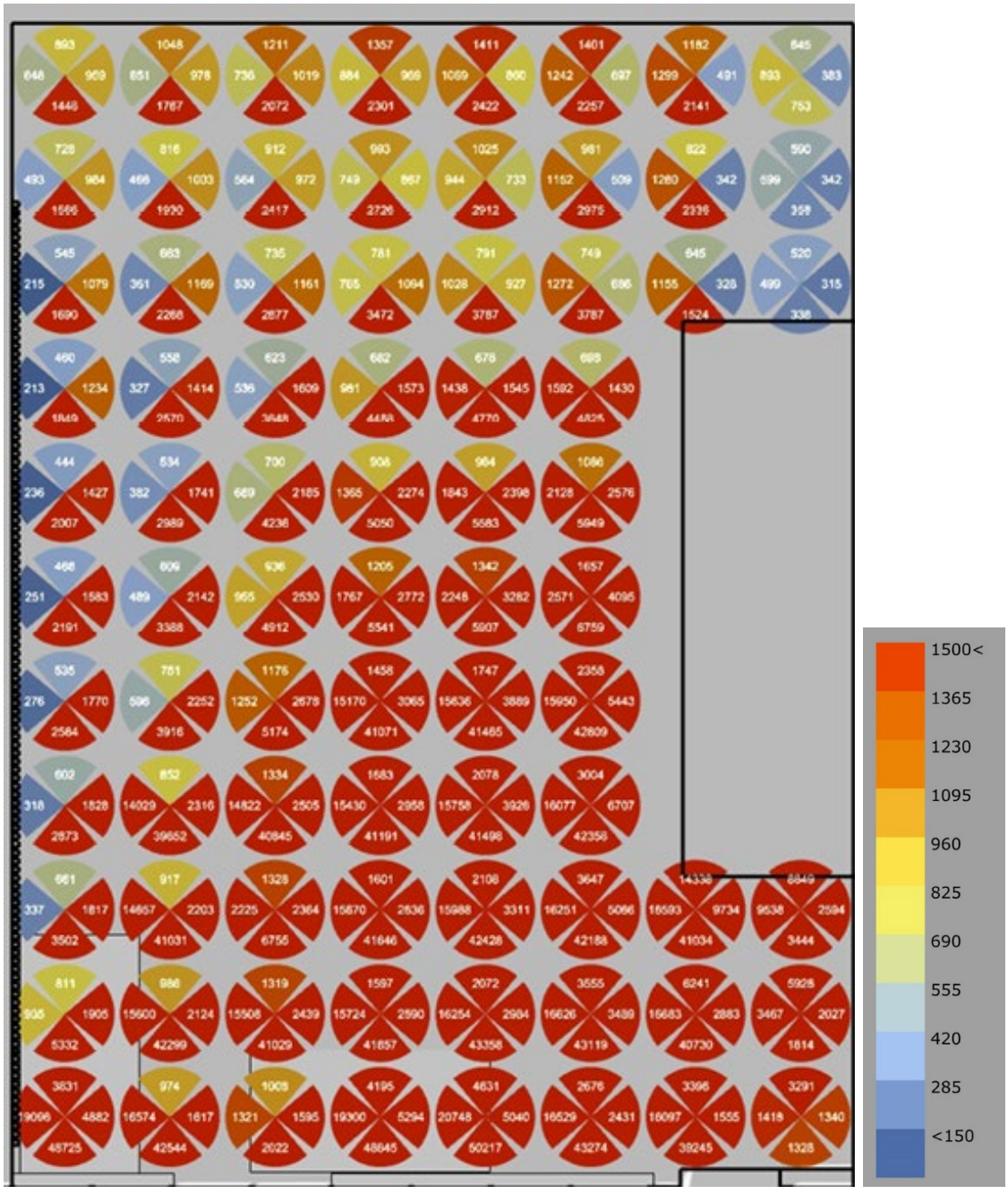

Fig. 4.37: Grid-based analysis of photopic lux on November 19, 2022, at 1pm

When the simulations are performed for November 19 at 1:00pm, excessive photopic lighting becomes more dominant (Fig 4.37). As the sun altitude is much lower, more direct sunlight can enter, causing extremely high photopic lux values. This can cause discomfort glare and difficulty in reading computer screens (i.e. veiling reflections). The light levels are not ideal and shading devices are necessary.

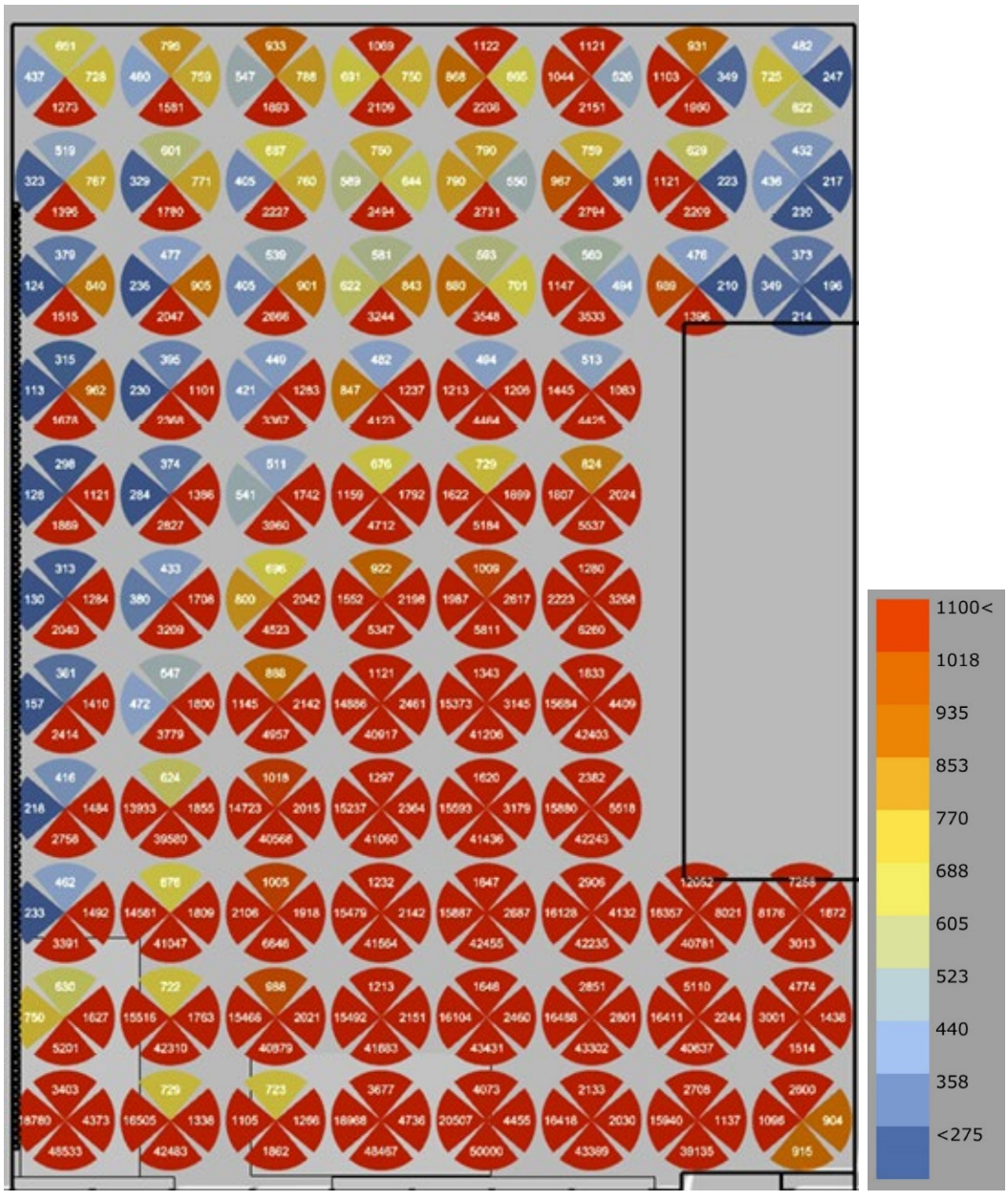

Fig. 4.38: Grid-based analysis of EML on November 19, 2022, at 1pm

Although most of the sensor points are above the single-dose threshold for EM.lx at all orientations, the extremely high photopic lux levels still means that shading devices are needed (Fig 4.38).

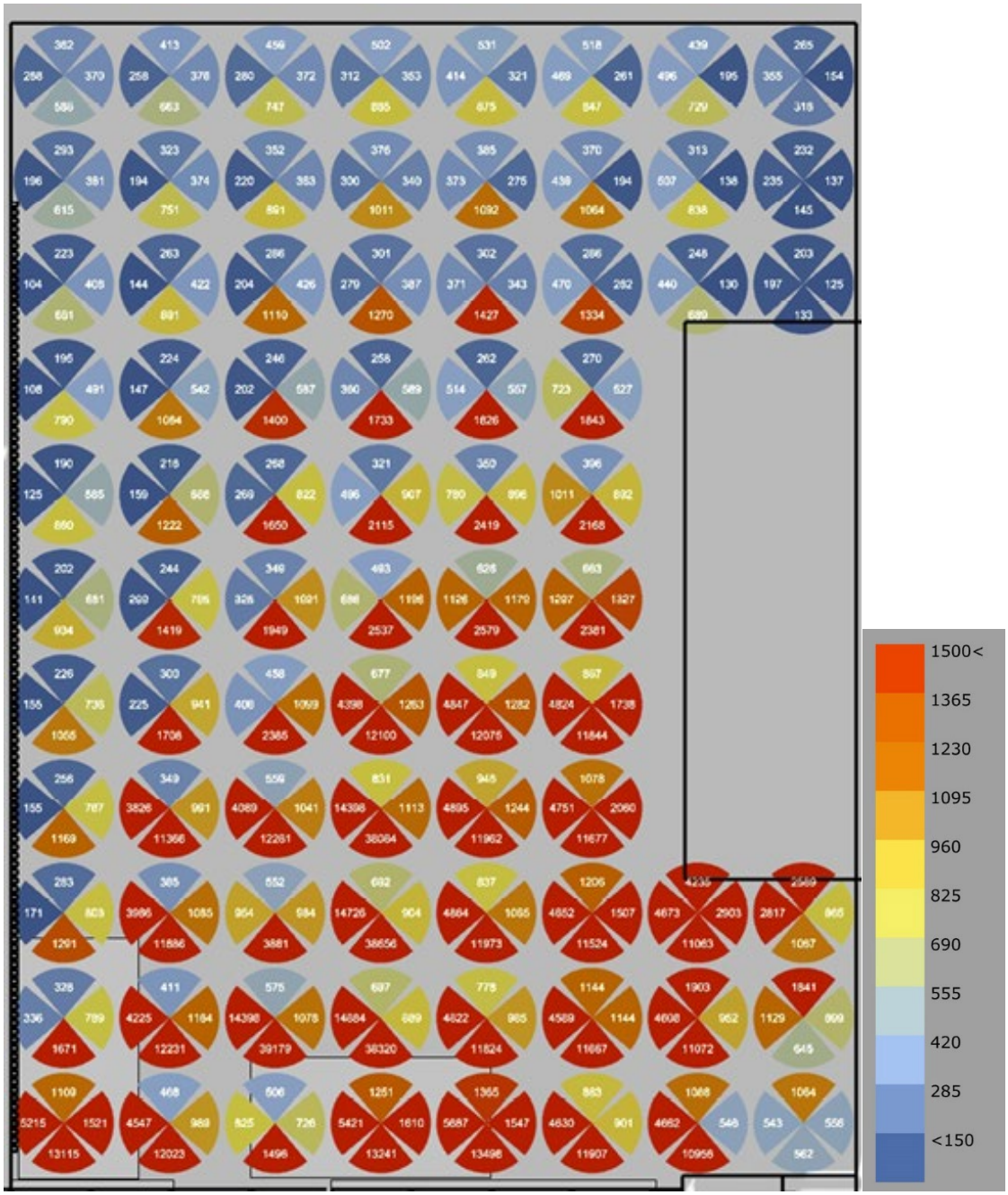

Fig. 4.39: Grid-based analysis of photopic lux on November 19, 2022, at 1pm with blinds down

The shade fabric in the classroom is modeled for the simulation illustrated in Fig 4.39. Although photopic lux levels are greatly reduced, there are still areas without fabric (corresponding to the door) and excessive daylight can enter. Secondary shading is necessary for better control.

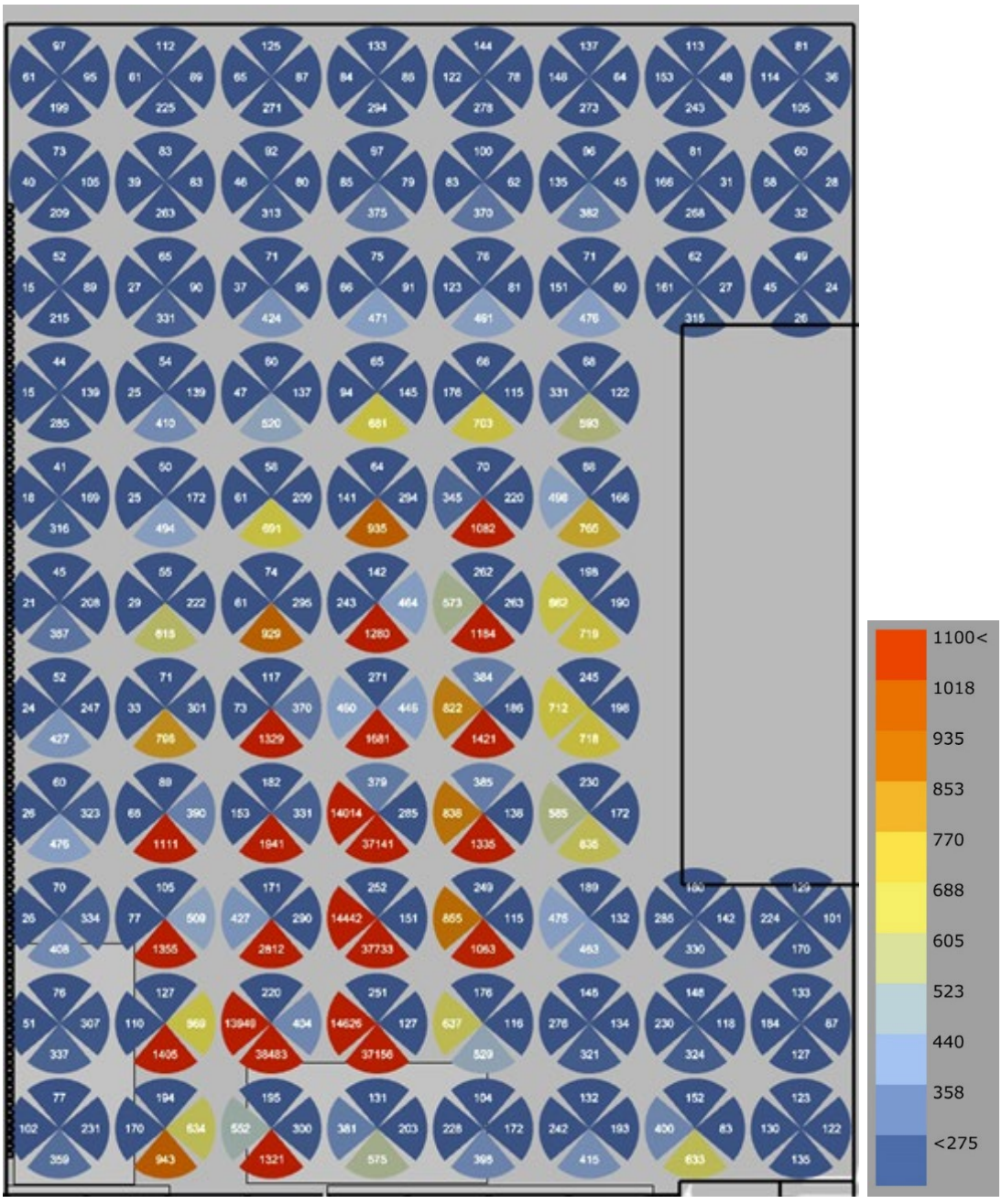

Fig. 4.40: Grid-based analysis of EML on November 19, 2022, at 1pm with blinds down

Although photopic lux levels are only slightly reduced, the EML values are drastically reduced (Fig 4.40). This highlights the prevalent problem where visual and circadian needs compete with each other. High photopic lux may correspond to higher EML, but it is not ideal for visual comfort.

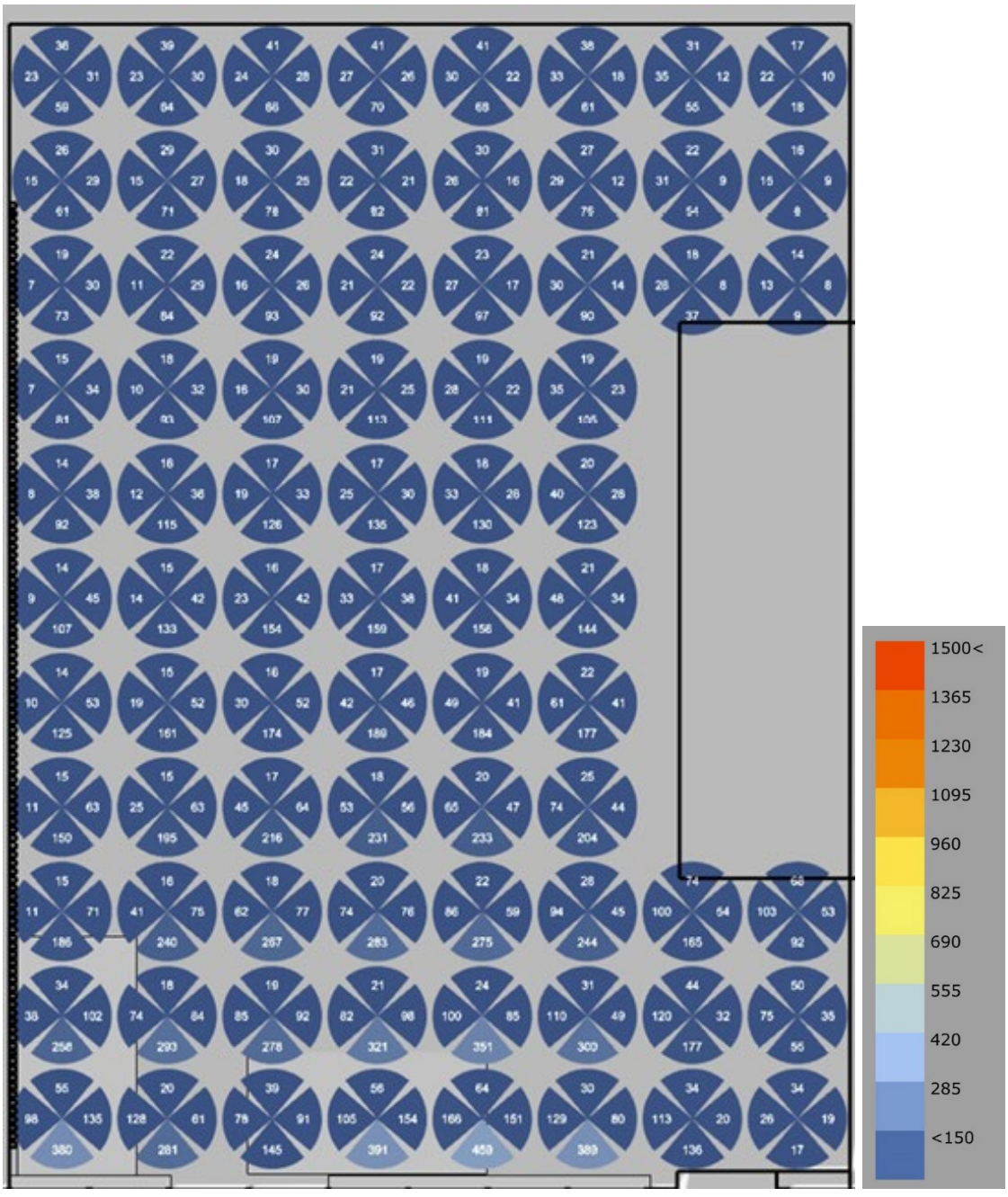

Fig. 4.41: Grid-based analysis of photopic lux on January 21, 2022, at 1pm

An overcast day is simulated to study low daylighting availability (January 21, 2022). The light levels in the classroom are insufficient for common visual tasks, and supplemental electric lighting is needed (Fig 4.41).

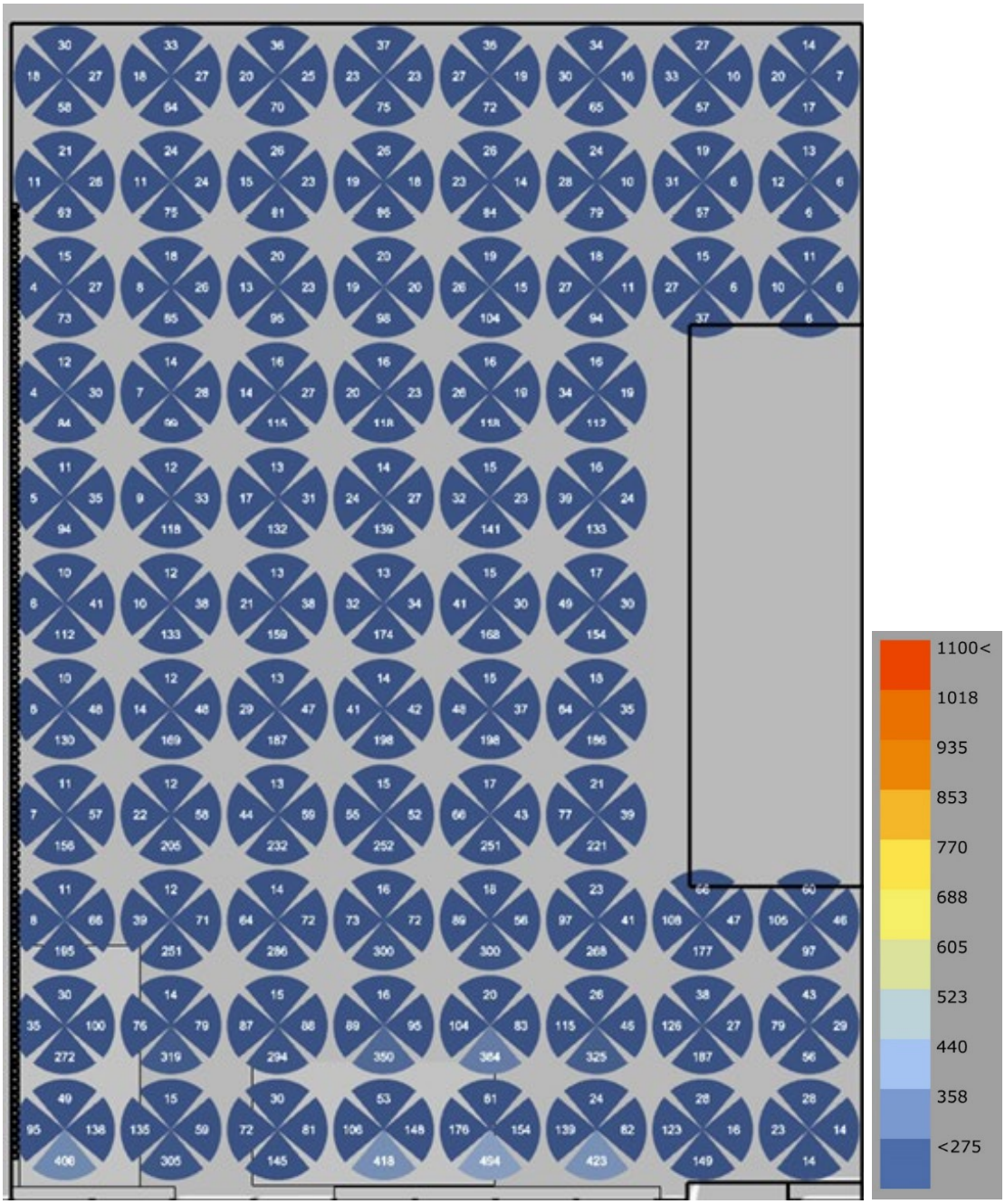

Fig. 4.42: Grid-based analysis of EML on January 21, 2022, at 1pm

There are, however, a few simulated EML values above the minimum required EM.lx of 275 which means that even with overcast skies you can still get circadian entrainment, albeit a low amount, at some locations in the classroom (Fig 4.42).

4.3 – Discussion

Although there are instances of simulation with large discrepancies between measured values and simulated results, the acceptable range of error is < 20% for Radiance RGB simulations.

Our findings support a newer understanding of circadian rhythm that light intensity drives circadian entrainment much more than the spectral qualities of light. However, past a certain threshold of light intensity, there is the potential to cause visual discomfort, and shading would be necessary to mitigate that. If the blue wavelength of light is not suppressed by such shading techniques, the lower light intensity will still be beneficial for circadian entrainment. For electric lighting, as intensity is limited and much lower than daylight, circadian entrainment is primarily driven by spectral characteristics, which means that having enriched blue light in the spectra of these electric lights is beneficial in driving the indoor circadian rhythm when needed. While not a replacement for the circadian entrainment by daylight, it is still a means for people to gain circadian entrainment whilst indoors.

Chapter 5 – Conclusion

This thesis research seeks to understand the changing circadian stimulus of Seattle skies throughout the year. This is achieved via field data measurement of luminance and spectral characteristics using multiple measurement devices. HDR images captured as part of field data collection also serves as a method to visualize luminance distributions of the scene. The measurement values are used as inputs for LARK simulation where a digital twin of the field data collection setting was built. Results of the simulations are compared against the field data measurements to validate LARK's accuracy and its ability to predict EML, as well as identify areas for improvement. The comparisons show that there are discrepancies, primarily due to the fact that the digital models may not align perfectly with the physical world. There were also factors during data measurement that contributed to these discrepancies.

This year-long research endeavor in field data measurement of luminance and spectral characteristics has yielded valuable insight into the patterns in which changes in the sky conditions of Seattle affects the CCT and resulting circadian entrainment. The values are measured using a handheld spectrophotometer, from the perspective of an office worker with a workstation looking towards a south-facing window, and a workstation looking towards the wall, adjacent to the window. In the summer months of May to August, clear skies are more prevalent and thus both photopic lux and EMLs measured were more consistent. The measured sky CCTs typically fall within the range of 7000K to 9000K. As a result, the measured EMLs during these months tend to be higher than measured photopic lux values. The measurements become more varied in the months of September to February, with peaks of photopic lux values as high as 80,000 lux and CCTs measured are lower at around 5000K to 6000K. Due to the lower CCTs,

measured EML tends to be lower than measured photopic lux values. During these months, the overcast skies cause more atmospheric scattering of daylight, resulting in lower measured sky CCTs. The sun is also at a lower altitude, which means daylight can enter the field measurement classroom and hit the sensor directly, causing the extremely high lux readings. Moreover, the measured CCTs at times of extremely high photopic lux is due to the fact that the sun is around 5200K, and the sun's CCT is able to completely overpower the CCT of the sky. These measurements, taken over the span of a year, show how the sun's position and cloud conditions can affect the values of CCT and luminance distributions of the sky. It is our hope that these findings will advance our collective understanding of the non-visual characteristics of daylight by contributing to existing efforts in daylight measurement, as well as serve as data points for future work in improving daylight simulation sky models and LARK.

Although LARK has demonstrated that it can predict indoor circadian stimulus from measured sky data, it is still a new software that is under development. Further validation on top of the ones conducted as part of this thesis is needed, through more comparative studies. Early studies have already highlighted that LARK has greater accuracy in producing simulation results in controlled settings when compared to other circadian lighting simulation tools such as ALFA (Balakrishnan et al. 2019). However, through this thesis, we can identify the shortcomings that LARK currently has when undertaking real world simulations. One of the main sources of discrepancies in simulation results, particularly for the EML side, is the sky model. In the current version of LARK, its sky models are colored by measured global horizontal spectra, while the sun is modeled as an equal energy white source. The simulation sky dome is of a uniform color, but in the real world, the sky changes color across the sky dome. Earlier research (Inanici 2019) have shown that CCT and spectra of the sky changes with orientation of measurement, but the

LARK sky dome is not currently modeled as such. The color variation across the sky dome and the spectra of the direct component can affect EML simulation results. Further research is thus needed to identify how the CCT of the sky dome changes throughout, and be able to model that to ultimately improve the accuracy of EML simulations in LARK. Another challenge is that LARK relies on measured GHI and spectral data to run its simulations. This means that it is imperative that our field measurements are reliable and accurate to minimize discrepancies. However, field measurements are imperfect, as human errors and equipment malfunctions can happen. One of the challenges is the positioning of the handheld spectrophotometer, as just a slight tilt can significantly impact the readings. Moreover, as we relied upon third-party sources for the GHI data, their measurement devices were at a separate physical location, and we do not know whether the equipment were adequately calibrated. Having all measurement devices in proximity to each other and ensuring that they are taking readings as accurate as possible will improve the discrepancies between measured values and simulation results. All measurements are taken in an urban environment, with the assumption that they were not overshadowed at any time.

As aforementioned, both daylight measurement and LARK are continued efforts that will benefit from further observations and research. With more field measurement data, we can better identify the factors that drive the photopic lux and CCT values of the sky, as well as the changing spectral qualities throughout the sky dome. As research in circadian rhythm, and especially circadian stimulus in the built environment, is a relatively new field of study, our findings will be able to contribute to the growing collective knowledge. LARK, along with other circadian lighting simulation tools under development, are instrumental for researchers and designers to aid in identifying strategies to improve circadian entrainment of occupants in indoor

environments. They should continue to be developed as new findings expand our understanding of circadian rhythms.

Bibliography

Abboushi, B., and S. Safranek. "Determining Critical Points to Control Electric Lighting to Meet Circadian Lighting Requirements and Minimize Energy Use." In *Proceedings of Annual Modeling and Simulation Conference (ANNSIM)*, 559–68. San Diego, CA: IEEE, July 18 – 21, 2022.

Acosta, I., R. P. Leslie, and M. G. Figueiro. "Analysis of Circadian Stimulus Allowed by Daylighting in Hospital Rooms." *Lighting Research & Technology* 49, no. 1 (February 1, 2016): 49–61. https://doi.org/10.1177/1477153515592948.

Aguilar-Carrasco, M. T., S. Domínguez-Amarillo, I. Acosta, and J. J. Sendra. "Indoor Lighting Design for Healthier Workplaces: Natural and Electric Light Assessment for Suitable Circadian Stimulus." *Optics Express* 29, no. 19 (2021): 29899. https://doi.org/10.1364/oe.430747.

Alight, A., and J. A. Jakubiec. "Evaluating the Use of Photobiology-Driven Alertness and Health Measures for Circadian Lighting Design." In *Proceedings of Building Simulation 2021*. Bruges, Belgium, September 1 – 3, 2021.

Amundadottir, M. L. "Light-Driven Model for Identifying Indicators of Non-Visual Health Potential in the Built Environment." Thesis, Lausanne, EPFL, 2016.

Amundadottir, M. L., S. Rockcastle, M. Sarey Khanie, and M. Andersen. "A Human-Centric Approach to Assess Daylight in Buildings for Non-Visual Health Potential, Visual Interest and Gaze Behavior." *Building and Environment* 113 (2017): 5–21. https://doi.org/10.1016/j.buildenv.2016.09.033.

Andersen, M., S. J. Gochenour, and S. W. Lockley. "Modelling 'Non-Visual' Effects of Daylighting in a Residential Environment." *Building and Environment* 70 (August 29, 2013): 138–49. https://doi.org/10.1016/j.buildenv.2013.08.018.

Anderson, G., S. Clough, F. Kneizys, J. Chetwynd, and E. Shettle, (1986). AFGL Atmospheric Constituent Profiles (0.120km).

Balakrishnan, P., and J. A. Jakubiec. "Spectral Rendering with Daylight: A Comparison of Two Spectral Daylight Simulation Platforms." In *Proceedings of Building Simulation Conference*, 1191–98. Rome, Italy: IBPSA, September 2 – 4, 2019 https://doi.org/10.26868/25222708.2019.211158.

Bellia, L., and F. Fragliasso. "Good Places to Live and Sleep Well: A Literature Review about the Role of Architecture in Determining Non-Visual Effects of Light." *International Journal of Environmental Research and Public Health*, 1002, 18, no. 3 (February 23, 2021): 1–27. https://doi.org/10.3390/ijerph18031002.

Berman, S. M., and R. D. Clear. “A Practical Metric for Melanopic Metrology.” *Lighting Research & Technology* 51, no. 8 (December 29, 2019): 1178–91. https://doi.org/10.1177/1477153518824147.

Berson, D. M., F. A. Dunn, and M. Takao. “Phototransduction by Retinal Ganglion Cells That Set the Circadian Clock.” *Science (American Association for the Advancement of Science)* 295, no. 5557 (2002): 1070–73. https://doi.org/10.1126/science.1067262.

Bierman, A., T. R. Klein, and M. S. Rea. “The Daysimeter: A Device for Measuring Optical Radiation as a Stimulus for the Human Circadian System.” *Measurement Science and Technology* 16, no. 11 (October 2005): 2292–99. https://doi.org/10.1088/0957-0233/16/11/023.

Boyce, P. R. *Human Factors in Lighting*. 3rd ed. Boca Raton: CRC Press/Taylor and Francis, 2014.

Brainard, G. C., J. P. Hanifin, J. M. Greeson, B. Byrne, G. Glickman, E. Gerner, and M. D. Rollag. “Action Spectrum for Melatonin Regulation in Humans: Evidence for a Novel Circadian Photoreceptor.” *The Journal of Neuroscience* 21, no. 16 (August 15, 2001): 6405–12. https://doi.org/10.1523/jneurosci.21-16-06405.2001.

Brennan, M., and Z. Cheng. “Improving Outcomes for Cincinnati’s Tiniest Patients.” ZGF Architects, February 4, 2022. https://www.zgf.com/ideas/3942-improving-outcomes-for-cincinnati-s-tiniest-patients.

Breslav, S., R. Goldstein, A. Tessier, and A. Khan. “Towards Visualization of Simulated Occupants and Their Interactions with Buildings at Multiple Time Scales.” In *Symposium on Simulation for Architecture & Urban Design*, 1–8. Tampa, FL: Autodesk Research, April 13 – 16, 2014.

Brown, T. M. “Melanopic Illuminance Defines the Magnitude of Human Circadian Light Responses under a Wide Range of Conditions.” *Journal of Pineal Research* 69, no. 1 (March 27, 2020): 1–14. https://doi.org/10.1111/jpi.12655.

Brown, T. M., G. C. Brainard, C. Cajochen, C. A. Czeisler, J. P. Hanifin, S. W. Lockley, R. J. Lucas, et al. “Recommendations for Daytime, Evening, and Nighttime Indoor Light Exposure to Best Support Physiology, Sleep, and Wakefulness in Healthy Adults.” *PLOS Biology* 20, no. 3 (March 17, 2022): 1–24. https://doi.org/10.1371/journal.pbio.3001571.

Chang, A., F. A. Scheer, and C. A. Czeisler. “The Human Circadian System Adapts to Prior Photic History.” *The Journal of Physiology* 589, no. 5 (January 25, 2011): 1095–1102. https://doi.org/10.1113/jphysiol.2010.201194.

Chang, A., N. Santhi, M. St Hilaire, C. Gronfier, D. S. Bradstreet, J. F. Duffy, S. W. Lockley, R. E. Kronauer, and C. A. Czeisler. "Human Responses to Bright Light of Different Durations." *The Journal of Physiology* 590, no. 13 (July 30, 2012): 3103–12. https://doi.org/10.1113/jphysiol.2011.226555.

Cheng, Z. "Visual and Non-Visual Effects of Light on Health in Neonatal Intensive Care Units." Dissertation, University of Washington, 2022.

CIE S 026/E:2018. *CIE system for metrology of optical radiation for IPRGC-influenced responses to light* Vienna: CIE Central Bureau (2018). https://doi.org/10.25039/s026.2018.

Danell, M., S. Rockcastle, and M. L. Amundadottir. "Evaluating Temporal and Spatial Light Exposure Profiles for Typical Building Occupants." In *Proceedings of Symposium in Simulation in Architecture and Urban Design*, 539–46. Vienna, Austria: Simulation Councils, inc., May 25 – 27, 2020.

Dewan, K., S. Benloucif, K. Reid, L. F. Wolfe, and P. C. Zee. "Light-Induced Changes of the Circadian Clock of Humans: Increasing Duration Is More Effective than Increasing Light Intensity." *Sleep* 34, no. 5 (May 1, 2011): 593–99. https://doi.org/10.1093/sleep/34.5.593.

Duijnhoven, J. van, M. Aarts, and H. Kort. "The Importance of Including Position and Viewing Direction When Measuring and Assessing the Lighting Conditions of Office Workers." *Work* 64, no. 4 (October 28, 2019): 877–95. https://doi.org/10.3233/wor-193028.

Durmus, D. "Correlated Color Temperature: Use and Limitations." *Lighting Research & Technology* 54, no. 4 (June 25, 2021): 363–75. https://doi.org/10.1177/14771535211034330.

Figueiro, M. G., B. Steverson, J. Heerwagen, K. Kampschroer, C. M. Hunter, K. Gonzales, B. Plitnick, and M. S. Rea. "The Impact of Daytime Light Exposures on Sleep and Mood in Office Workers." *Sleep Health* 3, no. 3 (April 2017): 204–15. https://doi.org/10.1016/j.sleh.2017.03.005.

Figueiro, M., G. Brainard, S. Lockley, V. Revell, and R. White. *Light and Human Health: An Overview of the Impact of Optical Radiation on Visual, Circadian, Neuroendocrine, and Neurobehavioral Responses. IES TM-18-08*. New York, NY: Illuminating Engineering Society of North America, 2008.

Fritz, R., and A. McNeil. "About Radiance." Radsite, January 4, 2019. https://www.radiance-online.org/about.

Gkaintatzi-Masouti, M., C. Pierson, J. van Duijnhoven, M. Andersen, and M. Aarts. "A Simulation Tool for Building and Lighting Design Considering IPRGC-Influenced Light Responses." *E3S Web of Conferences* 362 (December 1, 2022a): 1–7. https://doi.org/10.1051/e3sconf/202236201001.

Gkaintatzi-Masouti, M., J. van Duijnhoven, and M. Aarts. “Simulations of Non-Image-Forming Effects of Light in Building Design: A Literature Review.” *Lighting Research & Technology*, December 22, 2022b, 1–21. https://doi.org/10.1177/14771535221142812.

Gkaintatzi-Masouti, M., J. van Duijnhoven, and M. P. Aarts. “Review of Spectral Lighting Simulation Tools for Non-Image- Forming Effects of Light.” *Journal of Physics: Conference Series* 2042, no. 1 (November 1, 2021): 1–6. https://doi.org/10.1088/1742-6596/2042/1/012122.

Gooley, J. J., S. M. Rajaratnam, G. C. Brainard, R. E. Kronauer, C. A. Czeisler, and S. W. Lockley. “Spectral Responses of the Human Circadian System Depend on the Irradiance and Duration of Exposure to Light.” *Science Translational Medicine* 2, no. 31 (May 12, 2010). https://doi.org/10.1126/scitranslmed.3000741.

Hattar, S., H. Liao, M. Takao, D. M. Berson, and K.-W. Yau. “Melanopsin-Containing Retinal Ganglion Cells: Architecture, Projections, and Intrinsic Photosensitivity.” *Science* 295, no. 5557 (February 8, 2002): 1065–70. https://doi.org/10.1126/science.1069609.

Hernández-Andrés, J., J. Romero, J. L. Nieves, and R. L. Lee. “Color and Spectral Analysis of Daylight in Southern Europe.” *Journal of the Optical Society of America A* 18, no. 6 (June 1, 2001): 1325–35. https://doi.org/10.1364/josaa.18.001325.

Hyde, E. P. “A New Determination of the Selective Radiation from Tantalum.” *Physical Review (Series I)* 32, no. 6 (June 1, 1911): 632–33. https://doi.org/10.1103/physrevseriesi.32.632.

Inanici, M. “Applications of Image Based Rendering in Lighting Simulation: Development and Evaluation of Image Based Sky Models.” In *Proceedings of the Eleventh International IBPSA Conference*, 265–71. Glasgow, Scotland: IBPSA, July 27 – 30, 2009.

Inanici, M. “Evaluation of High Dynamic Range Photography as a Luminance Data Acquisition System.” *Lighting Research & Technology* 38, no. 2 (June 1, 2006): 123–36. https://doi.org/10.1191/1365782806li164oa.

Inanici, M. “Evalution of High Dynamic Range Image-Based Sky Models in Lighting Simulation.” *LEUKOS* 7, no. 2 (October 1, 2010): 69–84. https://doi.org/10.1582/leukos.2010.07.02001.

Inanici, M., and A. Jakubiec. “Introduction to HDR Photography.” Workshop Presented at the 32nd International Conference on PLEA. (July 11 – 13, 2016).

Inanici, M., B. Abboushi, and S. Safranek. “Evaluation of Sky Spectra and Sky Models in Daylighting Simulations.” *Lighting Research & Technology*, February 15, 2022, 1–28. https://doi.org/10.1177/14771535221103400.

Inanici, M., M. Brennan, and E. Clark. “Spectral Daylighting Simulations: Computing Circadian Light.” In *Proceedings of BS2015: 14th Conference of International Building Performance Simulation Association*, 1245–52. Hyperabad, India: IBPSA, December 7 – 9, 2015.

IWBI. “WELL v2 Certification.” International Well Building Institute. Accessed December 18, 2022. https://www.wellcertified.com/certification/v2/.

Jackson, M. A., and M. Bollinger. “Section 1: How Blue Light Affects The Eye and Body; Chapter 4: Circadian Rhythm.” Essay. In *How to Save Your Eyes in the Digital Age: The Handbook on Blue Light, Screen Time, Health, and Electronics*, 29–36. Eden Prairie, MN: Eyesafe Inc., 2022.

Jakubiec, J. A., and A. Alight. “Spectral and Biological Simulation Methods for the Design of Healthy Circadian Lighting.” In *Proceedings of Building Simulation 2021: 17th Conference of IBPSA*, 1–8. Bruges, Belgium: IBPSA, September 1 – 3, 2021.

Jakubiec, J. A., M. Inanici, K. Van Den Wymelenberg, and A. Mahic. “Improving the Accuracy of Measurements in Daylit Interior Scenes Using High Dynamic Range Photography.” In *36th International Conference on Passive and Low Energy Architecture - Cities, Buildings, People: Towards Regenerative Environments*, 1–8. Los Angeles, CA: PLEA, July 11 – 13, 2016.

Jung, B., and M. Inanici. “Measuring Circadian Lighting through High Dynamic Range Photography.” *Lighting Research & Technology* 51, no. 5 (July 10, 2019): 742–63. https://doi.org/10.1177/1477153518792597.

Khademagha, P., M. Aries, A. Rosemann, and E. van Loenen. “Implementing Non-Image-Forming Effects of Light in the Built Environment: A Review on What We Need.” *Building and Environment* 108 (November 1, 2016): 263–72. https://doi.org/10.1016/j.buildenv.2016.08.035.

Khademagha, P., M. Aries, A. Rosemann, and E. Van Loenen. “Why Directionality Is an Important Light Factor for Human Health to Consider in Lighting Design?” *International Journal of Sustainable Lighting* 18 (December 31, 2016): 3–8. https://doi.org/10.26607/ijsl.v18i0.15.

Khanie, M. S., M. Andersen, and J. Wienold. “Human Responsive Daylighting in Offices: A Gaze-Driven Approach for Dynamic Discomfort Glare Assessment.” Dissertation, EPFL, 2015.

Klepeis, N. E., W. C. Nelson, W. R. Ott, J. P. Robinson, A. M. Tsang, P. Switzer, J. V. Behar, S. C. Hern, and W. H. Engelmann. “The National Human Activity Pattern Survey (NHAPS): A Resource for Assessing Exposure to Environmental Pollutants.” *Journal of Exposure Science & Environmental Epidemiology* 11, no. 3 (June 2001): 231–52. https://doi.org/10.1038/sj.jea.7500165.

Knoop, M., O. Stefani, B. Bueno, B. Matusiak, R. Hobday, A. Wirz-Justice, K. Martiny, et al. "Daylight: What Makes the Difference?" *Lighting Research & Technology* 52, no. 3 (July 18, 2019): 423–42. https://doi.org/10.1177/1477153519869758.

Li, Y., T. Ru, Q. Chen, L. Qian, X. Luo, and G. Zhou. "Effects of Illuminance and Correlated Color Temperature of Indoor Light on Emotion Perception." *Scientific Reports* 11, no. 1 (November 12, 2021): 1–12. https://doi.org/10.1038/s41598-021-93523-y.

Lucas, R. J., S. N. Peirson, D. M. Berson, T. M. Brown, H. M. Cooper, C. A. Czeisler, M. G. Figueiro, et al. "Measuring and Using Light in the Melanopsin Age." *Trends in Neurosciences* 37, no. 1 (January 2014): 1–9. https://doi.org/10.1016/j.tins.2013.10.004.

Mardaljevic, J. "Chapter 5 - Sky Models for Lighting Simulation." Essay. In *Daylight Simulation: Validation, Sky Models and Daylight Coefficients*, 163–209. Leicester, UK: De Montfort University, 1999.

Mardaljevic, J., M. Andersen, N. Roy, and J. Christoffersen. "A Framework for Predicting the Non-Visual Effects of Daylight – Part II: The Simulation Model." *Lighting Research & Technology* 46, no. 4 (August 4, 2013): 388–406. https://doi.org/10.1177/1477153513491873.

Mayer, B., and A. Kylling. "Technical Note: The LIBRADTRAN Software Package for Radiative Transfer Calculations - Description and Examples of Use." *Atmospheric Chemistry and Physics* 5, no. 7 (July 26, 2005): 1855–77. https://doi.org/10.5194/acp-5-1855-2005.

Münch, M., A. Wirz-Justice, S. A. Brown, T. Kantermann, K. Martiny, O. Stefani, C. Vetter, K. P. Wright, K. Wulff, and D. J. Skene. "The Role of Daylight for Humans: Gaps in Current Knowledge." *Clocks & Sleep* 2, no. 1 (February 28, 2020): 61–85. https://doi.org/10.3390/clockssleep2010008.

Ohno, Y. "Practical Use and Calculation of CCT and DUV." *LEUKOS* 10, no. 1 (October 18, 2013): 47–55. https://doi.org/10.1080/15502724.2014.839020.

Perez, R., R. Seals, and J. Michalsky. "All-Weather Model for Sky Luminance Distribution—Preliminary Configuration and Validation." *Solar Energy* 50, no. 3 (March 1993): 235–45. https://doi.org/10.1016/0038-092x(93)90017-i.

Pierson, C., E. M. Soto, M. Aarts, and M. Andersen. "A Conceptual Simulation Workflow to Guide Design Decisions Regarding the Effects of Daylight on Occupants' Alertness." *Journal of Physics: Conference Series* 2042, no. 1 (2021): 1–6. https://doi.org/10.1088/1742-6596/2042/1/012116.

Pierson, C., M. Gkaintatzi-Masouti, M.P.J. Aarts, and M. Andersen. “Validation of Spectral Simulation Tools for the Prediction of Indoor Electric Light Exposure.” *Proceedings of the Conference CIE 2021*, December 6, 2021, 52–62. https://doi.org/10.25039/x48.2021.op05.

Pierson, C., M. P. Aarts, and M. Andersen. “Validation of Spectral Simulation Tools in the Context of IPRGC-Influenced Light Responses of Building Occupants.” *Journal of Building Performance Simulation* 16, no. 2 (September 26, 2022): 179–97. https://doi.org/10.1080/19401493.2022.2125582.

Potočnik, J., and M. Košir. “Influence of Geometrical and Optical Building Parameters on the Circadian Daylighting of an Office.” *Journal of Building Engineering* 42 (March 24, 2021): 1–19. https://doi.org/10.1016/j.jobe.2021.102402.

Rea, M. S., and M. G. Figueiro. “Light as a Circadian Stimulus for Architectural Lighting.” *Lighting Research & Technology* 50, no. 4 (June 1, 2018): 497–510. https://doi.org/10.1177/1477153516682368.

Rea, M. S., M. G. Figueiro, A. Bierman, and J. D. Bullough. “Circadian Light.” *Journal of Circadian Rhythms* 8, no. 0 (February 13, 2010): 2–2. https://doi.org/10.1186/1740-3391-8-2.

Rea, M. S., M. G. Figueiro, and J. D. Bullough. “Circadian Photobiology: An Emerging Framework for Lighting Practice and Research.” *Lighting Research & Technology* 34, no. 3 (September 1, 2002): 177–87. https://doi.org/10.1191/1365782802lt057oa.

Reindl, D. T., W. A. Beckman, and J. A. Duffie. “Evaluation of Hourly Tilted Surface Radiation Models.” *Solar Energy* 45, no. 1 (1990): 9–17. https://doi.org/10.1016/0038-092x(90)90061-g.

“Rhinoceros 3D.” www.rhino3d.com. Accessed December 18, 2022. https://www.rhino3d.com/.

Ruppertsberg, A. I., and M. Bloj. “Rendering Complex Scenes for Psychophysics Using Radiance: How Accurate Can You Get?” *Journal of the Optical Society of America A* 23, no. 4 (May 1, 2006): 759–67. https://doi.org/10.1364/josaa.23.000759.

Saiedlue, S., A. Amirazar, J. Hu, and W. Place. “Assessing Circadian Stimulus Potential of Lighting Systems in Office Buildings by Simulations.” In *Proceedings of ARCC Conference Repository*, 719–27. Toronto, Canada: ARCC, May 29 – June 1, 2019.

Schwiegerling, J. *Field Guide to Visual and Ophthalmic Optics*. Bellingham, WA: SPIE Press, 2004.

Spitschan, M., O. Stefani, P. Blattner, C. Gronfier, S. Lockley, and R. Lucas. “How to Report Light Exposure in Human Chronobiology and Sleep Research Experiments.” *Clocks & Sleep* 1, no. 3 (July 26, 2019): 280–89. https://doi.org/10.3390/clockssleep1030024.

Stevens, R. G., G. C. Brainard, D. E. Blask, S. W. Lockley, and M. E. Motta. “Breast Cancer and Circadian Disruption from Electric Lighting in the Modern World.” *CA: A Cancer Journal for Clinicians* 64, no. 3 (2013): 207–18. https://doi.org/10.3322/caac.21218.

Stiles, W. S., and G. Wyszecki. *Color science: Concepts and methods, quantitative data and formulae*. New York, NY: John WIley and Sons, 2000.

Stockman, A., D. I. MacLeod, and N. E. Johnson. “Spectral Sensitivities of the Human Cones.” *Journal of the Optical Society of America A* 10, no. 12 (December 1, 1993): 2491–2521. https://doi.org/10.1364/josaa.10.002491.

Sánchez-Cano, A., and J. Aporta. “Optimization of Lighting Projects Including Photopic and Circadian Criteria: A Simplified Action Protocol.” *Applied Sciences* 10, no. 22 (November 13, 2020): 8068. https://doi.org/10.3390/app10228068.

Tekieh, T., S. W. Lockley, P. A. Robinson, S. McCloskey, M. S. Zobaer, and S. Postnova. “Modeling Melanopsin-mediated Effects of Light on Circadian Phase, Melatonin Suppression, and Subjective Sleepiness.” *Journal of Pineal Research* 69, no. 3 (July 1, 2020): 1–16. https://doi.org/10.1111/jpi.12681.

Thapan, K., J. Arendt, and D. J. Skene. “An Action Spectrum for Melatonin Suppression: Evidence for a Novel Non-rod, Non-cone Photoreceptor System in Humans.” *The Journal of Physiology* 535, no. 1 (2001): 261–67. https://doi.org/10.1111/j.1469-7793.2001.t01-1-00261.x.

Vos, J. J. “Reflections on Glare.” *Lighting Research & Technology* 35, no. 2 (August 18, 2003): 163–75. https://doi.org/10.1191/1477153503li083oa.

Wyszecki, G., and W. S. Stiles. *Color science: Concepts and methods, quantitative data and formulae*. 1st Editioned. New York, NY: Wiley, 1982.

Zeitzer, J. M., D. Dijk, R. E. Kronauer, E. N. Brown, and C. A. Czeisler. “Sensitivity of the Human Circadian Pacemaker to Nocturnal Light: Melatonin Phase Resetting and Suppression.” *The Journal of Physiology* 526, no. 3 (August 1, 2000): 695–702. https://doi.org/10.1111/j.1469-7793.2000.00695.x.

Østergård, T., R. L. Jensen, and S. E. Maagaard. “Building Simulations Supporting Decision Making in Early Design – A Review.” *Renewable and Sustainable Energy Reviews* 61 (April 6, 2016): 187–201. https://doi.org/10.1016/j.rser.2016.03.045.